"Methods for optimization of power transits": Toolbox for Common Forecasting, Risk assessment, and Operational Optimization in Grid Security Cooperations of Transmission System Operators (TSOs)

Toolbox for Common Forecasting, Risk assessment, and Operational Optimization in Grid Security Cooperations of Transmission System Operators (TSOs)

Report

Author(s):
Roald, Line; Köck, Klaus; De Jong, Martijn; Krause, Thilo; Andersson, Göran; Renner, Herwig; Lahaye, Domenico; Papaefthymiou, Georgios

Publication date:
2015

Funding acknowledgement:
282775 - Toolbox for Common Forecasting, Risk assessment, and Operational Optimisation in Grid Security Cooperations of Transmission System Operators (TSOs) (EC)

SEVENTH FRAMEWORK PROGRAMME

SEVENTH FRAMEWORK PROGRAMME

THEME [ENERGY.2011.7.2-1]

[Innovative tools for the future coordinated and stable operation of the pan-European electricity transmission system]

Project Deliverable

Deliverable D 4.3 "Methods for optimization of power transits"

Project acronym: UMBRELLA

Project full title: **Toolbox for Common Forecasting, Risk assessment, and Operational Optimization in Grid Security Cooperations of Transmission System Operators (TSOs)**

Grant agreement no.: *282775-2*

Version: Final *2015-01-27*

Contents

1 Introduction

This deliverable describes work performed within Task 4.3 “Technological Measures to Optimize Power Transits” and Task 4.4 “Operational Rules for Enhancing System Security” of the UMBRELLA project. The overall objective of Work Package 4 is to develop a risk-based security assessment method and the present work builds on methods developed as part of Task 4.1 “Development of risk-based concepts for system security” and Task 4.2 “Assessment of risks regarding cascading events”.

The objective of Task 4.3 is to study how different state-of-the-art technological means such as Flexible AC Transmission Systems (FACTS), Phase Shifting Transformers (PSTs), and High Voltage Direct Current (HVDC) lines can be used to positively influence the overall power system security. We will refer to the above mentioned devices as power flow control devices (PFCCs), and split our work in an implementation and an application phase. The implementation phase was mainly concerned with the modelling of PFCCs, and was split into two sub steps. In the first one a model per PFCC was derived to be able to mathematically describe the impact of such devices on the system risk. In the second step of the implementation phase these models were integrated into the different tools developed for Deliverables D4.1 and D4.2.The application phase presents a set of case studies where these setups were used to study how the incorporation of the different technologies can improve the power system security and optimise the power flows. The results from the implementation and application phase on the effect of PFCCs on the system risk are concluded chapter wise for the three power system risk assessment tools developed in Deliverables D4.1 and D4.2. The first methods is based on stochastic optimisation, the second method assesses the overall system risk for a future system state, while the third method can be used for more through analysis of critical system states. The use of these three models, which vary in their scope and model fidelity, allows for a holistic analysis of the role that power flow control devices can play on reducing the system operational risk. Work done covering the objective of Task 4.3 can be found in the Chapters 2, 4 and 6.

Task 4.4 is dealing with the topic of market designs and operational rules for enhanced system security. Current coordination concepts and prevailing methods in market designs and congestion management are analyzed with the tools developed in Task 4.3. In the course of the work concerning this task market models are compared in terms of overall system risk and complementary procedures are proposed. The Chapters 3, 5 and 6 contribute to Task 4.4.

In the following, a short introduction to each of the subchapters is provided:

The method presented in Chapter 2 is an extension to the probabilistic security constrained optimal power flow (pSCOPF) developed as part of Deliverable D4.1. The original OPF formulation used chance constrained optimisation to guarantee that the system will remain secure with a given probability, even in presence of uncertain in-feeds from Renewable Energy Sources (RES). In the modelling part of Chapter 2 the formulation has been extended to include corrective control actions from HVDC and PSTs, as well as more flexible use of the reserves to balance power mismatches in the system. The

corrective control of HVDC and PSTs incorporate both “traditional” post-contingency corrective control, where the devices react if an outage occurs, and the new concept of uncertainty corrective control, where the devices react to unscheduled changes in the power output of RES, loads or generators. In the application part of Chapter 2, a case study investigating the impact of both corrective control from HVDC and PSTs and more flexible use of the reserves is presented. It is shown how additional flexibility from the reserves, HVDC and PSTs can lower the overall system cost, and how HVDC and PSTs can help the system operator to cope with uncertainty at a low cost.

In Chapter 3, an OPF formulation is used to evaluate two different market designs, a central-dispatch and a self-dispatch market, with respect to the cost of operation and how they react to uncertain in-feeds. In addition, we assess how the use of real-time redispatch as a reaction to in-feed uncertainty can help lower cost. Chapter 3 is structured in a similar way as Chapter 2. In the first part, we show how the reserves and redispatch can be modelled within the OPF. Then, the simplified model of the two different market designs is described, and the corresponding OPF problems are shown. In the second part, results from a case study are used to highlight the effect of the different market designs on the total operating cost. It is shown how redispatch actions can be shifted from the planning phase to real time, and how this allows to operate the system at a lower cost without lowering the system security.

In the first part of Chapter 4, newly implemented enhancements of the probabilistic cascading risk assessment method are described in detail. They contain a turnaround from an event-based approach to a state-based one. While the former method was based on the simulation of branch outages whereas the new one is based on the simulation of system states by single or multiple branch outages. Also some simplifications were performed, mainly to reduce the computational effort to obtain results in a reasonable time horizon. Therefore the manual redispatch modules - representing congestion management done by the TSO - as well as the automatic secondary frequency control were neglected, assuming that during a running cascade there is no time to initiate remedial actions. The second part of Chapter 4 describes the modelling of PFCCs - here the technology of TCSCs, HVDC lines and PSTs - and their implementation in the probabilistic cascading risk assessment method. Finally two case studies are presented showing the influence of different PFCCs on the overall system risk, measured in terms of Lost Load, as well as the risk mitigating effect of central vs. decentral coordination of PFCCs in a multi-zone power system.

Chapter 5 is about analyzing different market models in terms of their costs and the effect on the system risk. The market models are differ in the way they handle congestion management, which has an influence on the system security. The market models compared are uniform pricing (no transmission constraints), nodal pricing (constraints on all lines in the N case), a cross between nodal and uniform pricing – the so called zonal pricing using market splitting (constraints on inter-zonal exchanges). As a benchmark for comparison in terms of system risk the currently prevailing concept - the N-1 secure dispatching method (constraints on the power flows of the N as well the N-1 scenarios) – is used. As a first part of this chapter the market models and their implementation are

presented, followed by the visualisation of the particular results. Two case studies are shown giving advantages and drawbacks of the different market models. The chapter is concluded by a discussion of the results.

In Chapter 6 we present an enhancement to the Monte-Carlo and AC power flow based risk-based security assessment method. This tool can obtain specific inputs from the tools presented in Chapters 2 and 4 (such as a set of contingencies) and assesses the system risk in two complementary implementations using different sets of risk metrics: a) fast screening, based on severity functions and b) detailed assessment including optimal remedial actions determined using an AC OPF framework, with the risk measured based on Lost Load. The analysis allows an increased level of detail by investigating voltage-related security aspects by the utilisation of an AC power flow, as well as the impact of a more detailed depiction of the uncertainty in system inputs by the utilisation of Monte-Carlo sampling techniques (modelling of non-standard marginal distribution and complex stochastic dependencies on load and renewable forecast errors). In the model presentation we discuss explicitly how PFCCs can be incorporated in both implementations. In the second part of the chapter we present a set of study cases where we investigate the voltage security aspects of the system, the role of uncertainty modelling and the impact of PFCCs on reducing system risk. Since a key concern on the applicability of Monte-Carlo based methods is computational aspects, we further present the application of the methodology on a full scale network model and discuss how it can be implemented in a realistic timeframe.

A summary concluding this deliverable is given in Chapter 7, references are given in Chapter 8 and detailed data for the 118 bus system is given in the Appendix.

1.1 Basic definitions and terminology

In this section, we will introduce some of the basic definitions and terminology we have used within this deliverable.

- *Outage:* Single outage of an element, such as a line or a generator. Can either be an independent outage or an outage which is induced by another contingency.
- Initial Outage: The first outage of an event
- *Line/Generator trip:* Outage of a line/generator.
- *Secondary trip*: Dependent outage.
- *Contingency:* Single or Multiple Outage, could be line(s) and/or generator(s). Only used for „initial outages“.
- *Disturbance:* Single or Multiple Outage, could be line(s) and/or generator(s). Could also be another type of disturbance (e.g., extreme wind-infeed deviations, inter-area oscillations, changes in flow on a tie line, etc.).

- *Event:* All outages that „belong together“, either in time or in terms of why they happen, form an event. The “size of an event” can be overall parameters like “amount of load shed” or “number of outages involved in the event”.

1.2 Acronyms and abbreviations

AC ..... Alternating Current

AC OPF ..... AC Optimal Power Flow (considering both active and reactive power)

AC PF ..... AC Power Flow (considering both active and reactive power)

AGC..... Automatic Generator Control

CDF ..... Cumulative Distribution Function

DACF..... Day Ahead Congestion Forecast

DC.....Direct Current

DC OPF ..... (Linearised / DC) Optimal Power Flow (considering only active power)

DSA.....Deterministic Security Assessment

FACTS..... Flexible AC Transmission Systems

HV.....High Voltage

HVAC.....High Voltage AC

HVDC.....High Voltage DC

LMP.....Location Marginal Pricing

LODF..... Line Outage Distribution Factor

MC ……..Monte-Carlo

N-1 outage.....Outage of one single element

OL-RBSA.....Online Risk-Based Security Assessment

OPF ..... Optimal Power Flow

PFCC..... Power Flow Controlling Component

PLF ..... Probabilistic Load Flow

pSCOPF ..... Probabilistic Security Constrained Power Flow

PST.....Phase Shifting Transformer

PTDF ..... Power Transfer Distribution Factor

RBSA..... Risk-Based Security Assessment

RES ..... Renewable Energy Sources

RMS.....Root Mean Square

PV..... Photovoltaics

SCOPF ..... Security Constrained Optimal Power Flow

SOCP.....Second-Order Cone Program

STATCOM .... Static Synchronous Compensator

SVC.....Static Var Compensator

TCSC.....Thyristor Controlled Series Compensator

TSO……Transmission System Operator

1.3 Notation and symbols

General notation

$X_{(i,j)}$ ..... Reference to the $(i,j)^{th}$ entry of the matrix X

$x_{(i)}$ ..... Reference to the i^{th} entry of the vector x

x_{ij} ..... In case of lines, reference to the line from bus i to j

x^i ..... Refers to the value of the parameter in case of outage situation i

$\|x\|_2$ ..... Euclidian norm of x

Outage probabilities

p_k ..... Outage probability for contingency k for an independent outage

$p_{k,ij}$ ..... Probability of a secondary line trip of line ij after contingency k

p_{load} ..... Probability distribution of the load flow

p_{trip} ..... Line trip probability function

$\overline{p_{trip}}$ ..... Cumulated tripping probability

Line Power flows

P_{line} ..... Vector of active power flows on the lines

$P_{line,ij}$ ..... Load flow on line from bus i to bus j (double index)

$P_{line,l}$ ..... Load flow on line l (single index)

$P_{line,ij}^{pre}$ ..... Power flow before the contingency k on line ij

$P_{line,ij}^{post}$ ..... Power flow after the contingency k

$P_{line\ L,M}^{post}$ ..... Power flow in lines l after an outage of line set M

$P_{line,ij}^{max}$ ..... Thermal rating of the line ij

$P_{line,ij}^{trip}$ ..... Post contingency power flow leading to a certain trip

Power injections

P_B ..... Bus active power injections (vector)

$P_{B,b}$ ..... Active power injection at bus b

Q_B ..... Bus reactive power injections (vector)

$Q_{B,b}$ ..... Reactive power injection at bus b

P_D ..... Active power demand (vector)

$P_{D,d}$ ..... Active power demand at bus b

Q_D ..... Reactive power demand (vector)

$Q_{D,d}$ ..... Reactive power demand at bus b

P_{dacf} ..... Nodal power forecast

$P_{\mu,fce}$ ..... Mean value of the forecast error

$P_{\sigma,fce}$ ..... Standard deviation of the forecast error

μ ..... Mean value

σ ..... Standard deviation

ρ_{ij} ..... Correlation coefficient between node i and j

Σ_W ..... Covariance matrix of all uncertain in-feeds

ΔP ..... Inbalance in power

Q_G ..... Reactive power generated by conventional power plants

$Q_{G,g}$ ..... Reactive power generated by conventional power plant g

P_G ..... Active power generated by conventional power plants

$P_{G,g}$ ..... Active power generated by conventional power plant g

$P_{G,g}^0$ ..... Initial active power from generator

P_G^{max} ..... Maximum power production at the generators

P_G^{min} ..... Minimum power production at the generators

P_G^+ ..... Purchased up-reserves from each generator

P_G^- ..... Purchased down-reserves from each generator

R_G^+ ..... Used up-reserves from each generator

R_G^- ..... Used down-reserves from each generator

$\triangle P_G^i$ ..... Change in generation after outage i

D_G^i ..... Reaction of AGC after an outage in case of pro-rata activation

D_W^i (or d_W^i) .... Reaction of generators to wind power fluctuations

ΔP_G^+ ..... Day-ahead up redispatch

ΔP_G^- ..... Day-ahead down redispatch

R_W ..... Real-time redispatch related to wind power fluctuations

β ..... Additional available generation in case of an emergency

C..... Generation costs vector

P_W ..... Power generated by wind power plants

$P_{W,w}$ ..... Power generated by wind power plant w

P_W^f ..... Forecasted power generated by wind power plants

δP_W ..... Deviation from forecasted power

ΔP_W ..... Total deviation from forecasted power HVDC

P_{DC} ..... Scheduled power flow on the HVDC lines

$\triangle P_{DC}^i$ ..... Change in power flow on the HVDC lines after outage i

H_W^i ..... Change in power flow on the HVDC lines after outage i

R_{DC}^+..... Reserve capacity for increasing flow on the HVDC lines

R_{DC}^-..... Reserve capacity for decreasing flow on the HVDC lines

PST

α ..... Phase angle for the PSTs

$\triangle \alpha^i$ ..... Change in phase angle for the PSTs, after outage i

S_W^i ..... Reaction of the PSTs to change in the uncertain in-feeds

B_α ..... Influence of the PSTs on power injections in all lines

s_L ..... Direct influence of the PSTs on power flows in lines where connected

Voltage

$|V|$..... Voltage magnitude

V_m ..... Voltage magnitude at bus m

θ ..... Voltage angle

θ_i ..... Voltage angle of bus i

θ_{ref} ..... Slack node voltage angle

Frequency deviations

f ..... system frequency

f_{min}..... lower limit of the system frequency

f_{max} ..... upper limit of the system frequency

$\frac{\Delta P_l}{\Delta f}$ ..... Self-regulation of the load

$\frac{\Delta P_g}{\Delta f}$ ..... Generator droop

System parameters

N_G ..... Number of generators

N_B ..... Number of buses

N_L ..... Number of circuits

x_{ij} ..... Reactance of line from bus I to bus j

$\boldsymbol{Y_{bus}}$ ..... Nodal admittance matrix

$\boldsymbol{B_{bus}}$ ..... Nodal admittance matrix with DC approximation

$\widehat{\boldsymbol{B}}_{\boldsymbol{bus}}$ ..... Nodal admittance matrix with DC approximation without slack bus

$\boldsymbol{A^i}$ ..... Mapping from nodal injections to line power flows

$LODF_{mn,ij}$ ..... Line outage distribution factor of line mn to line ij

$LODF_{M,O}$ ..... LODF from the outaged lines O to the monitored lines M

$GGDF_{ij,g}$ ..... Load flow change in line ij after an generator outage g

$\widehat{PTDF}$ ..... PTDF matrix without slack bus

$PTDF_M$ ..... PTDF matrix for the set of lines M

$PTDF_{l,b}$ ..... Element of the PTDF matrix regarding to line l and bus b

$d_{l,k}$ ..... Element l,k of the weighting matrix

$\mathbf{r}_g$ ..... Bus mapped weighting factor matrix d

C_G ..... Generation connectivity matrix

C_L ..... Branch connectivity matrix

M_G ..... Mapping of generators to buses

M_D ..... Mapping of demand to buses

M_W ..... Mapping of uncertain in-feeds to buses

M_{DC} ..... Mapping of HVDC lines to buses

Risk parameters

$Risk_{k,ij}$ ..... Risk of a secondary tripping of line ij after contingency k

$Risk_{k,ij}^{max}$ ..... Contingency and line specific risk bound

$C_{k,ij}$ ..... Upper bound to the contingency and line specific constraint

$Risk_k$ ..... Risk related to contingency k

$Risk_{tot}$ ..... Risk of a secondary tripping of line ij after contingency k

Redispatch parameters

$P_{redispatch}$..... Vector of redispatched generator powers

$N_{P_{max}}$..... Maximum number of power plants to redispatch

$P_{dispatch}^{min}$..... Minimum redispatchable power

Overall method related parameters

$lsl(i)$ ..... Weighting factor discretisation step's lower limit

$usl(i)$ ..... Weighting factor discretisation step's lower limit

p_{ns} ..... Weighting factor of the particular discretisation step

q_i ..... Counter probability

$p_{2|1}$..... Joint probability

ρ_{ij} ..... Correlation coefficient

ρ ..... Correlation matrix

Σ ..... Covariance matrix

State of the art measures

$P_{HVDC,t}$..... Nodal injection at the from bus

$P_{HVDC,f}$ ..... Nodal injection at the from bus

α_0..... HVDC no-load losses

α_1..... HVDC linear losses

P_n ..... Vector of nodal injections

α_{PST} ..... Phase shift angle

P_f ..... Fictitious power injection

X_{TCSC}..... Reactance of the TCSC at a given set point

X_{TCSC}^{min}..... Minimum reactance of the TCSC

X_{TCSC}^{max}..... Maximum reactance of the TCSC

Branch loading parameters

$P_{q97.5}$..... 97.5%-quantile in power

P_B^{max} ..... Branch loading limit vector

P_B^{μ} ..... Vector of branch loadings' mean values

P_B^{σ} ..... Vector of branch loadings' standard deviations

2 Probabilistic Security Constrained Optimal Power Flow with Corrective Control

The method presented in this section is an extension to the probabilistic security constrained optimal power flow (pSCOPF) presented in [1], [2]. The original formulation used chance constrained optimisation to guarantee that the system will remain secure with a given probability, even in presence of uncertain in-feeds.

The current method extends this formulation by incorporating *corrective control* actions from HVDC and PSTs, as well as activation of reserves based on their location in the system (meaning that the reserves can be activated in a way which avoids congestions). *Corrective control* actions are often referred to as control actions that are taken *after* a disturbance has occurred in the system, to bring the system back into a secure operating state. Thus, corrective control is often referred to as *post-contingency corrective control*. A system state which requires post-contingency corrective control to avoid violating technical limits is referred to as a *correctively secure* system state.

It has been shown that post-contingency corrective control can reduce the cost of ensuring N-1 security, i.e., reduce the cost difference between an OPF with and without security constraints [3]. This is because the use of corrective actions allows for smaller security margins in the normal operating state, since many violations can be taken care of after a contingency has occured.

Here, we propose to introduce the notion of *uncertainty corrective control.* Uncertainty corrective control are corrective actions taken to mitigate violations which arise due to deviations from the planned generation schedule, e.g., due to forecast errors for renewables or intra-day trading. As for post-contingency corrective control, the uncertainty corrective control actions are only applied *after* the deviation from the forecast has accured, and thus are functions of the realisation of the uncertain variables. A system state which might require uncertainty corrective control to avoid overloads can be said to be *correctively secure against uncertainties*, analog to corrective security for contingencies.

Considering the way transmission systems are operated today, corrective control actions such as switching actions and redispatch are widely used to handle deviations from the planned generation schedule (whether this is due to forecast errors for renewable in-feeds or intra-day trading). However, there are very few OPF formulations that model corrective actions which explicitly depend on a deviation from the generation schedule. This is partly because uncertainty is a new and increasing problem, due to market liberalisation and higher shares of renewables. Another reason is that modelling uncertainty in the OPF is a challenging task, since uncertain variables such as wind power in-feeds are better characterised as a continuous probability distribution than by discrete values. While outages are discrete (they happen or they do not), forecast errors can take on an infinite number of values, such that a different modelling approach is necessary.

Some existing OPF methods account for a set of critical scenarios within the optimisation and ensure that suitable corrective actions are available for those (e.g., [4], [5]). Due to the low number of considered scenarios and the heuristics used to define which scenarios to

include, there are however no guarantees that the obtained solution is representative for other scenarios. To a certain extent, the OPF formulations in [1] (which are similar to [6], [2], [7]) can also be said to introduce uncertainty corrective control from generators, since it is assumed that the generators react to the uncertainty in real-time. These actions were, however, not considered to be corrective actions that are included to reduce the cost of uncertainty or the amount of congestion in the system, but rather actions that are necessary to ensure a balanced system state.

In [6], [2], [7], the reaction to the forecast deviations is modelled as an affine control policy, where the generators are increasing/descreasing their in-feed proportionally to the forecast deviation. Modelling the reactions as a function avoids the need to define a finite number of scenarios, but allows us to treat the forecast uncertainty as a continuous variable. Moreover, the use of an affine control policy allows for an analytical reformulation of the chance constraints [2], [7]. Therefore, a similar affine control policy is applied here, but with two extensions. First, HVDC and PSTs are allowed to react correctively to the forecast deviations (according to an affine control policy). Second, we extend the affine policy to not only consider the overall power mismatch in the system (which could be measured through the frequency), but allow for reactions to each forecast deviation separately (assuming local measurements). This enables the controls to react locally.

Note that although it is assumed that the HVDC and PSTs are reacting continuously to the forecast deviations, this does not necessarily have to be implemented as an automatic control. The solution to the OPF with uncertainty corrective control from HVDC and PSTs will stay within the operational limits (with a given probability) if the control policies are followed, but there can be many (minor) forecast deviations that do not lead to violations of any limits. Since HVDC and PSTs are not necessary to, e.g., keep the system balanced, the TSO might choose to change their set points manually only if the forecast deviation exceeds a certain threshold or if an N-1 violation is observed.

The formulation presented below is based on chance constraints, which guarantee that the limit is kept with a given probability. This does however mean that there is also a non-zero probability that a violation will occur. This is usually not a problem, as most of the constraints in power systems are “soft constraints”, e.g., the thermal limits of a line can be violated for a short while without incurring major problems. N-1 constraints, which are usually binding in power system optimisation, are also soft. If they are violated, there is usually no immediate violation of operational limits in the system, but only the risk of violation in case the corresponding outage would happen at the same point in time. Therefore, the TSO usually has more time to take action against adverse effects from forecast deviations than what is normally available for corrective control after outages (where the system might be operating above the long-term technical limits). Additionally, large forecast deviations typically build up over a longer time horizon. Because of these two time aspects, it is possible to define alternative strategies to handle the cases where a violation would occur before a violation of an actual limit occurs.

The chapter is organised as follows: First, we introduce the model for the uncertain in-feeds. Second, the modelling of corrective control actions addressing both type of disturbances (contingencies and in-feed deviations) are a shown for both generators,

HVDC and PSTs. Third, the pSCOPF problem incorporating corrective control for both uncertainty realisations and contingencies is stated. Finally, the method is demonstrated in a case study for the IEEE 118 bus system.

2.1 System modelling

In the following, we will consider a system with N_G generators, N_W uncertain in-feeds and N_D loads. There are N_L transmission lines, N_{DC} HVDC connections and N_α PSTs.

2.1.1 Model of the uncertain in-feeds

The uncertain in-feeds are denoted by a subscript $_W$, which refers to uncertain wind in-feeds. The uncertainty is however not limited to wind in-feeds, but can also be related to uncertain loads, PV in-feeds or changes to the power plants schedules due to intra-day trading. We model realised power in-feeds $P_W \in R^{N_W}$ of the uncertain in-feeds as the sum of a forecasted value $P_W^f \in R^{N_W}$ and a forecast error $\delta P_W \in R^{N_W}$:

$$P_W = P_W^f - \delta P_W.$$

We assume that the forecast errors δP_W are Gaussian random variables with zero mean, and have a covariance matrix $\Sigma_W \in R^{N_W \times N_W}$. Different from the approach in the previous deliverables, it is not assumed that the random variables are independent. In the following, we will refer to the sum of all forecast errors as $\Delta P_W = 1^T_{\{1,N_W\}} \delta P_W$.

Note that it is straight forward to extend the formulation to Gaussian random variables with non-zero mean, and that it is possible to extend the formulation to random variables that are non-Gaussian.

2.1.2 Generator modelling

The power output $P_G \in R^{N_G}$ of each generator is an optimisation variable, but is chosen to fulfill the power balance constraint

$$1^T_{\{1,N_B\}}\left(M_G P_G + M_W P_W^f - M_D P_D\right) = 0, \tag{2-1}$$

where $P_D \in R^{N_D}$ are the loads and M_G, M_W, M_D are matrices that map the in-feeds to their respective buses.

2.1.2.1 Balancing power

In addition to providing energy according to their schedule, the generators provide reserve power to ensure that the power balance is kept during disturbances. We consider two type of disturbances, i) generator outages and ii) forecast errors (i.e., deviations from the

forecasted renewable in-feeds). Incorporating corrective control both for uncertainty and contingencies, we obtain an expression of the following form for the generator outputs:

$$P_G^i = P_G + \Delta P_G^i + D_W^i \delta P_W.$$

Here, $i = 0$ refers to a normal operating condition (no outages) and $i = 1, \dots, N$ to specific outage situations (N-1 cases). P_G^i are the generator outputs during each disturbance. P_G refers to the scheduled power output, ΔP_G^i are the changes in generation due to generator outages and the term $D_W^i \delta P_W$ refers to changes in the generation due to forecast deviations.

Balancing of generator outages

During a generator outage, ΔP_G^i is the amount by which each of the generator outputs are adjusted. The definition of ΔP_G^i is subject to the following constraints,

$$\Delta P_{G(i)}^i = -P_{G(i)}, \qquad \Sigma_j \Delta P_{G(j)}^i = 0, \qquad \Delta P_G^0 = 0, \tag{2-2}$$

where the notation $P_{G(i)}$ refers to the ith entry of the vector P_G. Note that ΔP_G^i can also be defined as

$$\Delta P_G^i = D_{G(\cdot,i)}^i P_{G(i)}. \tag{2-3}$$

This notation is particularly useful when the compensation factors $D_{G(\cdot,i)}^i \in R^{N_G \times N_G}$ are defined before the simulation starts (i.e., in systems with pro-rata activation of reserves).

Balancing of forecast deviations

When the wind power deviates from the forecasted in-feeds, the generators must increase or reduce their outputs to keep the system balanced. The decrease/increase from each generator depend either on the overall power mismatch introduced by the forecast deviations, ΔP_W, or on the forecast deviation of the different uncertain in-feeds, δP_W.

If the balancing depends on the mismatch of the different uncertain in-feeds δP_W, we obtain a balancing matrix $D_W^i \in R^{N_G \times N_W}$, subject to the following constraints

$$D_{W(i,l)}^i = 0, \quad \Sigma_j D_{W(j,l)}^i = 1, \quad \forall \text{ columns } l \quad \text{and} \quad D_W^i \geq 0 \tag{2-4}$$

If the balancing depends only on the overall power deviation (also denoted as “power mismatch” in the following) ΔP_W, the amount of increase or decrease can be defined as $d_W^i \Delta P_W = d_W^i \cdot 1_{\{1,N_W\}}^T \delta P_W$, where $d_W^i \in R^{N_G}$ is defined subject to the following constraints:

$$d_{W(i)}^i = 0, \qquad \Sigma_j d_{W(j)}^i = 1, \qquad d_W^i \geq 0 \tag{2-5}$$

Note that the index i in d_W^i and D_W^i refers to the i^{th} outage situation (i.e., a generator or line outage), and not to the forecast deviation. Forecast deviations are continuous, and

can thus not be completely defined through a finite set of scenarios i. Further, $d_W^i \cdot 1_{\{1,N_W\}}^T$ is a matrix with the same dimensions as D_W^i. In the following, the equations will be stated using D_W^i to avoid unnecessary notation.

2.1.2.2 Reserve power

In order to ensure that there is enough generation capacity available to keep the power balance, the transmission system operators purchase reserve power. Here, we assume that each generator will be scheduled to provide up and down reserves denoted by $R_G^+, R_G^- \in R^{N_G}$ for the considered OPF time step, with

$$R_G^+ > 0, \quad R_G^- < 0. \tag{2-6}$$

These reserves will cover all deviations from the scheduled power output of the generators P_G, including reserves which are needed to balance the system after generator outages and reserves that are needed to balance wind power in-feeds. Since reserve capacities are usually purchased on a longer time scale than the power (i.e., for a day or a week at the time), we assume that the reserves scheduled to be provided by each generator during the considered time step must stay within the purchased reserve capacities $P_G^+, P_G^- \in R^{N_G}$:

$$R_G^+ < P_G^+, \quad -R_G^- < P_G^-. \tag{2-7}$$

where

$$P_G^+, P_G^- > 0\,. \tag{2-8}$$

The purchased reserve capacities are assumed to be fixed for the given time horizon, and are not subject to optimisation.

2.1.2.3 Generator constraints

The generation capacities $P_G^{min}, P_G^{max} \in R^{N_G}$ are the minimum and maximum capacities that are available to the market. For generators that provide reserves, the reserve capacity P_G^+, P_G^- must be kept free at all times, and cannot be scheduled in the energy market. The total capacity of a generator is the sum of the generation capacity available at the market and the generation capacity used for reserve provision:

$$P_{G(g)}^{tot,min} = P_{G(g)}^{min} - P_{G(g)}^-, \tag{2-9}$$

$$P_{G(g)}^{tot,max} = P_{G(g)}^{max} + P_{G(g)}^+, \tag{2-10}$$

To ensure that the generator output does not exceed the maximum output $P_{G(g)}^{tot,max}$ and does not fall below the minimum output $P_{G(g)}^{tot,min}$, we assume that $P_G^{min}, P_G^{max}, P_G^+, P_G^-$ are defined according to (2-9), (2-10) and enforce the following constraints:

$$P_{G(g)} \geq P_{G(g)}^{min}, \tag{2-11}$$

$$P_{G(g)} \leq P_{G(g)}^{max}, \tag{2-12}$$

$$-R_{G(g)}^{-} \geq P_{G(g)}^{-} \tag{2-13}$$

$$R_{G(g)}^{+} \leq P_{G(g)}^{+} \tag{2-14}$$

$$\mathbb{P}\left(R_{G(g)}^{-} \leq \Delta P_{G(g)}^{i} + D_{W(g,\cdot)}^{i} \delta P_W\right) \geq 1 - \varepsilon, \tag{2-15}$$

$$\mathbb{P}\left(\Delta P_{G(g)}^{i} + D_{W(g,\cdot)}^{i} \delta P_W \leq R_{G(g)}^{+}\right) \geq 1 - \varepsilon, \tag{2-16}$$

for all generators $g = 1, \dots, N_G$ and all outages $i = 0, \dots, N$. Since (2-15) and (2-16) depend on the random variables δP_W, we use chance constraints to ensure that the constraints will hold with a certain probability.

2.1.3 HVDC

HVDC connections are able to change their set points within a very short timeframe. This makes the HVDC connection very suitable for corrective control, which has to happen quickly after the contingency takes place.

The HVDC set point in normal operation is denoted as P_{DC} and the HVDC set-point in each post-contingency state as P_{DC}^{i}. The post-contingency corrective control (change in set-point between pre- and post-contingency state) is denoted by ΔP_{DC}^{i}.

In order to use the HVDC connections to influence the uncertainty margins, we need to allow the HVDC connection to react to the uncertainty. Since there exist an infinite number of possible uncertainty realisations, it is not possible to define a HVDC set-point for each uncertainty state (as we did for the contingencies i). Instead, we assume that the HVDC connection is continuously adjusting the set point based on the changes in wind power in-feed, similar to the reserves.

Incorporating corrective control both for uncertainty and contingencies, we can obtain an expression similar to the expression for the generators

$$P_{DC}^{i} = P_{DC} + \Delta P_{DC}^{i} + H_W^{i} \delta P_W.$$

where ΔP_{DC}^{i} is the reaction to contingency i and $H_W^{i} \delta P_W$ models the reaction to the uncertain in-feeds. Different from the generators, there are no restrictions on how to choose ΔP_{DC}^{i}, since the HVDC are not required for the power balance in the system. However, in case of an outage of the HVDC connection itself, the power flow on that line should be set to zero. Therefore, for an outage of the h^{th} HVDC connection corresponding to the i^{th} outage, we require

$$\Delta P_{DC(h)}^{i} = -P_{DC(h)}. \tag{2-17}$$

As for the generators, the reaction to the uncertain in-feeds can be modelled based on either the overall power mismatch ΔP_W or the separate mismatches δP_W. If the reaction is based on the deviation of separate in-feeds, we define the reaction as $H_W^i \delta P_W$. Here, $H_W^i \in R^{N_{DC} \times N_W}$ is a matrix where each entry is the reaction of one HVDC connection to a specific in-feed. In case of an outage of the h^{th} HVDC connection corresponding to the i^{th} outage,the following constraint must be fullfilled

$$H^i_{W(h,l)} = 0, \quad \forall \text{ columns } l \tag{2-18}$$

If the reaction is based on the overall power deviation, we define the reaction as $h_W^i \Delta P_W = h_W^i \cdot 1^T_{\{1,N_W\}} \delta P_W$, where $h_W^i \in R^{N_{DC}}$. In case of an outage of the h^{th} HVDC connection corresponding to the i^{th} outage, we set the balancing to zero

$$h^i_{W(h)} = 0\,. \tag{2-19}$$

Assuming that some of the HVDC connections might be merchant lines where the power capacity must be purchased, we also introduce two new variables $R^+_{DC}, R^-_{DC} \in R^{N_{DC}}$. These capacities are analogue to the reserve capacities of the generators, and denote the capacity that must be kept free to cope with outages and forecast deviations. By definition,

$$R^+_{DC} > 0, \quad R^-_{DC} < 0. \tag{2-20}$$

Thus, in addition to (2-17) and (2-20), the following constraints must hold for the HVDC lines:

$$-P^{max}_{DC(g)} \leq P_{DC(g)} + R^-_{DC(g)}, \tag{2-21}$$

$$P_{DC(g)} + R^+_{DC(g)} \leq P^{max}_{DC(g)}, \tag{2-22}$$

$$\mathbb{P}\left(R^-_{DC(g)} \leq \Delta P^i_{DC(g)} + H^i_{W(g,\cdot)} \delta P_W\right) \geq 1 - \varepsilon, \tag{2-23}$$

$$\mathbb{P}\left(\Delta P^i_{DC(g)} + H^i_{W(g,\cdot)} \delta P_W \leq R^+_{DC(g)}\right) \geq 1 - \varepsilon, \tag{2-24}$$

for all HVDC connections $g = 1, \dots, N_{DC}$ and all outages $i = 0, \dots, N$. P^{max}_{DC} denotes the maximum transfer capacity of an HVDC line. Since (2-23) and (2-24) depend on the random variables δP_W, we use chance constraints to ensure that the constraints will hold with a certain probability.

2.1.4 PST

Although phase shifting transformers (PSTs) cannot compete with HVDC in their reaction time, we still assume that the PSTs are able to change their set-point within a time frame which is short enough to provide corrective control (e.g., for congestion management after

wind power deviations and to relieve temporary transmission line overloads post-contingency).

Here, the vector of PST angle set-points in normal operation is denoted as α and the PST set-point in each post-contingency state as α^i. The corrective control (change in set-point between pre- and post-contingency state) is given by $\Delta\alpha^i = \alpha^i - \alpha$. The limits of α are given by $\alpha \in [\alpha^{min}, \alpha^{max}]$. We assume that the taps of the transformers are close enough, such treating α as a continuous variable is a good approximation of the problem. As for the HVDC connections, we allow the PSTs to act correctively after the occurrence of wind power deviations according to an affine control policy, which can be defined as $S_W^i \delta P_W$ if the reaction depend on the separate deviations, or as $s_W^i \Delta P_W = s_W^i \cdot 1_{\{1,N_W\}}^T \delta P_W$ if the reaction depends on the overall power deviation ΔP_W.

Incorporating corrective control for both uncertainty and contingencies leads to an expression of the following form:

$$\alpha^i = \alpha + \Delta\alpha^i + S_W^i \delta P_W.$$

As for the HVDC connections, there are no restrictions to how $\Delta\alpha^i, S_W^i$ can be chosen, except in case of the outage of the s^{th} PST (corresponding to outage i), where

$$\Delta\alpha_{(s)}^i = -\alpha_{(s)},\ S_{W(s,l)}^i = 0 \quad \forall \text{ columns } l. \tag{2-25}$$

or

$$\Delta\alpha_{(s)}^i = -\alpha_{(s)},\ s_{W(s)}^i = 0. \tag{2-26}$$

These equations must hold for the outage of all PSTs $s = 1, \dots, N_\alpha$. For the PSTs, there is no need to keep "reserve capacities" for the PST angle α. Apart from (2-25), there are two PST constraints,

$$\mathbb{P}\left(\alpha_{(s)}^{min} \le \alpha_{(s)} + \Delta\alpha_{(s)}^i + S_{W(s,\cdot)}^i \delta P_W\right) \ge 1 - \varepsilon, \tag{2-27}$$

$$\mathbb{P}\left(\alpha_{(s)} + \Delta\alpha_{(s)}^i + S_{W(s,\cdot)}^i \delta P_W \le \alpha_{(h)}^{max}\right) \ge 1 - \varepsilon, \tag{2-28}$$

which must for all PSTs $s = 1, \dots, N_\alpha$ and all outages $i = 0, \dots, N$. Since (2-27) and (2-28) depend on the random variables δP_W, we use chance constraints to ensure that the constraints will hold with a certain probability.

2.1.5 Line flow modelling

The line flows are a function of the system topology, the power injections (modified by the generators and the HVDC) and the set-points of the PSTs. Incorporating all those effects, the line flows can be modelled as [8], [9]:

$$P_F = A^i\left(P_{inj}^i + B_\alpha \alpha^i\right) + s_L \alpha^i$$

Here, P_F are the line flows and $A^i = B_f^i\left(\tilde{B}_{bus}^i\right)^{-1}$ are the matrices describing the topology in the ith operating condition. P_{inj} are the nodal power injections from generators, uncertain in-feeds, loads and HVDC, and is given by

$$P_{inj}^i = M_G\left(\boldsymbol{P_G} + \boldsymbol{d_W^i}\Delta P_W\right) + M_{DC}\left(\boldsymbol{P_{DC}} + \Delta\boldsymbol{P_{DC}^i} + \boldsymbol{h_W^i}\Delta P_W\right) + M_W\left(P_W^f - \delta P_W\right) - M_D P_D\,.$$

The matrix $M_{DC} \in R^{N_B \times N_{DC}}$ is a matrix relating the HVDC connections to the buses where they are connected, with a -1 entry at the sending bus, and a +1 at the receiving bus.

In the matrix $B_\alpha \in R^{N_B \times N_\alpha}$, each column corresponds to one PST. For the PST at line l with angle α_l, the corresponding column has only zero entries except for $+1/x_l$ at position k (corresponding to the from bus) and $-1/x_l$ at position m (corresponding to the to bus). This term corresponds to a virtual power injection at the buses k and m, and models the indirect effect of the PST on all lines in the system through the resulting change in voltage angles (this also includes a change in the line flow on the line where it is located).

To incorporate the direct change in power flow at the line where the PST is located, we include the last term. $b_L \in R^{N_L \times N_\alpha}$ describes the direct influence of the PST on the line where it is located. Each column has only zero entries, except for a $1/x_l$ at position l (corresponding to the line where the PST is located).

With this, we get the following line constraints:

$$\begin{aligned}&\mathbb{P}\Big(A_{L(l,\cdot)}^i\Big(M_G\left(P_G + D_W^i\delta P_W + \Delta P_G^i\right) + M_{DC}\left(P_{DC} + \Delta P_{DC}^i + H_W^i\delta P_W\right) + \\ &M_W\left(P_W^f - \delta P_W\right) - M_L P_L + B_\alpha\left(\alpha + \Delta\alpha^i + S_W^i\delta P_W\right)\Big) + b_{L(l,\cdot)}\left(\alpha + \Delta\alpha^i + \right. \\ &\left.S_W^i\delta P_W\right) \le P_{L(l)}^{max}\Big) \ge 1 - \varepsilon,\end{aligned} \tag{2-29}$$

$$\begin{aligned}&\mathbb{P}\Big(-P_{L(l)}^{max} \le A_{L(l,\cdot)}^i\Big(M_G\left(P_G + D_W^i\delta P_W + \Delta P_G^i\right) + M_{DC}\left(P_{DC} + \Delta P_{DC}^i + H_W^i\delta P_W\right) + \\ &M_W\left(P_W^f - \delta P_W\right) - M_L P_L + B_\alpha\left(\alpha + \Delta\alpha^i + S_W^i\delta P_W\right)\Big) + b_{L(l,\cdot)}\left(\alpha + \Delta\alpha^i + \right. \\ &\left.S_W^i\delta P_W\right)\Big) \ge 1 - \varepsilon,\end{aligned} \tag{2-30}$$

which must hold for all transmission lines $l = 1, \dots, N_L$ and all line and generator outages $i = 1, \dots, N$.

2.1.6 Objective function

The objective of the OPF is to minimise operational cost, while keeping the system secure. Minimise operational cost is in this context similar to maximising power transits from low cost generators to high load areas, as well as ensuring integration of as much RES energy as possible. Depending on how the system is organised, we can formulate different objective functions. In this part of the deliverable, the system is assumed to be a central dispatch system.

In a central dispatch system, the market players submit bids to the TSO. The TSO optimises the dispatch such that the operational cost is minimal while all constraints are met. The most important cost component is the cost of the generation dispatch P_G. Additional sources of cost include procurement of the reserve capacities P_G^+, P_G^- and possibly the cost of reserving HVDC capacities R_{DC}^+, R_{DC}^- to cope with uncertainties. Here, we will assume that P_G^+, P_G^- are procured for a longer time horizon (such that they induce no cost to the current OPF problem) and that the HVDC capacities have zero cost, such that these parameters don't occur in the objective function.

The objective function can thus be expressed as

$$\min\ {c_G}^T P_G, \tag{2-31}$$

where $c_G \in R^{N_G}$ is the cost of energy.

1.1.1 Optimisation variables

Depending on the system structure, different parameters can either be assigned a fixed value before the optimisation starts or be included in the problem as optimisation variables. The following variables are always optimisation variables:

P_G Generator output

P_{DC} HVDC transmitted power

α Angle of the PST

Depending on the time horizon of the problem, the following parameters might be considered as optimisation variables, or as fixed quantities (reserve capacities for generators are often reserved for a week or a day at a time, and are fixed for all smaller time steps):

R_G^+ Up reserves (per generator)

R_G^- Down reserves (per generator)

In some systems, the reserves might be activated on a pro-rata basis. In this case, d_W^i and $\Delta P_G^i = d_G^i P_{G(i)}$ will be fixed before the optimisation starts. In other systems, these might be optimised along with the generation dispatch:

d_W^i / D_W^i Distribution vector (among generators) for wind power balancing energy

ΔP_G^i Compensation of the generator outages

If we allow for corrective control related to outages and wind power deviations from HVDC and PSTs, the following variables can also enter the problem as optimisation variables:

h_W^i / H_W^i Reaction of the HVDC lines to wind power deviations

ΔP_{DC}^i Reaction of the HVDC lines to outages

R_{DC}^+ Reserve capacity (per HVDC)

R_{DC}^- Reserve capacity (per HVDC)

s_W^i / S_W^i Reaction of the PSTs to wind power deviations

α^i Reaction of the PSTs to outages

2.1.7 Chance constraint reformulation

The chance constraints are used to guarantee that constraints which include random variables will hold with at least a given probability. To reformulate the chance constraints to tractable constraints (yielding a solvable optimisation problem), we use an analytic reformulation approach, based on the assumption of a normal distribution [10]. The reformulation of the chance constraint is done in the following way:

1. The terms within the chance constraint are rearranged in the following way:

$$\mathbb{P}(a(x)^T \delta P_W + b(x) \leq c) \geq 1 - \varepsilon, \tag{2-32}$$

   Here, x denotes the decision variables.

2. Assuming that δP_W is distributed according to a multivariate normal distribution, with zero mean and covariance matrix Σ_W, (2-32) can be reformulated as

$$b(x) \leq c - \Phi^{-1}(1-\varepsilon) \cdot \| \Sigma_W^{1/2} a(x) \|_2, \tag{2-33}$$

   where $\Phi^{-1}(1-\varepsilon)$ represents the $1-\varepsilon$ quantile of the normal distribution and $\| \Sigma_W^{1/2} a(x) \|_2$ refers to the euclidian norm.

2.2 Optimisation problem formulation

Based on the above considerations formulation, we obtain the following optimisation problem:

$$\min c_G{}^T P_G, \tag{2-34}$$

subject to

$$1_{\{1,N_B\}}^T \left(C_G P_G + C_W P_W^f - C_D P_D\right) = 0, \tag{2-35}$$

$$P_{G(g)} \geq P_{G(g)}^{min}, \tag{2-36}$$

$$P_{G(g)} \leq P_{G(g)}^{max}, \tag{2-37}$$

$$-R_{G(g)}^- \geq P_{G(g)}^- \tag{2-38}$$

$$R_{G(g)}^+ \leq P_{G(g)}^+ \tag{2-39}$$

$$\Delta P^i_{G(g)} \le R^+_{G(g)} - \Phi^{-1}(1-\varepsilon) \parallel \Sigma_W^{\frac{1}{2}} D^i_{W(g,\cdot)} \parallel_2, \quad (2\text{-}40)$$

$$\Delta P^i_{G(g)} \ge R^-_{G(g)} + \Phi^{-1}(1-\varepsilon) \parallel \Sigma_W^{\frac{1}{2}} D^i_{W(g,\cdot)} \parallel_2, \quad (2\text{-}41)$$

$$\sum \Delta P^i_G = 0, \quad (2\text{-}42)$$

$$\Delta P^i_{G(i)} = -P^0_{G(i)}, \quad (2\text{-}43)$$

$$D^i_{W(i)} = 0, \quad (2\text{-}44)$$

$$\sum_k D^i_{W(l,k)} = 1\,, \quad \forall \text{ columns l}\,, \quad (2\text{-}45)$$

$$P_{DC(h)} + R^+_{DC(h)} \le P^{max}_{HVDC(h)}, \quad (2\text{-}46)$$

$$P^{min}_{DC(h)} \le P_{DC(h)} + R^-_{DC(h)}, \quad (2\text{-}47)$$

$$\Delta P^i_{DC(h)} \le R^+_{DC(h)} - \Phi^{-1}(1-\varepsilon) \parallel \Sigma_W^{\frac{1}{2}} H^i_{W(h,\cdot)} \parallel_2, \quad (2\text{-}48)$$

$$\Delta P^i_{DC(h)} \ge R^-_{DC(h)} + \Phi^{-1}(1-\varepsilon) \parallel \Sigma_W^{\frac{1}{2}} H^i_{W(h,\cdot)} \parallel_2, \quad (2\text{-}49)$$

$$\Delta P^i_{DC(i)} = -P_{DC(i)}, \quad (2\text{-}50)$$

$$h^i_{W(i)} = 0, \quad (2\text{-}51)$$

$$\alpha_{(h)} + \Delta\alpha^i_{(h)} \le \alpha^{max}_{(h)} - \Phi^{-1}(1-\varepsilon) \parallel \Sigma_W^{\frac{1}{2}} S^i_{W(h,\cdot)} \parallel_2 \quad (2\text{-}52)$$

$$\alpha_{(h)} + \Delta\alpha^i_{(h)} \ge \alpha^{min}_{(h)} + \Phi^{-1}(1-\varepsilon) \parallel \Sigma_W^{\frac{1}{2}} S^i_{W(h,\cdot)} \parallel_2 \quad (2\text{-}53)$$

$$\Delta\alpha^i_{(i)} = -\alpha_{(i)} \quad (2\text{-}54)$$

$$s^i_{W(i)} = 0 \quad (2\text{-}55)$$

$$A^i_{L(l,\cdot)}\left(M_G\left(P_G + \Delta P^i_G\right) + M_W P^f_W + M_{DC}\left(P_{DC} + \Delta P^i_{DC}\right) - M_L P_L + B_\alpha \alpha^i\right) + b_L \alpha^i \quad (2\text{-}56)$$
$$\le P^{max}_{L(l)} - \Phi^{-1}(1-\varepsilon) \parallel \Sigma_W^{\frac{1}{2}}\left(A_{L(l,\cdot)}\left(M_G D^i_W - M_W + M_{DC} H^i_W + B_\alpha S^i_W\right) + b_{L(l,\cdot)} S^i_W\right) \parallel_2,$$

$$A^i_{L(l,\cdot)}\left(M_G\left(P_G + \Delta P^i_G\right) + M_W P^f_W + M_{DC}\left(P_{DC} + \Delta P^i_{DC}\right) - M_L P_L + B_\alpha \alpha^i\right) + b_L \alpha^i \ge \quad (2\text{-}57)$$
$$-P^{max}_{L(l)} + \Phi^{-1}(1-\varepsilon) \parallel \Sigma_W^{\frac{1}{2}}\left(A_{L(l,\cdot)}\left(M_G D^i_W - M_W + M_{DC} H^i_W + B_\alpha S^i_W\right) + b_{L(l,\cdot)} S^i_W\right) \parallel_2$$

Eq. (2-34) is the objective function, reflecting the costs of both the scheduled dispatch and the reserves, and (2-35) is the power balance constraint. Eqs. (2-36) - (2-45) are generation constraints, while (2-46) - (2-51) are related to the HVDC connections. Eqs.(2-52) - (2-55) are PST constraints, (2-56) and (2-57) are the transmission line constraints.

All equations hold for all generators, HVDC connections, PSTs and transmission lines, respectively, and must be enforced for all operating conditions i.

Note that the problem (2-1) - (2-57) is a Second-Order Cone Program (SOCP) if the variables D_W, S_W or H_W are optimisation variables. An SOCP is convex. Efficient solution algorithms are available, although it is computationally more complex to solve than a linear program.

2.3 Uncertainty margins

Note that all constraints that were originally formulated as chance constraints contain the term $\Phi^{-1}(1-\varepsilon) \cdot \| \Sigma_W^{1/2} a(x) \|_2$. Comparing the constraints to their deterministic counterparts (obtained by setting both the fluctuations from the single wind in-feeds δP_W, and the fluctuations from the overall wind deviation ΔP_W to zero), this term represents a tightening of the constraint, leading to a smaller feasible domain.

This tightening can be interpreted as the security margin which is necessary to secure the system against uncertainty, from now on called the *uncertainty margin*.

Note that the uncertainty margins of the problem (2-34) - (2-57) depend on the choice of the decision variables. This is a difference to the original problem formulation presented in Deliverable D4.2, where the uncertainty margins were fixed and could be precalculated before the optimisation started. By including optimisation variables in the uncertainty margins, two things happen:

- The uncertainty margins are no longer fixed, but can be optimised along with the rest of the problem. In this way, it is possible to reduce the necessary uncertainty margin on congested lines, which leads to a lower cost solution.
- The optimisation problem becomes more complex, since the reformulated chance constraints are no longer linear, but second-order cone constraints.

In the case study, we will investigate the saving potential related to optimised uncertainty margins, to better understand the trade-off between problem complexity and cost reduction.

2.4 Case study

The main objective of this case study is to investigate how corrective control actions for forecast deviations – allowing controls such as HVDC and PST to react to forecast errors – can help to reduce the cost of renewables integration. In particular, we will investigate how this type of control can help us optimise the uncertainty margins.

As presented in [4], [2], the need to secure the system against outages and forecast errors increases operational cost. The cost increase related to securing the system against outages (i.e., the costs arising from enforcing the N-1 constraints) can be quantified as the cost difference between two OPFs with/without security constraints. The cost increase related to securing the system against forecast errors (i.e., the cost increase incurred by the introduction of an uncertainty margin) can be quantified as the cost difference between a deterministic/probabilistic OPF.

Previous studies [3] have shown that post-contingency corrective control can reduce the cost of security. In the above section, we have introduced an OPF formulation with *post-uncertainty corrective control actions* from HVDC and PSTs, by allowing them to act against wind power deviations using h_W and s_W. The aim is that post-uncertainty corrective control will decrease the cost of uncertainty, just as post-contingency corrective control decrease the cost of security.

In this section, we assess the quantitative impact of post-uncertainty corrective control from HVDC and PSTs on uncertainty margins and cost-of-uncertainty. Since we are mainly concerned with the cost of uncertainty (and not with the cost of security, which has been studied before), the case study does not consider any security constraints (i.e., we only consider $i = 0$) for the sake of clarity of the results. We also omit the index i in the notation (corresponding to the operating condition of the system), since $i = 0$ in all cases.

The balancing power provided by the generators, represented through the distribution vector d_W, can also be seen as a post-contingency corrective control. In previous work [1], [2], we assumed that d_W was fixed. The impact of corrective control from HVDC and PSTs is therefore compared to the impact of a more flexible use of reserves, where d_W is introduced as an optimisation variable as in [7]. Introducing such flexibility implies that the reserves can be deployed based on their location in the system, meaning that they can be used not only for balancing, but also for congestion management. To assess only the impact of the location of reserves in the system, we assume that the available reserve capacities P_G^+, P_G^- have already been fixed through a longer term auction, and that we are only optimising how to used the already allocated reserve capacities (i.e., optimising d_W).

2.4.1 Test system

We consider the IEEE 118 bus system, as described in the Appendix. The following modifications are made:

- The system is divided into three zones as seen in Figure 1.

- The transfer capacities of the transmission lines is decreased to 75% of the original capacity.
- The load is increased by 150% of the original system load in zone 1 and 2, and is increased by 200 % in zone 3.
- The generation capacity of all generators is increased by 300%, and the available reserves capacities for both up and down reserves are 15% of the available capacity.

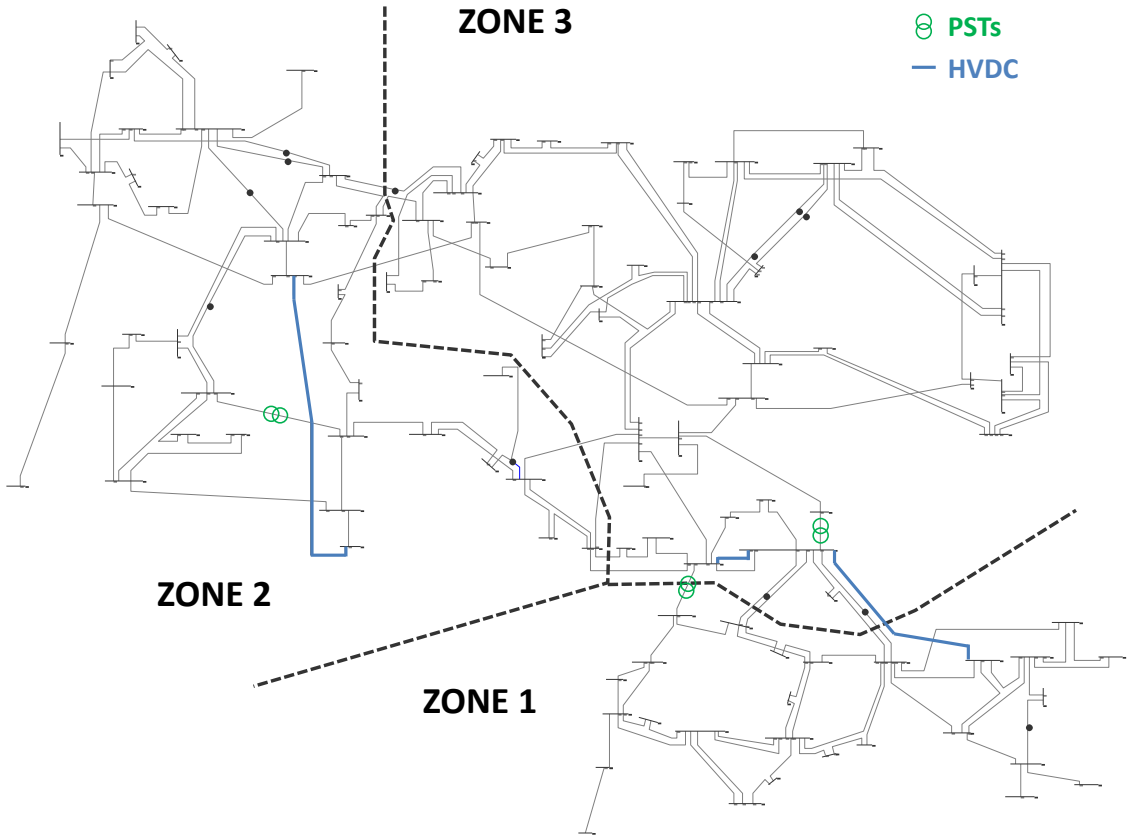

Figure 1: IEEE 118 bus system split into three zones, with additional PSTs and HVDC connections.

2.4.1.1 Forecast uncertainty

In this case study, we assume that the systems loads can be interpreted as a mix between load and renewables connected at a lower voltage level. Instead of considering that particular wind in-feeds are uncertain, we assume that all loads (connected to 91 of the 118 buses) have a forecast error. The forecast errors are normally distributed, and that the standard deviation of each load is equal to 20% of the forecast. Further, it is assumed that the forecast errors are uncorrelated, although the method can include correlation between forecast errors.

2.4.1.2 Reserves

We assume that all generators are providing up and down reserves P_G^+, P_G^- on top of their maximum capacities. We define the available reserves based on the maximum capacity of each generators, such that

$$P_G^+ = P_G^- = 0.15 \cdot P_G^{max} \ . \tag{2-58}$$

In the cases where the activation of reserves is not optimised, we assume that each generator participates (i.e., provides balancing energy) according to it's maximum capacity. The compensation vector for these cases, where d_W is fixed, is given by

$$d_W = P_G^{max} / \sum_g P_{G(g)}^{max} \ . \tag{2-59}$$

2.4.1.3 Phase shifting transformers

We assume that there are three PSTs in the system, installed in lines 41, 95 and 128 (as marked in Figure 1.The minimum and maximum phase shift is $-30°$ to $+30°$.

2.4.1.4 HVDC connections

The HVDC connections and their corresponding transfer capacities are listed in Table 1, and shown in Figure 1. Note that the capacity of HVDC was chosen equal to the capacity of the lines they replace, and that the new line is deliberately chosen to have a relatively small capacity (only 100 MW) to not introduce too much new capacity in the system.

Table 1: HVDC connections and their capacity.

HVDC #	From Bus	To Bus	Replacing Line	Capacity [MW]
1	26	77	38	375
2	30	80	123	375
3	62	81	-	100

2.4.2 Investigations

In the following, we investigate how flexible use of reserves for balancing, HVDC lines and PSTs can be used to handle uncertain variables in the system, and compare them with each other. For each type of flexibility (reserves, HVDC and PST) we consider four cases:

1. No consideration of uncertainty
2. No use of reserves/HVDC/PST to handle uncertainty (except pro rata activation of balancing energy)

3. Optimised reaction of reserves/HVDC/PST to the uncertainty, based on the overall power mismatch in the system
4. Optimised reaction of reserves/HVDC/PST to the uncertainty, based on local measurements of the forecast deviations.

In total, we have 12 different cases, which are listed in Table 2.

Table :2 Simulated cases.

Case	Uncertainty	d_W	P_{DC}	h_W	a_0	s_W
R1	-	-	-	-	-	-
R2	Yes	Defined based on (2-59)	-	-	-	-
R3	Yes	Optimised based on overall power mismatch	-	-	-	-
R4	Yes	Optimised based on locational signal	-	-	-	-
H1	-	-	Yes	-	-	-
H2	Yes	Defined based on (2-59)	Yes	-	-	-
H3	Yes	Defined based on (2-59)	Yes	Optimised based on overall power mismatch	-	-
H4	Yes	Defined based on (2-59)	Yes	Optimised based on locational signal	-	-
P1	-	-	-	-	Yes	-
P2	Yes	Defined based on (2-59)	-	-	Yes	-
P3	Yes	Defined based on (2-59)	-	-	Yes	Optimised based on overall power mismatch
P4	Yes	Defined based on (2-59)	-	-	Yes	Optimised based on locational signal

2.4.3 Results

The cases are compared based on the generation cost of the dispatch. We then explain the cost differences based on the uncertainty margins, and show how the flexibility of the reserves, HVDC lines and PSTs are used to obtain the lowest possible cost.

2.4.3.1 Generation cost

The generation cost of the 12 different cases can be seen in Figure 2.

The results are grouped in three plots, where the left plot shows the costs for a dispatch with flexible reserves, the middle plot shows the costs with HVDC and the right plot shows the costs with PSTs in the system. All costs are normalised by cost which is obtained running an OPF without consideration of uncertainty, HVDC and PSTs (case R1). Note that the plots are zoomed in (i.e., the y-axis starts at 0.98 rather than at zero).

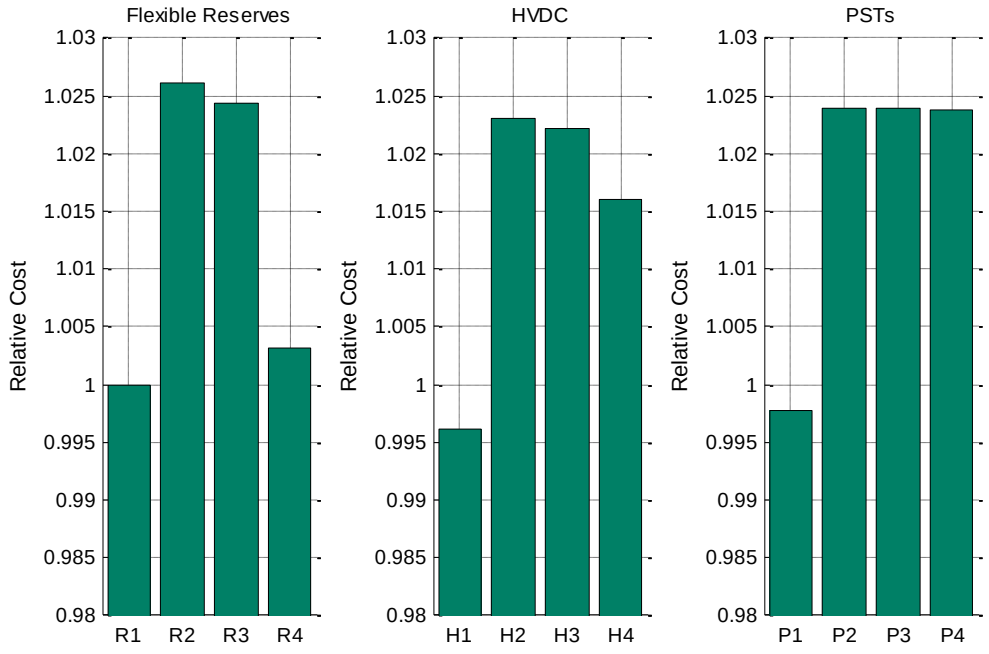

Figure 2: Cost of generation dispatch obtained with flexible reserves, HVDC lines and PSTs as described in Table :2. The costs are normalised be the cost of the OPF without uncertainty or HVDC/PSTs (case R1). Note that the y-axis is cropped and starts at 0.98, not at zero.

For both reserves, HVDC lines and PSTs, the case without consideration of uncertainty (the left bar in each subplot) has the lowest cost. The cost is lower when an HVDC or a PST is in the system, due to the additional flexibility this brings to increase and control the power flows. When we introduce uncertainty to the problem, the cost increases by approximately 2.5% for both reserves, HVDC lines and PSTs (cost difference between the first and the second bar in each subplot). If more flexibility to handle the uncertainty is introduced, i.e. if d_W, h_W or s_W are included and can be optimised, the cost of uncertainty is decreased (third and fourth bar in each subplot). Although the benefit of including

d_W, h_W and s_W is different for reserves, HVDC lines and PSTs, the cost is always lower if we optimise based on a locational mismatch (the fourth bar in each subplot).

As explained above, accounting for uncertainty in the optimisation problem leads to a tightening of the constraints, i.e., to the introduction of an uncertainty margin. Because of this margin, the cost increases. This uncertainty margin is a function of d_W, h_W and s_W. In the cases R2, H2 and P2, the uncertainty margin is the same, since d_W is fixed and h_W and s_W are not introduced. Therefore, the cost of uncertainty (cost increase from the first to the second bar) is approximately the same in all cases, namely 2.5%.

By introducing d_W, h_W and s_W as optimisation variables, we are able to influence the uncertainty margins. By reducing the margins on congested lines (while possibly increasing them at other lines), we can reduce the overall amount of congestion and thus reduce generation cost. The congested lines in the R1 case are seen in Figure 3 where three particularly interesting lines 96, 97 and 104 are labelled. These lines are important for the transfer of power from the cheap generators in zone 1 and 2 to the main load center in zone 3, and are congested. In Figure 4 the uncertainty margins for those three lines are shown for all 12 cases. In the cases where the uncertainty is not considered (R1, H1 and P1), the uncertainty margins are zero, while they are highest in the cases where the uncertainty margins are not optimised (R2, H2 and P2). When we optimise based on the overall power mismatch, a small reduction in the margins can be seen (R3, H3 and P3). The reduction is relatively small because the overall power mismatch does not contain a lot of information, so the controls have to “guess” where the mismatch takes place and how they should react. The uncertainty margins are smallest when they are optimised based on a localised deviation signal (R4, H4 and P4), because the controls can react to each uncertainty source separately. Because congestion is location dependent, such an approach can reduce congestion more effectively.

Introducing more flexible reserves has the highest potential to reduce the cost. This is reasonable, as there are many generators in the system compared to the number of HVDC and PSTs (54 generators compared to 3 HVDC and 3 PSTs). It seems like the HVDC is more effective than the PST in reducing the uncertainty margins and thus the cost of uncertainty. However, this result is case dependent and might be different for other systems.

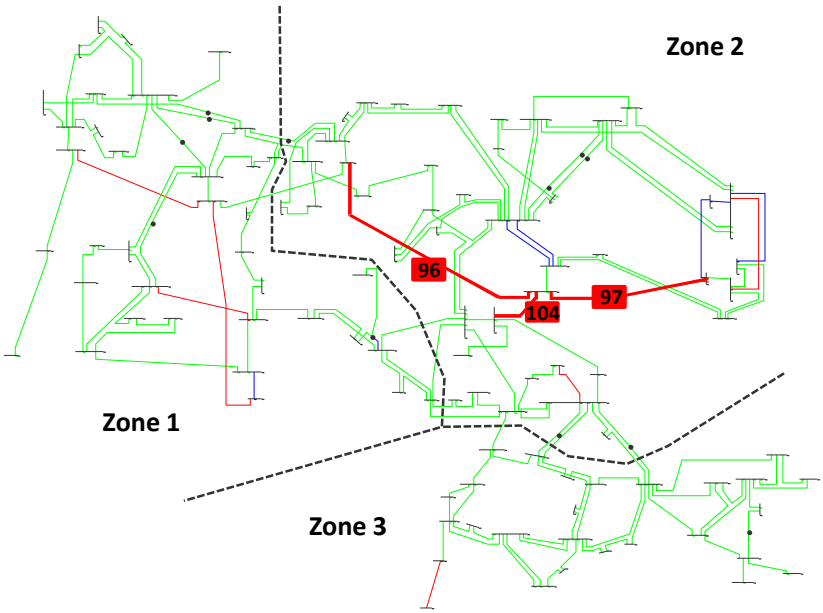

Figure 3: IEEE 118 bus system with line loadings from case R1, with markings of the lines 96, 97 and 104. Green: Loading < 90%. Blue: Loading 90-99.9%. Red: Loading > 99.9%.

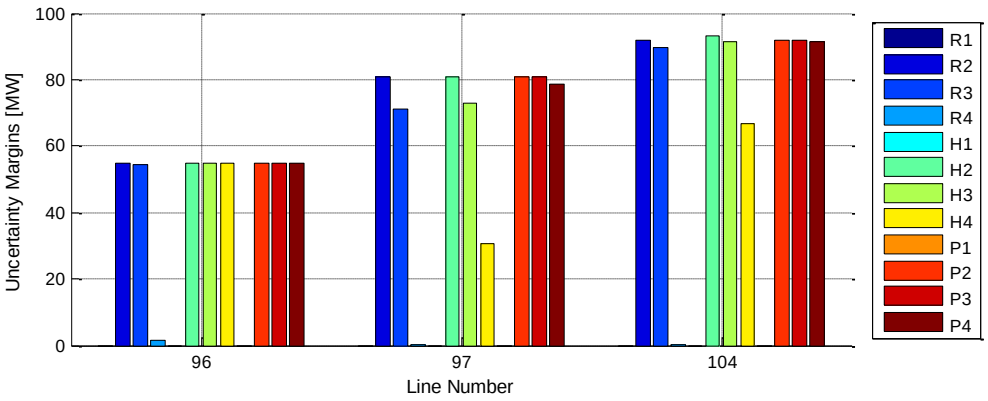

Figure 4: Uncertainty margins for lines 96, 97 and 104 for the twelve different cases. When uncertainty is not considered in the optimisation (R1, H1 and P1), the uncertainty margins are zero. When compared to Figure 2, it is seen that the cases with smaller uncertainty margins (e.g., due to flexible use of reserves, HVDC and PSTs) have lower generation cost.

How the generators react to the uncertainties is given through the entries of d_W, which are defined such that each deviation is balanced exactly by the other generators (i.e., each column of d_W, whether d_W is a vector as in R2, R3 or a matrix D_W as in R4, sums to one). In Figure 5 the entries of d_W and D_W are plotted. On the left (R2), the pro rata activation of reserves is plotted, and it is seen that each generator contributes a small amount. Further right (R3), the optimised d_W based on the overall generation mismatch is shown, and it is seen that generator 24 contributes more significantly to the balancing. Finally, to the right

(R4), d_W is plotted for the case where each generator reacts separately to each forecast deviation. In this case, d_W is a matrix with $N_G \times N_W$ entries. It is seen that for most buses, there are a few generators that contribute most of the balancing power, while most of the other generators contributes very little. Moreover, the buses that are located close to each other are typically balanced by the same generators. This means that an aggregated signal representing the power mismatch from buses in a particular region might also be able to achieve a similar reduction in cost as the signal based on the power mismatch at each bus.

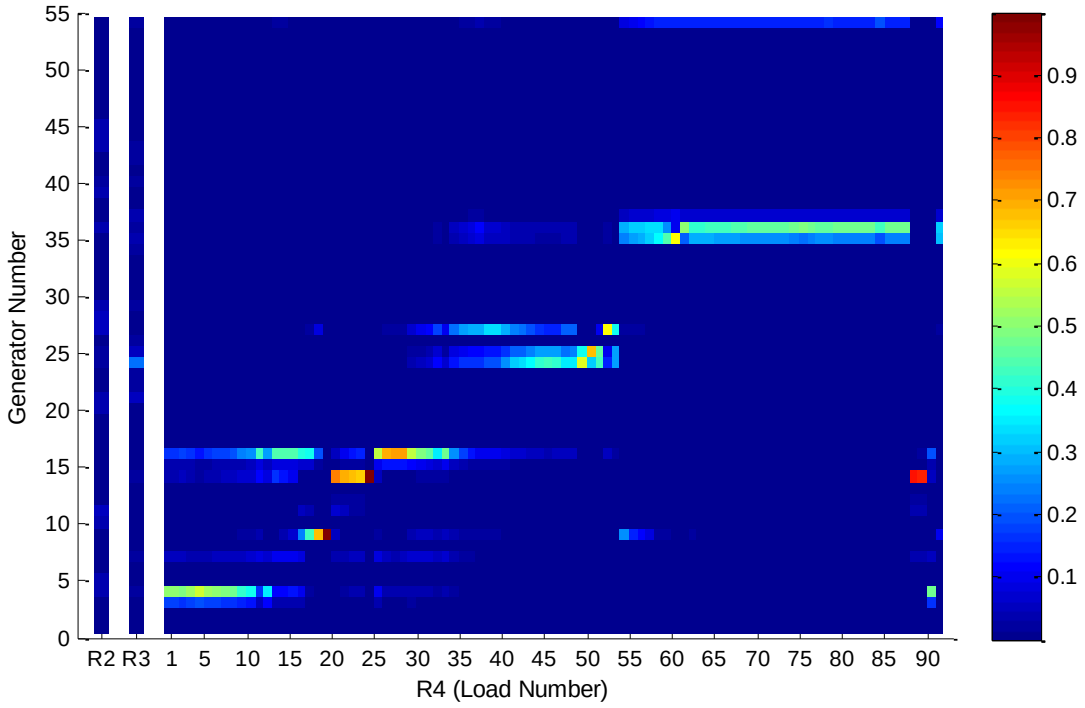

Figure 5: Balancing vector d_W for the cases R2 and R3 (left) where the generators react to the overall power mismatch only, and balancing entries for the balancing matrix d_W (right), where the generators react to each uncertain in-feed separately. The sum for all entries in each column is one to ensure that the system is always balanced.

Similar plots as Figure 5 can be made for h_W (HVDC) and s_W (PST), for the cases based on overall power mismatch and locational power mismatch (H3, H4 and P3, P4). These plots are seen in Figure 6. For h_W and s_W, the entries are not obliged to sum up to any given number, meaning that the HVDC and PST can react as less or more dependent on how large their influence is in the congestion. When h_W and s_W are optimised considering only the overall power mismatch (H3 and P3, to the left), the entries are very small, meaning that not much can be gained by adjusting the power flow on the HVDC or the phase angle of the PST. However, when h_W and s_W are allowed to react to the individual power mismatches (H4 and P4, entries to the right), the entries are much larger, meaning the reaction from the HVDC and the PSTs to the power mismatches are much more significant.

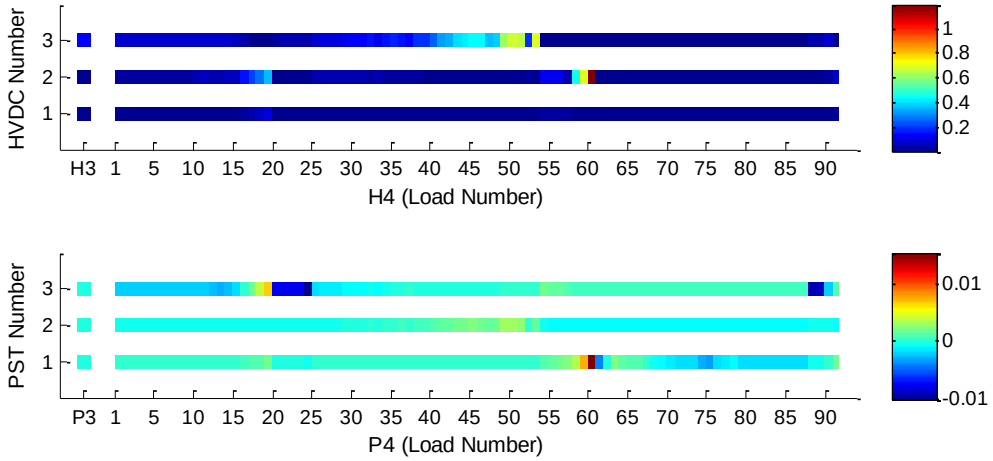

Figure 6: When the HVDC and the PST can react to individual forecast deviations, their reaction is larger. This is seen by comparing the reaction in the left part (which is cloase to zero) to the reaction in the right part (which has a higher absolute value). Upper part (HVDC): The entries of the vector h_W for the case H3 (where the HVDC reacts to the overall power mismatch only), and the entries of the matrix h_W for the case H4 (where the HVDC reacts to each uncertain in-feed separately). Lower part (PST): The entries of the vector h_W for the case H3 (where the HVDC reacts to the overall power mismatch only), and the entries of the matrix h_W for the case H4 (where the HVDC reacts to each uncertain in-feed separately).

This effect is also seen in Figure 7 where the scheduled power flows P_{DC} and the uncertainty margins of the HVDC are shown, and Figure 8, there the scheduled phase angle and the uncertainty margin of the PSTs are shown. Interestingly, in the H4 case, the scheduled power flow P_{DC} is lower than in the other cases, while the uncertainty margins are larger. This is particularly clear for the third HVDC connection, where the scheduled power flow is close to zero and the uncertainty margin is “using” the full capacity of the line. The same tendency is seen for the PSTs in Figure 8. In the P4 case, all PSTs have scheduled angles close to zero and very large uncertainty margins. This means that in this case, both HVDC and PSTs lower the operational cost not by increasing transfer capacity in the nominal case (when no deviation occurs), but rather by reducing the uncertainty margins and allowing for a better handling of the forecast deviations.

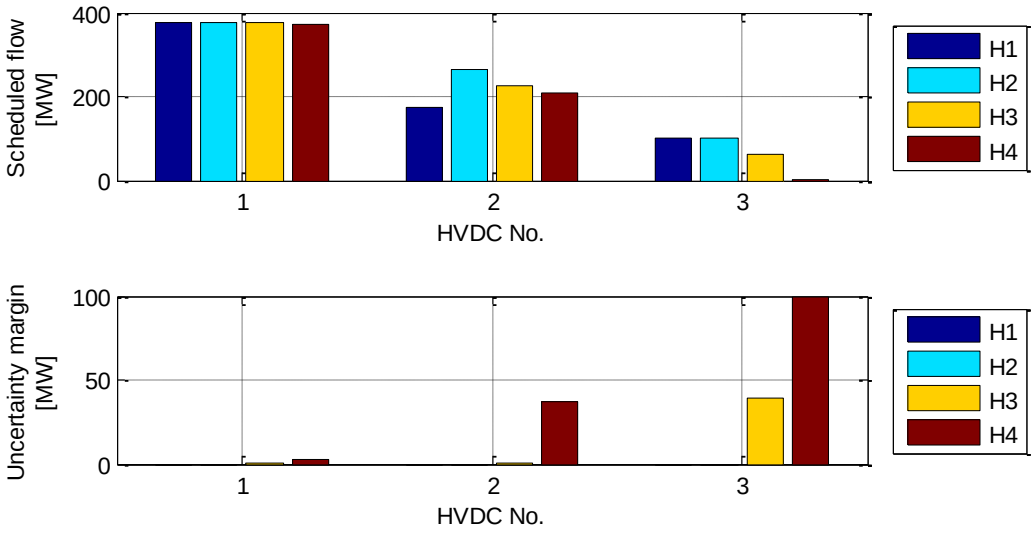

Figure 7: Scheduled power flow P_{DC} and necessary uncertainty margins $R_{DC}^{+/-}$ for the HVDC connections.

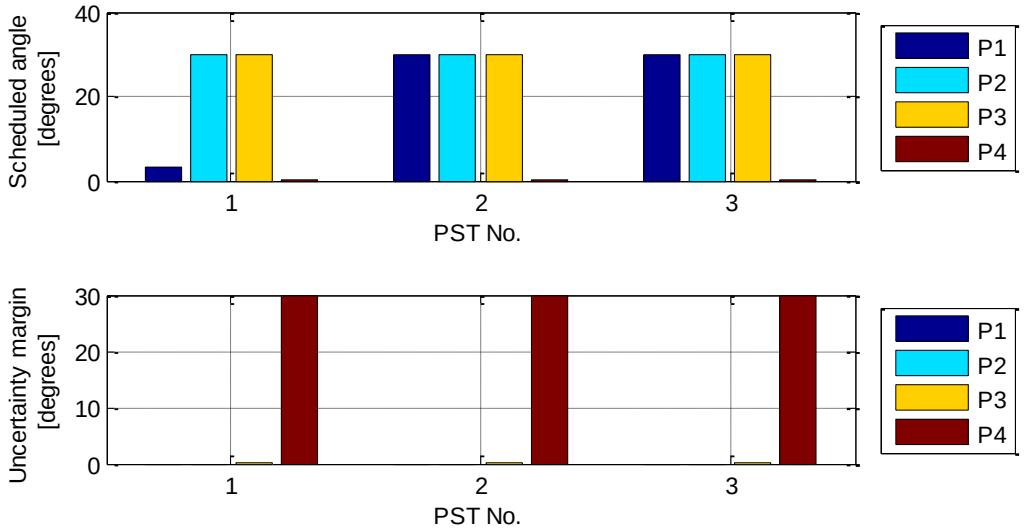

Figure 8: Scheduled angle and uncertainty margins for the PSTs.

2.5 Summary and conclusions

In this chapter, a method to integrate the flexibility from reserves, HVDC and PSTs in a probabilistic OPF formulation have been shown. The method extends current formulations in two ways. First, corrective actions acting to mitigate the effect of forecast deviations are introduced for reserves, HVDC and PSTs. Second, the corrective actions are made dependent not only on the overall power mismatch in the system (the net forecast

deviations), but on the forecast deviations of the separate uncertain in-feeds. This allows the controls to act locally and to reduce congestion to a larger extent.

In the case study, it was seen that the OPF based on locational signals from the separate uncertainty sources leads to a significant reduction in the cost of uncertainty. The most effective measure appears to be a more flexible use of the reserves.

Interestingly, the use of HVDC and PSTs to handle uncertainty leads to a situation where the scheduled setting is close to zero, and most of the capacity (power flow or angle change) is used to react to forecast deviations. This is an interesting result, since it indicates that HVDC and PSTs might have an important role in handling uncertain in-feeds. In the future, those devices and particularly their effect on uncertainty should be accounted for in the scheduling process.

3 Evaluation of Market Designs

The choice of market design has an impact on both operational cost and security in the system. Here, we assess how two different market designs react in presence of uncertainty, a central dispatch system and a self-dispatch system. Further, we will look into how the use of balancing and redispatch can be used to handle congestions that are induced by changes in the generation schedule due to, e.g., forecast uncertainty related to the power in-feeds from RES.

The chapter is divided in two parts. First, we introduce the modelling of the balancing reserves and redispatch actions, and the modelling of the central and self-dispatch systems, before we formulate the corresponding OPF problems. Second, we present a case study where the two market designs are illustrated. We also investigate how the option to do redispatch in both day-ahead and real-time operation affects the OPF solution. Note that we formulate the problem without consideration of outages of lines or generators, but focus only on disturbances due to forecast uncertainty (i.e., deviations from the schedule due to RES forecast errors or intraday trading).

3.1 Balancing and redispatch

In this section, the modelling of balancing energy and redispatch is described.

3.1.1 Balancing energy from reserves

Balancing energy provided by the primary, secondary and tertiary reserves are used to keep the power balance in the system during disturbances (as described in Chapter 2). In order to keep the system balanced, it is important to ensure that any deviation from the (balanced) generation schedule is compensated by the corresponding amount of power from another generation source. As an example, if the wind energy production is *higher* than the forecasted wind production, the generators will be asked to *decrease* their output. On the other hand, if the wind energy production is *lower* than the forecasted wind production, the generators will be asked to *increase* their output.

As described in Chapter 2, we can model the decrease or increase in generation output from each generator depending either on the overall power mismatch introduced by the forecast deviations, ΔP_W, or on the forecast deviation of the different uncertain in-feeds, δP_W.

If the balancing depends on the mismatch of the different uncertain in-feeds δP_W, we can model the reaction of the generators through a balancing matrix $D_W^i \in R^{N_G \times N_W}$, which is subject to the following constraints

$$\Sigma_j D_{W(j,l)} = 1, \quad \forall \text{ columns } l \qquad \text{and} \qquad D_W \geq 0. \tag{3-1}$$

If the balancing depends only on the overall mismatch ΔP_W, the amount of increase/ decrease can be defined through a balancing vector $d_W \in R^{N_G}$, which is defined subject to the following constraints:

$$\Sigma_j d_{W(j)} = 1 \quad \text{and} \quad d_W \geq 0. \tag{3-2}$$

Note that d_W can also be restated to depend on δP_W by setting

$$d_W \Delta P_W = d_W 1^T_{\{1,N_W\}} \delta P_W, \tag{3-3}$$

where the term $d_W 1^T_{\{1,N_W\}}$ has the same dimensions as D_W.

The constraints $D_W \geq 0$, $d_W \geq 0$ ensures that all elements of the balancing vector are larger than zero, meaning that all generators change their output in the same direction (i.e., all generators increase production or all generators decrease production to compensate the deviation of a power plant).

3.1.2 Redispatch

If the market based generation dispatch $P_G \in R^{N_G}$ and the infeed deviation $\delta P_W \in R^{N_W}$leads to violation of operational constraints such as transmission limits of power lines, the TSO needs to take actions to bring the system back within the operational limits. There are different actions available, such as transmission switching or the use of redispatch. Here, we only consider redispatch. Different from balancing energy, which is used to keep the power balance in the system, redispatch is used only to handle congestion. During a redispatch, the power output of one or more generators downstream of a congestion are increased, while the power output of other generators upstream of a congestion are decreased by the same amount. No additional power is produced, it is simply a shift between different generators (such that the overall change in generation sums to zero). This shift in generation does however affect the power flows in the system, and are thus useful to keep power flows within the power limits of the transmission lines.

Redispatch can either be scheduled in the operational planning phase, or be applied during real time operation.

Redispatch scheduled during the operational planning phase

If the market based generation dispatch $P_G \in R^{N_G}$ leads to violation of operational constraints such as transmission limits of power lines, the TSO might want to schedule redispatch already as part of the day-ahead operational planning phase to ensure that the base-case dispatch (based on the forecasted values) can be considered secure. The redispatch scheduled during the operational planning phase is modelled as two vectors $\Delta P_G^+, \Delta P_G^- \in R^{N_G}$, which are subject to the following constraints

$$\Delta P_G^+, \Delta P_G^- \geq 0 \quad \text{and} \quad \sum_g \Delta P^+_{G(g)} - \sum_g \Delta P^-_{G(g)} = 0\ . \tag{3-4}$$

Where the first constraint ensures that both vectors are positive, and the second constraint ensures that redispatch actions sum up to zero. The planned power output of all generators are then given by

$$P_G^{sched} = P_G + \Delta P_G^+ - \Delta P_G^- \tag{3-5}$$

where $P_G \in R^{N_G}$ is the market based generation dispatch.

Redispatch applied during real time operation

During real time operation, additional redispatch can be necessary due to deviations from the planned generation schedule $\delta P_W \in R^{N_W}$, which might occur due to RES forecast errors, load forecast errors or intra-day trading.

Redispatch is per definition locational, i.e., redispatch is always applied at specific locations in the system, since this is the most effective way to reduce congestion. When modelling redispatch as a reaction to a RES deviation, we assume that the generators react based on the deviation of each power plant δP_W. We define a redispatch matrix R_W, similar to the balancing matrix D_W. The matrix $R_W \in R^{N_G \times N_W}$ is subject to the following constraint

$$\sum_g R_{W(g,l)} = 0 \qquad \forall \text{ columns l}, \tag{3-6}$$

which ensures that the redispatch does not affect the power balance in the system. Note that R_W can contain both positive and negative values (which is necessary if the terms should sum to zero). This means that a RES production which is lower than expected, it will lead to a an increase in production of some generators, and a decrease in production at other generators. This is different from the balancing, which will introduce either an increase or a decrease in all generators.

3.1.3 Generator constraints with balancing and redispatch

When we introduce both balancing and redispatch in the generator constraints, we obtain the following set of constraints:

$$\mathbb{P}\left(P_{G(g)} + \Delta P_{G(g)}^+ - \Delta P_{G(g)}^- + R_{W(g)}\delta P_W \geq P_{G(g)}^{min}\right) \geq 1 - \varepsilon \tag{3-7}$$

$$\mathbb{P}\left(P_{G(g)} + \Delta P_{G(g)}^+ - \Delta P_{G(g)}^- + R_{W(g)}\delta P_W \leq P_{G(g)}^{max}\right) \geq 1 - \varepsilon \tag{3-8}$$

$$-R_{G(g)}^- \geq P_{G(g)}^- \tag{3-9}$$

$$R_{G(g)}^+ \leq P_{G(g)}^+ \tag{3-10}$$

$$\mathbb{P}\left(R_{G(g)}^- \leq D_{W(g,\cdot)}\delta P_W\right) \geq 1 - \varepsilon, \tag{3-11}$$

$$\mathbb{P}\left(D_{W(g,\cdot)}\delta P_W \leq R_{G(g)}^+\right) \geq 1 - \varepsilon, \tag{3-12}$$

The two first constraints ensure that the power generation will stay within the acceptable limits P_G^{min}, P_G^{max}, while the four last constraints ensure that the scheduled reserves of each generator, denoted by R_G^-, R_G^+, stay within the reserves capacities $P_{G(g)}^-, P_{G(g)}^+$which have been procured from each generator (for more information, see Section 2.1.2.2). Note that the balancing energy is taken from the reserve capacities, while redispatch can be done within the "normal" operating range of the generators (i.e., it is not necessary to reserve redispatch capacity apriori).

3.2 Central dispatch and self-dispatch systems

As mentioned above, a simplified representation of the two market types is considered in this part of the deliverable:

- Central dispatch system: The generation dispatch is obtained by solving an OPF (overall cost minimisation) in the day ahead, and any changes to the market during intraday is assumed to be due to RES fluctuations, balancing or redispatch
- Self-dispatch system: The generation dispatch is obtained from a separate market clearing without consideration of the grid. The TSO solves an OPF (minimisation of redispatch volume) based on the market outcome in the day ahead. Any changes to the market during the intraday are assumed to be due to RES fluctuations, balancing or redispatch.

In the following, a more detailed description of the market models is given.

3.2.1 Central dispatch system

In a central dispatch system, the market players submit bids to the TSO. The TSO optimises the dispatch such that the overall operational cost is minimal while all constraints (both related to generating units and transmission system) are met and that the power balance is kept. The OPF problem solved by the TSO is shown below.

Here, we assume that the TSO is solving the OPF some time before real-time (e.g., in the day-ahead planning). The only changes that occur to the dispatch until real time come from the forecast errors from the RES, or from balancing and redispatch from the generators. As in the previous part of the deliverable, we do not consider the cost of reserve procurement (i.e., no cost related to P_G^+, P_G^- or R_G^+, R_G^-).

Balancing energy can be provided either based on the overall power mismatch ΔP_W or on the power mismatch of the different uncertainty sources δP_W, as explained above. For simplicity, we show the equations for a balancing matrix $D_W \in R^{N_G \times N_W}$.

Since the market clearing is done under consideration of transmission constraints, the market based generation dispatch P_G does not require any scheduled redispatch $\Delta P_G^-, \Delta P_G^+$. However, redispatch might be necessary in real time, to ensure that deviations from the scheduled dispatch do not lead to constraint violations, which means that R_W can be non-zero.

The OPF problem for a central dispatch system can thus be written as

$$\min_{P_G, R_W, D_W} \; {c_G}^T P_G \tag{3-13}$$

subject to

$$1^T_{\{1,N_B\}}\left(C_G P_G + C_W P_W^f - C_D P_D\right) = 0 \tag{3-14}$$

$$P_{G(g)} + \Delta P^+_{G(g)} - \Delta P^-_{G(g)} \leq P^{max}_{G(g)} - \Phi^{-1}(1-\varepsilon) \parallel \Sigma_W^{\frac{1}{2}} R_{W(g,\cdot)} \parallel_2 \tag{3-15}$$

$$P_{G(g)} + \Delta P^+_{G(g)} - \Delta P^-_{G(g)} \geq P^{min}_{G(g)} + \Phi^{-1}(1-\varepsilon) \parallel \Sigma_W^{\frac{1}{2}} R_{W(g,\cdot)} \parallel_2 \tag{3-16}$$

$$-R^-_{G(g)} \geq P^-_{G(g)} \tag{3-17}$$

$$R^+_{G(g)} \leq P^+_{G(g)} \tag{3-18}$$

$$0 \leq R^+_{G(g)} - \Phi^{-1}(1-\varepsilon) \parallel \Sigma_W^{\frac{1}{2}} D_{W(g,\cdot)} \parallel_2 \tag{3-19}$$

$$0 \geq R^-_{G(g)} + \Phi^{-1}(1-\varepsilon) \parallel \Sigma_W^{\frac{1}{2}} D_{W(g,\cdot)} \parallel_2 \tag{3-20}$$

$$D_W \geq 0, \tag{3-21}$$

$$\sum_k D_{W(k,l)} = 1, \quad \forall \text{ columns l} \tag{3-22}$$

$$\Delta P^+_G \geq 0, \tag{3-23}$$

$$\Delta P^-_G \geq 0, \tag{3-24}$$

$$\sum_k R_{W(k,l)} = 0, \quad \forall \text{ columns l} \tag{3-25}$$

$$A_{L(l,\cdot)}\left(C_G\left(P_{G(g)} + \Delta P^+_{G(g)} - \Delta P^-_{G(g)}\right) + C_W P_W^f - C_L P_L\right) \tag{3-26}$$
$$\leq P^{max}_{L(l)} - \Phi^{-1}(1-\varepsilon) \parallel \Sigma_W^{\frac{1}{2}} \left(A_{L(l,\cdot)}(C_G(D_W + R_W) - C_W)\right) \parallel_2$$

$$A_{L(l,\cdot)}\left(C_G\left(P_{G(g)} + \Delta P^+_{G(g)} - \Delta P^-_{G(g)}\right) + C_W P_W^f - C_L P_L\right) \tag{3-27}$$
$$\geq -P^{max}_{L(l)} + \Phi^{-1}(1-\varepsilon) \parallel \Sigma_W^{\frac{1}{2}} \left(A_{L(l,\cdot)}(C_G(D_W + R_W) - C_W)\right) \parallel_2$$

Eq. (3-13) is the objective function, reflecting the costs of the scheduled dispatch. Eq. (3-14) is the power balance. The constraints (3-15) - (3-16) are the generator constraints for the planned generation schedule, the constraints (3-17) - (3-20) are related to the balancing power and the constraints (3-21) - (3-25) are related to the definition of the variables. Eq. (3-26) - (3-27) are the line flow constraints.

3.2.2 Self-dispatch system

In a self-dispatch system, the market is cleared without any consideration of transmission constraints (with an exception of trade across international borders). A market based dispatch $\overline{P_G}$ is thus provided to the TSO from the market. Since each market participants is part of a so-called balancing group, which is obliged to present a balanced schedule to the TSO, the initial $\overline{P_G}$ should ensure that the power balance constraint is met. The objective of the TSO is to interfere as little as possible with the market based dispatch, while ensuring that no operational limits in the system are violated (e.g., transmission constraints) and by introducing as little cost as possible.

As for the central dispatch system, we assume that the TSO solves an OPF problem some time before real-time (e.g., in the day-ahead planning). The only changes that occur to the dispatch until real time come from the forecast errors from the RES, or from balancing and redispatch from the generators. As in the previous part of the deliverable, we do not consider the cost of reserve procurement (i.e., no cost related to P_G^+, P_G^- or R_G^+, R_G^-).

The cost in a self-dispatch market depends on the dispatch created by the market P_G. This market based dispatch was obtained without consideration of the transmission constraints. Therefore, such an approach might require redispatch measures $\Delta P_G^-, \Delta P_G^+$ already in the planning phase. In addition, further redispatch measures might be necessary in real time, to ensure that deviations from the scheduled dispatch do not lead to constraint violations, which means that R_W can be non-zero.

Balancing energy can be provided either based on the overall power mismatch ΔP_W or on the power mismatch of the different uncertainty sources δP_W, as explained above. For simplicity, we show the equations for a balancing matrix $D_W \in R^{N_G \times N_W}$.

The OPF problem for a self-dispatch system (after reformulation of the chance constraints, see Section 2.1.7) can thus be formulated as:

$$\min_{\Delta P_G^+, \Delta P_G^-, R_W, D_W} \; {c_G}^T P_G + c_R(\Delta P_G^+ + \Delta P_G^-) \tag{3-28}$$

subject to

$$1_{\{1,N_B\}}^T \left(C_G P_G + C_W P_W^f - C_D P_D\right) = 0 \tag{3-29}$$

$$P_{G(g)} + \Delta P_{G(g)}^+ - \Delta P_{G(g)}^- \leq P_{G(g)}^{max} - \Phi^{-1}(1-\varepsilon) \parallel \Sigma_W^{\frac{1}{2}} R_{W(g,\cdot)} \parallel_2 \tag{3-30}$$

$$P_{G(g)} + \Delta P_{G(g)}^+ - \Delta P_{G(g)}^- \geq P_{G(g)}^{min} + \Phi^{-1}(1-\varepsilon) \parallel \Sigma_W^{\frac{1}{2}} R_{W(g,\cdot)} \parallel_2 \tag{3-31}$$

$$-R_{G(g)}^- \geq P_{G(g)}^- \tag{3-32}$$

$$R_{G(g)}^+ \leq P_{G(g)}^+ \tag{3-33}$$

$$0 \leq R^{+}_{G(g)} - \Phi^{-1}(1-\varepsilon) \parallel \Sigma_W^{\frac{1}{2}} D_{W(g,\cdot)} \parallel_2 \tag{3-34}$$

$$0 \geq R^{-}_{G(g)} + \Phi^{-1}(1-\varepsilon) \parallel \Sigma_W^{\frac{1}{2}} D_{W(g,\cdot)} \parallel_2 \tag{3-35}$$

$$D_W \geq 0, \tag{3-36}$$

$$\sum_k D_{W(k,l)} = 1, \quad \forall \text{ columns l} \tag{3-37}$$

$$\Delta P^{+}_{G} \geq 0, \tag{3-38}$$

$$\Delta P^{-}_{G} \geq 0, \tag{3-39}$$

$$\sum_k R_{W(k,l)} = 0, \quad \forall \text{ columns l} \tag{3-40}$$

$$A_{L(l,\cdot)}\left(C_G\left(P_{G(g)} + \Delta P^{+}_{G(g)} - \Delta P^{-}_{G(g)}\right) + C_W P^{f}_{W} - C_L P_L\right) \tag{3-41}$$
$$\leq P^{max}_{L(l)} - \Phi^{-1}(1-\varepsilon) \parallel \Sigma_W^{\frac{1}{2}} \left(A_{L(l,\cdot)}(C_G(D_W + R_W) - C_W)\right) \parallel_2$$

$$A_{L(l,\cdot)}\left(C_G\left(P_{G(g)} + \Delta P^{+}_{G(g)} - \Delta P^{-}_{G(g)}\right) + C_W P^{f}_{W} - C_L P_L\right) \tag{3-42}$$
$$\geq -P^{max}_{L(l)} + \Phi^{-1}(1-\varepsilon) \parallel \Sigma_W^{\frac{1}{2}} \left(A_{L(l,\cdot)}(C_G(D_W + R_W) - C_W)\right) \parallel_2$$

Eq. (2-34) is the objective function, reflecting the costs of both the market based dispatch and the redispatch. Note that the market based dispatch P_G is not an optimisation variable, and that the cost component ${c_G}^T P_G$ is a fixed value. This value is only included in the objective to make the result comparable to the outcome of the central dispatch market (where the objective also contains the generation cost). Eq. (2-35) is the power balance. The constraints (2-36) - (3-31) are the generator constraints for the planned generation schedule, the constraints (3-32) - (3-35) are related to the balancing power and the constraints (3-36) - (3-40) are related to the definition of the variables. Eq. (2-56) - (2-57) are the line flow constraints.

3.3 Case study

The objective of this case study is to investigate how the central dispatch and the self-dispatch markets perform in presence of uncertainty, given different rules for how balancing and redispatch can be used.

We first investigate how the central dispatch market performs compared to the self-dispatch market in a system with congestion, and explain the differences. In a second part, we investigate the markets separately, and show how the use of balancing and reserves change the cost of operation.

3.3.1 Test system

We consider the IEEE 118 bus system, as described in the Appendix. The following modifications are made:

- The system is divided into three zones as seen in Figure 9.
- The transfer capacities of the transmission lines is decreased to 75% of the original capacity.
- The load is increased by 150% of the original system load in zone 1 and 2, and is increased by 200 % in zone 3.
- The generation capacity of all generators is increased by 300%, and the available reserves capacities for both up and down reserves are 15% of the available capacity.

3.3.1.1 Forecast uncertainty

All loads (connected to 91 of the 118 buses) are considered to be uncertain, as they are interpreted as a mix between load and renewables connected at a lower voltage level. We assume that the forecast errors are normally distributed, and that the standard deviation of each load is equal to 20% of the forecast. Further, it is assumed that the forecast errors are uncorrelated.

3.3.1.2 Reserves

We assume that all generators are providing up and down reserves P_G^+, P_G^- on top of their maximum capacities. We define the available reserves based on the maximum capacity of each generators, such that

$$P_G^+ = P_G^- = 0.15 \cdot P_G^{max} \ . \tag{3-43}$$

In the cases where the activation of reserves is not optimised, we assume that each generator participates (i.e., provides balancing energy) according to it's maximum capacity. The compensation vector for these cases, where d_W is fixed, is given by

$$d_W = P_G^{max} / \sum_g P_{G(g)}^{max} \ . \tag{3-44}$$

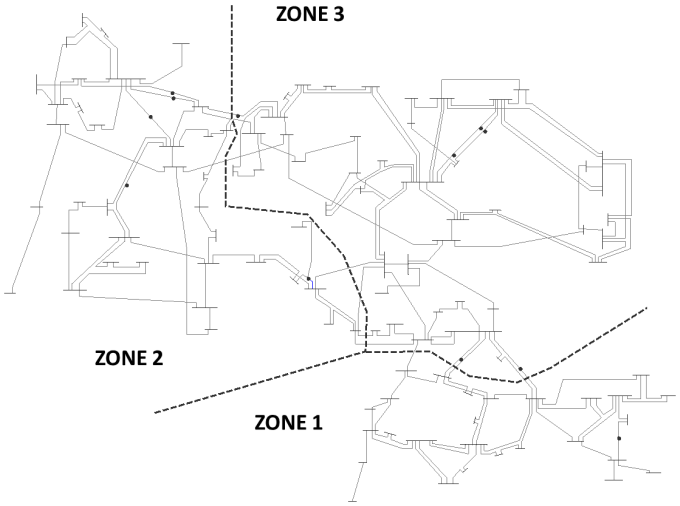

Figure 9: IEEE 118 bus system split into three zones.

3.3.1.3 Redispatch

We assume that all generators have to provide redispatch if they are asked to do so, within their operational limits. The price the TSO has to pay for redispatch is assumed to be 10% higher than the cost which is paid by the market participants, such that

$$c_R = 1.1 \cdot c_G \ . \tag{3-45}$$

In the current formulation, the TSO does not have to pay for the intraday redispatch. To model the cost of the intraday redispatch will be part of future work.

3.3.2 Investigations

As in Chapter X, we investigate four different ways of handling deviations from the forecast within the OPF:

1. No consideration of deviations from the forecast
2. Predefined activation of reserves d_W
3. Optimised reaction of reserves d_W, based on the overall power mismatch in the system ΔP_W
4. Optimised reaction of reserves D_W, based on local measurements of the forecast deviations δP_W.

Redispatch in the operational planning $\Delta P_G^+, \Delta P_G^-$ is included in all cases where a self-dispatch market is optimised, even in the cases where there is no real-time redispatch R_W.

The investigated cases are summarised in Table 3.

Table 3: Investigated cases.

Case	Market type	Uncertainty	Balancing D_W	Redispatch R_W
CD1	Central dispatch	-	-	-
CD2	Central dispatch	Yes	Defined based on (3-44)	-
CD3	Central dispatch	Yes	Optimised based on overall power mismatch	-
CD4	Central dispatch	Yes	Optimised based on locational signal	-
CDRe1	Central dispatch	-	-	-
CDRe2	Central dispatch	Yes	Defined based on (3-44)	Yes
CDRe3	Central dispatch	Yes	Optimised based on overall power mismatch	Yes
CDRe4	Central dispatch	Yes	Optimised based on locational signal	Yes
SD1	Self-dispatch	-	-	-
SD2	Self-dispatch	Yes	Defined based on (3-44)	-
SD3	Self-dispatch	Yes	Optimised based on overall power mismatch	-
SD4	Self-dispatch	Yes	Optimised based on locational signal	-
SDRe1	Self-dispatch	-	-	-
SDRe2	Self-dispatch	Yes	Defined based on (3-44)	Yes
SDRe3	Self-dispatch	Yes	Optimised based on overall power mismatch	Yes
SDRe4	Self-dispatch	Yes	Optimised based on locational signal	Yes

3.3.3 Results

Here, we first compare the central- and the self-dispatch markets to each other, and explain the differences in costs. Then, we compare the two markets designs separately with respect to the effect of redispatch. Finally, we summarise the results and draw some conclusions.

3.3.3.1 Comparison of central-dispatch and self-dispatch market outcome

Before looking into the effect of uncertainty in central-dispatch and self-dispatch systems, we explain the differences between the two market designs, and how the dispatches are obtained. In the following, we compare the central and the self-dispatch markets in the case where no uncertainty is considered (case CD1 and SD1 in Table 1).

In the central dispatch system, the generators are dispatched such that the minimal generation cost is obtained, while the transmission limits are kept. The line loadings that result from the dispatch obtained through the central dispatch market clearing (which is done through an OPF) is shown in Figure 10. It is seen that there are several lines with a line loading of 100%, but no line loadings above this limit. The lines with a loading of 100% are congested, meaning that an increase in the line loading would lead to a shift in generation from a high cost to a low cost generator and thus a decrease in the cost. However, the generation cannot be shifted, because it would lead to the overload of a line.

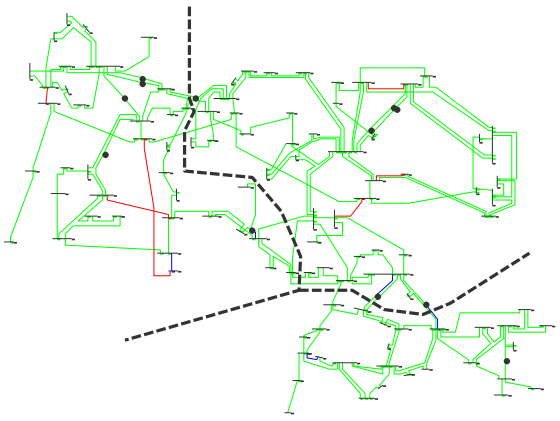

Figure 10: Line loadings throughout the system after the market clearing with the central dispatch system. Green corresponds to line loadings below 90% of the limit, blue corresponds to line loadings between 90-100%, red are line loadings at the limit.

In the self-dispatch system, the market is cleared based only on the generation cost of the generators, without consideration of the transmission constraints. In this case, the market clearing leads to a situation with several line overloads as seen in Figure 11. To avoid those line overloads, redispatch actions are needed. The outcome of the self-dispatch market after redispatch is shown in Figure 12. As for the central dispatch case, there are several lines that have a loading of 100%, but no lines that are overloaded.

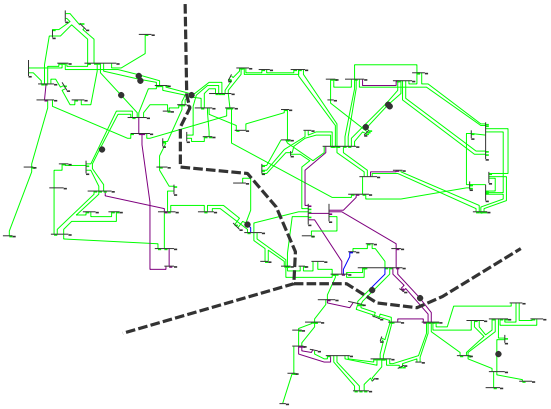

Figure 11: Line loadings throughout the system after the market clearing with the self-dispatch system, before any redispatch actions have been taken. Green corresponds to line loadings below 90% of the limit, blue corresponds to line loadings between 90-100%, red are line loadings at the limit, and purple corresponds to line loadings above 100%.

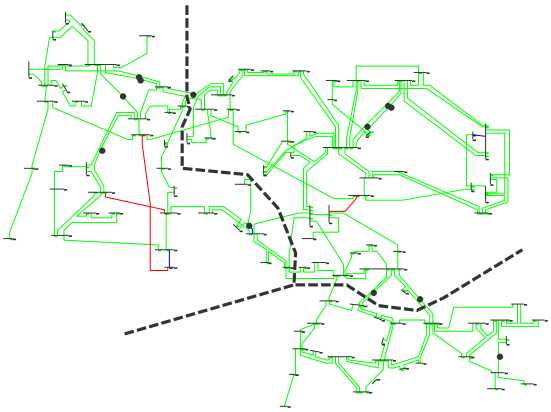

Figure 12: Line loadings throughout the system after the market clearing with the self-dispatch system, before any redispatch actions have been taken. Green corresponds to line loadings below 90% of the limit, blue corresponds to line loadings between 90-100%, red are line loadings at the limit, and purple corresponds to line loadings above 100%.

When comparing the congestions in Figure 12 with the congestions in Figure 10, it is seen that the congestions are similar, but not the same. This means that the dispatch of the self-dispatch system after redispatch is not the same as the dispatch after the central dispatch market clearing. Note that if the system was not congested (i.e., there is enough transmission capacity available such that the cheapest generator can produce without causing any congestions), the central dispatch and the self-dispatch systems should theoretically produce the same outcome. Further, no redispatch actions would be necessary.

In the specific case study we are looking at, there are however several congestions. In the self-dispatch case, the TSO has to implement several redispatch actions to reduce the loading of the lines, which he has to pay for. The result is seen in Figure 13, where the dark blue part of the bar represents the cost of the initial generation dispatch, while the light blue part represents the cost of redispatch actions. Since the central dispatch market considers transmission constraints in the market clearing process, while the self-dispatch market does not, the cost of the initial generation dispatch is higher in the central dispatch market. If we account for the cost of redispatch, the cost of secure operation (i.e., operation without overloads) is however much higher in the self-dispatch case.

The actual cost differences between the central dispatch and the self-dispatch systems are case dependent, and will differ depending on the system, the loading level and the amount of congested lines. However, the central dispatch system will always lead to an overall cost which is lower or equal to the cost of the self-dispatch system. Regardless of how much lower the initial generation cost in the self-dispatch system is, the use of redispatch to reduce the power flow on overloaded lines will always lead to a total cost which is higher

or equal to the cost of the central dispatch system. This is because the central dispatch system does the market clearing under consideration of transmission constraints, such that the cheapest possible generation dispatch (which do not violate any limits) is obtained. If there is no congestion in the system, or the congestion can be handled using zero cost operational means such as transmission switching, PSTs or HVDC, the systems will lead to the same operational cost. Assuming that the generators submit similar bids in the central and the self-dispatch systems and that the remedial actions are available in both cases, the central dispatch system will always lead to a cost which is lower or equal to the self-dispatch system.

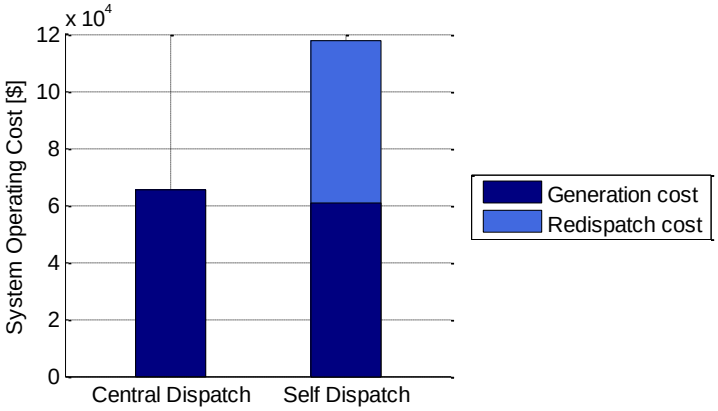

Figure 13: The total cost of the planned generation schedule, including generation cost for the central dispatch market and both generation cost and redisptch for the self-dispatch market.

3.3.3.2 Effect of flexible reserves and real-time redispatch

In the following, we analyze how a flexible use of reserves and modelling of redispatch influences the cost of operation in the central- and self-dispatch markets.

Central dispatch market

In Figure 14, the generation cost obtained with the central dispatch market design is shown. The four groups of bars corresponds to different use of reserves, i.e., different ways of defining d_W or D_W, respectively. Case 1) is the case with no consideration of uncertainty (i.e., the central dispatch case which is also shown in Figure 10). The cost of this dispatch is used as a benchmark cost to normalise the cost in the other cases. Case 2) uses a pre-defined d_W to balance the total power mismatch ΔP_W, while case 3) uses an optimised distribution vector d_W to balance ΔP_W. Case 4) uses an optimised balancing matrix D_W, which balances the power mismatch at each load δP_W separately. The blue and the red bars corresponds to the cases without and with real-time redispatch.

As mentioned in Chapter 2, accounting for uncertainty increases cost, due to the introduction of the uncertainty margins. We denote this cost increase as the cost of uncertainty. It is seen that the more flexible the reserves activation is (the flexibility is increasing from 2) to 3) to 4)), the lower the cost of uncertainty is. If the possibility to do

real-time redispatch (modelled through $R_W \cdot \delta P_W$) is considered, the cost of uncertainty is even lower, and decreases to approximately 0.2%. Note that the redispatch is so effective that it does not matter which model we use for the reserves. This might have changed if there was a cost allocated to keeping generation available to provide redispatch in real time (i.e., a cost related to $R_W \cdot \delta P_W$ for each generator) and an evaluation of the cost of using the redispatch. This should be refined in future work.

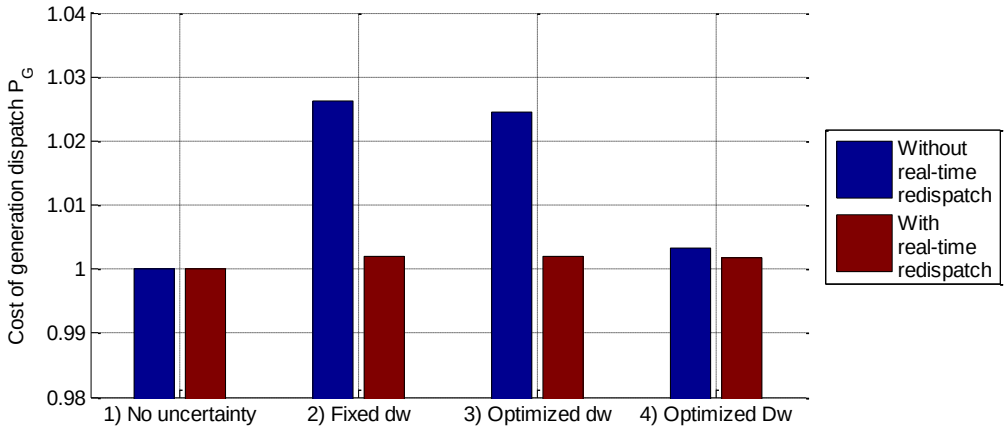

Figure 14: The difference in cost between different central dispatch market designs, normalised by case 1) which neglects the uncertainty. The different cases are defined based on how the uncertainty is handled with reserves and redispatch. The four different cases corresponds to different handling of the uncertainty using reserves, i.e., 1) no uncertainty, 2) fixed reserve activation d_W, 3) optimised reserve activation $d_W$based on the overall power mispatch ΔP_W and 4) optimised reserve activation D_W based on the power mismatch at each bus δP_W. The blue bars corresponds to the cases where no intra-day redispatch can be planned, while the red bars are the cases where intraday redispatch can be planned.

Self-dispatch market

Figure 15 shows the cost of the *redispatch* in the self-dispatch market. The cost of the generation dispatch is the same for all cases, and is thus not included in the comparison. The cases 1), 2), 3) and 4) for the reserve activation are similar to Figure 14 and the blue and red bars correspond to the cases with and without real-time redispatch, respectively. All results are normalised by the redispatch cost in the deterministic case (left), which corresponds to the value of the light blue bar in Figure 13. The cost of uncertainty is much higher in the self-dispatch market compared to the central dispatch market, and reaches more than 15% in the case without real-time redispatch where the reserves are activated according to a fixed balancing vector d_W. The cost of uncertainty is however reduced to less than 2% in the case where the reserves are activated according to the forecast deviations at each bus δP_W. A similar decrease in the cost of uncertainty is seen for all cases with real-time redispatch. Real-time redispatch based on the locational forecast deviation δP_W reduces the cost to around 2% for the Cases 2) and 3), and reduces the cost of uncertainty to almost zero in case 4.

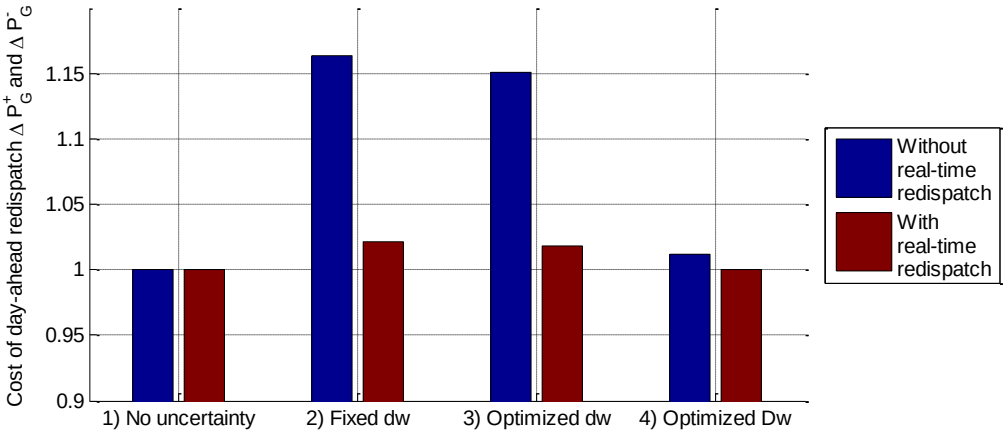

Figure 15: The difference in redispatch cost between different self-dispatch market designs, normalised by case 1) which neglects the uncertainty. The different cases are defined based on how the uncertainty is handled with reserves and redispatch. The four different cases corresponds to different handling of the uncertainty using reserves, i.e., 1) no uncertainty, 2) fixed reserve activation d_W, 3) optimised reserve activation $d_W$based on the overall power mispatch ΔP_W and 4) optimised reserve activation D_W based on the power mismatch at each bus δP_W. The blue bars corresponds to the cases where no intra-day redispatch can be planned, while the red bars are the cases where intraday redispatch can be planned.

3.3.3.3 Discussion

Although the numbers in the above case study are case dependent, some general conclusions can be drawn. The central market design allows for a less costly grid operation, since it accounts for the transmission constraints already in the market clearing process. However, the comparative advantage of the central dispatch market is smaller in systems with less congestions. Further, the comparison between the central dispatch and the self-dispatch systems rely on the assumption that the generators submit the same bids in both markets. If assuming that the bids are the same in both markets, the central dispatch market will always lead to a solution which is as cheap or cheaper than the self-dispatch market.

In the second part of the case study, it was seen that real-time redispatch and more flexible use of reserves can significantly lower the cost of uncertainty. The lowest cost of uncertainty is found when both the reserves and the redispatch can both react to the power mismatch at each bus (i.e., to a locational power mismatch). The most important factor is however whether or not real-time redispatch can be planned. Even in the cases where the reserves act based on the overall power mismatch, introduction of real-time redispatch significantly reduces the cost of uncertainty. In the case study above, the central dispatch system has a lower cost of uncertainty than the self-dispatch system in most cases.

Finally, it should be noted that even though it is assumed that the redispatch is a function of the forecast deviations, which might change continuously, this does not mean that there must be a continuous activation of redispatch. For most cases, it will be possible to wait until the forecast deviations reaches a certain threshold before any redispatch is applied.

When a critical error occurs, the redispatch matrix R_W can be multiplied by the forecast deviations, which will give an indication of which generators that should be used for redispatch.

3.4 Summary and conclusions

In this chapter, we have compared two different market designs, as well as different uses of balancing reserves and redispatch with respect to the their operational cost and the cost of uncertainty. First, we introduce the modelling of the balancing reserves and redispatch actions, and the modelling of the central and self-dispatch systems, before we formulate the corresponding OPF problems. Second, we present a case study for the IEEE 118 bus system, were the differences between a) the different market designs and b) the rules related to the activation of reserves and redispatch are illustrated.

The findings can be summarised as follows: The central dispatch market leads to higher generation cost than the self-dispatch market, but lower overall cost when the cost of redispatch to avoid line overloading is considered for the self-dispatch market. Further, the use of real-time redispatch leads to a significant reduction in operational cost, independent of whether the reserves are activated according to a fixed distribution vector, an optimised activation based on the overall dispatch or on optimised activation based on the local power mismatch at each bus.

4 Probabilistic Overall System Cascading Risk Assessment

In this chapter, a probabilistic method to assess the overall system risk is presented. The chapter is organised as follows. Section 4.1 revisits the method presented in Deliverable D4.2 and gives the enhancements and simplifications which were introduced since then. These enhancements contain the change from an event (branch tripping) based approach to a state based (power system topology after tripping branches) one, and a modification of the “line loading to outage probability”-function to better reflect reality. Further, the ability to handle inter- and intra-zonal correlations was implemented and a few simplifications to reduce the computational effort and feasibility of the method were introduced. The simplifications are the negligence of the manual and automatic redispatch during cascading events and the piecewise discretisation of the branch-loading to branch-outage function.

Section 4.2 is about the implementation of power flow controlling components (PFCCs) into the method. In this work Phase Shifting Transformers (PSTs), High Voltage DC-lines (HVDC lines) and a FACTS device, Thyristor Controlled Series Compensation (TSCS), are modelled to bring more flexibility to the grid. However these elements are assumed to have a fixed set-point during the entire simulation to be set by e.g., an additional optimisation algorithm a priori.

Section 4.3 presents different case studies to show the effect of PFCCs on the system’s power flows and the overall system risk. The first case study is about the different implemented types of PFCCs and their particular effect on the risk. The second one is about controlling strategies of PFCCs being either central or de-central coordinated.

4.1 Method enhancements

The method presented in Deliverable D4.2 was enhanced to provide more valuable results than the risk measure based on a product of outage probabilities, as it was the case in Deliverable D4.2. The here presented method gives a number for the overall system risk by simulating various line outages leading to new system states. The probability to end up in a system state and the value of lost load of it are multiplied to give the outage risk of this single state. During the simulation multiple branch outage combinations – and so system states – are simulated. Scanning all possible branch outage combinations, the sum of all single states’ risks gives the overall system risk. The extensions reach from simplifications, in detail the secondary control and the redispatch method have been omitted for the sake of computation speed and the feasibility of the simulation, to the implementation of correlations between loads and the linearisation of the branch-loading to branch-tripping-probability function.

Neglecting the presence of a secondary frequency control as well as redispatch leads to a tremendous reduction in computational effort. The two-time-horizon implementation presented in Deliverable D4.2 was not needed anymore after the simplification of the

method and so it was modified to solely handle immediate trippings. The mentioned simplifications imply that TSOs wouldn't react during an evolution of a cascade and the outage sequence is faster in time than the secondary control is able to react, leading to a worst case estimation. The primary frequency control is still implemented as well as the frequency estimation described in Deliverable D4.2.

4.1.1 Piecewise linearisation of the branch-loading to branch-tripping-probability function

The relation between loading and tripping probability of a branch was assumed to be a linear function previously (Figure 16). Multiple discussions with Transmission System Operators involved in the project lead to the conclusion that the tripping probability of highly loaded (close to the current protection device limit) equipment is rather exponentially increasing, due to branches tripped by undervoltage detection functions of distance protection relays as well as the non-linear influence of thermal overload causing line sag. Therefore, there are voltage magnitude caused branch-trippings close beneath the current protection limits leading to an increased tripping probability in this region of loading. The range between 100% line loading and the region where the number of voltage caused outages increases is assumed to reflect flashovers due to line sag and malfunction of protection equipment. So the exponential function shown in Figure 17 seems to be a better estimate to reflect the real evolution of the outage probability over the branch utilisation.

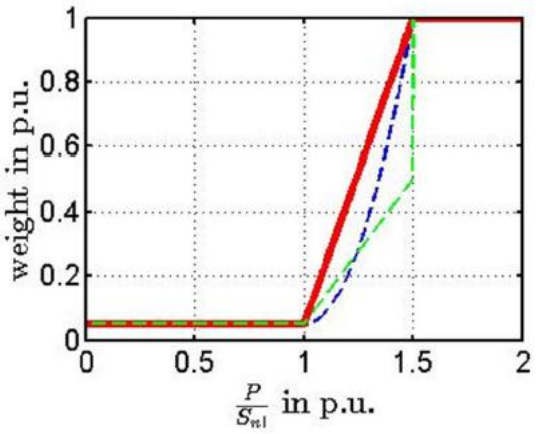

Figure 16: Line outage probability weighting function (Deliverable D4.2).

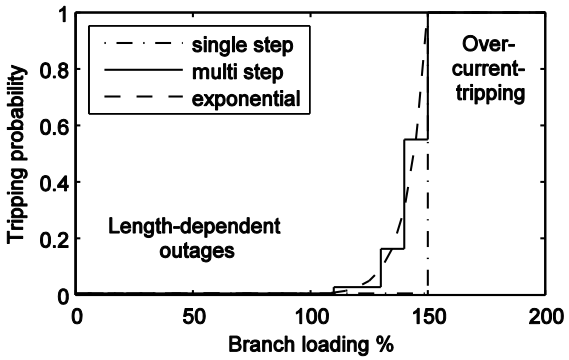

Figure 17: Modified Line outage probability weighting function.

In terms of computational effort it is much more time consuming to multiply a discrete probability density distribution (for each branch of the power system) with a continuous weighting function (4-1) than estimating the weighting function by an e.g., five step approximation (Figure 17) and then weighting ranges of the probability function which can easily be calculated for normal distributions according to Eq. (4-2). The present

implementation of the branch-loading to branch-tripping-probability function is a “multi step” exponential approach shown in Figure 17.

In Eq. (4-1), $\overline{p_{trip,b}}$ denotes the cumulative tripping probability for a given branch b, p_b is the probability of line utilisation according to the probability density function discretisation step i, and p_i is the weighting factor according to the “exponential function” in Figure 17.

$$\overline{p_{trip,b}} = \sum_{i=0}^{P_{max}} p_{b(i)} \cdot p_i. \tag{4-1}$$

Eq. (4-2) gives the simplified calculation method of the tripping probability. ns is the number of discretisation steps of the weighting function, $lsl(i)$ and $usl(i)$ are the steps upper and lower limit, p_b is again the probability for a given power flow, and p_{ns} again means the weighting factor of the particular approximation step.

$$\overline{p_{trip,b}} = \sum_{i=0}^{ns} p_{b(lsl(i)< P \leq usl(i))} \cdot p_{ns(i)}. \tag{4-2}$$

4.1.2 Selection procedure of outage candidates

The selection criterion for the next line to outage was simplified from multiple complex conditionals to only one number, which is the lower limit for a state probability (see Section 4.1.3).

4.1.3 State approach

The approach presented in Deliverable D4.2 by TUG was a type of depth search method finding likely cascades by following their propagation by always tripping the branches showing the highest outage probabilities. One problem of this approach is that the counter probability, reflecting the case that no line would trip and the system will stay in the present state, was neglected. This led to an effect where the method often performed the depth search starting from unlikely system states. To avoid this effect the following enhancement was developed and implemented. In Figure 18 a state graph is shown, consisting of four system states, all defined by a different branch outage combination.

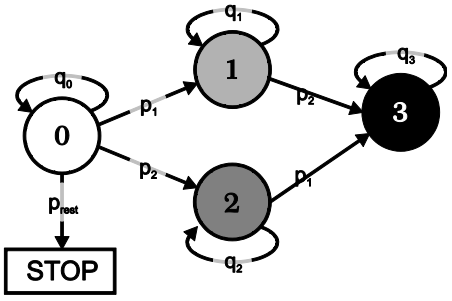

Figure 18: Simple example for the state approach.

In state 0 no branch is on outage so the system's probabilistic power flows can be calculated, according to the probabilistic load flow method presented in Deliverable D4.2. Each branch's tripping probability $\overline{p_{trip,b}}$ is determined according to the branch-loading to branch-outage-probability function presented in Section 4.1.1. By the knowledge of all tripping probabilities the counter probability can be determined by Eq. (4-3) and gives a number for the probability to stay in the actual simulated state. For the sake of simplicity $\overline{p_{trip,b}}$ is substituted by p_b in the following explanation.

$$q = \prod_{b=1}^{nb}(1 - p_b\ ). \tag{4-3}$$

The conditional probability to reach state 1 and stay there can be calculated by Eq. (4-4) where p_{11} is the "reach and stay" probability for state 1, p_1 is the tripping probability of branch 1 and q_1 is the counter probability of state 1 according to Eq.(4-5).

$$p_{11} = p_1 \cdot q_1. \tag{4-4}$$

This counter probability is given by in a generalised way by Eq. (4-5).

$$q_i = \prod_{\substack{b=1 \\ b \neq i}}^{nb}(1 - p_b). \tag{4-5}$$

Now there are multiple possibilities a cascade can propagate. One is that the cascade stops in state 1 (the probability is given by Eq. (4-4)), the other possible evolution is a simultaneously tripping of branch 2 leading to state 3. The probability of the latter case can be calculated by multiplying the tripping probability of branch 1 and branch 2 with the counter probability of state 3. In this example there are two ways to reach state 3 (either branch 1 and 2 or branch 2 and 1 trip coincidental) so the probability has to be divided by two. Another possibility for the evolution of the cascade is that the cascade reaches and stays in state 1 followed from this new system state by an outage of branch 2. The probability for this event can be calculated according to Eq. (4-6) and is called the joint probability of the event "reaching and staying in state 1" and a tripping of branch 2 out of state 1 ($p_{2|1}$). The outage after reaching one state - like in this example - is not illustrated, but it is meant that reaching a given state and staying there gives a new initial case like it was state 0 in the example. Simply the branches in operation differ from initial state to initial state.

$$p_{1\cap 2} = (p_1 \cdot q_1) \cdot p_{2|1}. \tag{4-6}$$

Referring back to the simple example there were two ways to reach state 3 and therefore the "reach and stay" probability was divided by the number of possible simultaneous outages leading to this particular state. For the sake of computational effort the order of outages is not relevant when the cascades stop in the same state. So instead of simulating six cascades to reach all states from 10 to 15 in the extended example shown in Figure 19 it is valid to simulate only one of the combinations leading to the particular state without dividing the resulting state probability by the number of possible tripping combinations [11].

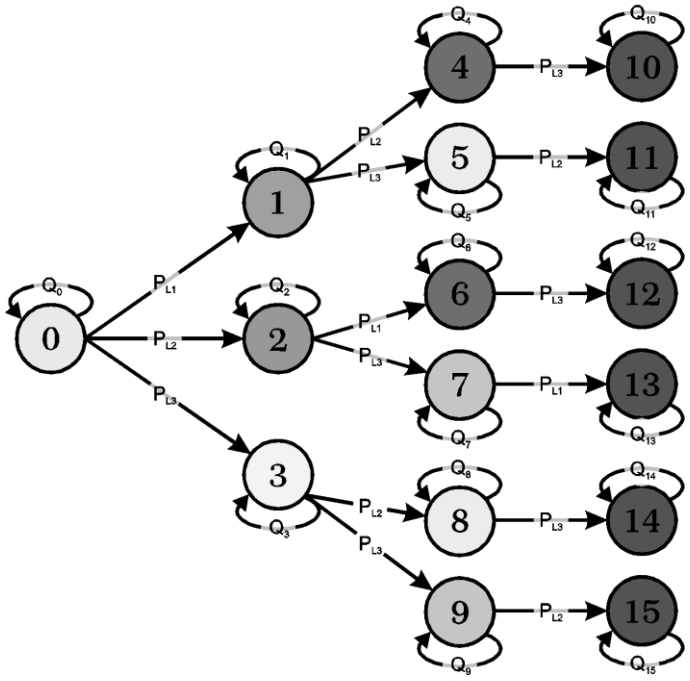

Figure 19: Extended example for the state approach.

Using this knowledge it is possible to reduce the number of new initial states, all leading to identical sub results, from 15 to 7 causing a tremendous decrease in computation time.

4.1.4 Correlation of nodal injections

In the method presented in Deliverable D4.2 did not to account for correlation between the fluctuating nodal in-feeds. The correlation of load fluctuations is implemented by the use of a correlation matrix. It is possible to provide either one full correlation matrix as an input value or to generate an artificial one by giving a correlation coefficient per zone and a number for inter-zonal correlation as exemplary shown in where ρ is the matrix of correlation coefficients and ρ_{ii} are intra-zonal correlation matrices while ρ_{ij} are inter-zonal correlation matrices ($i \neq j$).

$$\rho = \begin{bmatrix} \rho_{11} & \rho_{12} & \rho_{13} \\ \rho_{21} & \rho_{22} & \rho_{23} \\ \rho_{32} & \rho_{32} & \rho_{33} \end{bmatrix}. \tag{4-7}$$

By the knowledge of the variance of the loads (or the uncertainty afflicted nodal power injections) the covariance matrix can be calculated by the simple matrix multiplication of $\sigma_N \cdot {\sigma_N}^T$ and it's Hadamard with the correlation matrix given in (4-8) according to [12].

$$\Sigma = \sigma_N \cdot {\sigma_N}^T \circ \rho. \tag{4-8}$$

In Eq. (4-8) Σ denotes the covariance matrix, and σ_N is a vector of the standard deviations per node. The covariance matrix can be used in the further computation procedure of the probabilistic load flow to determine the variance of the line flows – the calculation of the mean values of load flows stays the same as presented in Deliverable D4.2. Power Transfer Distribution Factors (PTDFs) are used for this purpose.

$$\sigma_{\mathrm{B}}^2 = PTDF \circ PTDF \cdot \Sigma \cdot 1_{nb}. \tag{4-9}$$

4.1.5 Potential results and their visualisation

The method proposed in this work can give various system measures as results. An output could be e.g., the number of lost nodes, the amount of generation lost or the power not supplied. The latter one was found to give the best comparability between different simulation scenarios. The method provides both, an lower and an upper bound on the overall system risk. The lower bound represents the sum of the lost load which has been identified in all simulated states, weighted by the respective probability of the state. The upper bound corresponds to the total system risk, i.e. the highest possible risk we can have, after simulating a number of states. In the beginning of the simulation, the lower bound is initialised as zero, since no states with lost load have yet been identified. The upper bound is initialised as the worst possible loss, which corresponds to the case where all load is lost with a probability of 1. As the simulation goes on, the bounds come closer. The simulation ends, when all the probability to reach each remaining system state is beneath a given limit (see Section 4.1.2). This is exemplarily illustrated in Figure 20. The dashed line reflects the worst case assumption and the solid line the risk determined by the simulation. It is obvious that the worst case line starts in the first simulation stage with the assumption that all loads in the grid will be lost and the found risk starts at zero. During the simulation the two lines come closer to each other and so the uncertainty of the risk measure decreases. Due to the tremendous computational effort for perfect results there will always be an uncertainty in the risk value also for small power systems being simulated (e.g., the complete simulation of the IEEE 4-bus system is feasibly, the complete simulation of the IEEE 14-bus is not feasible in terms of simulation time.).

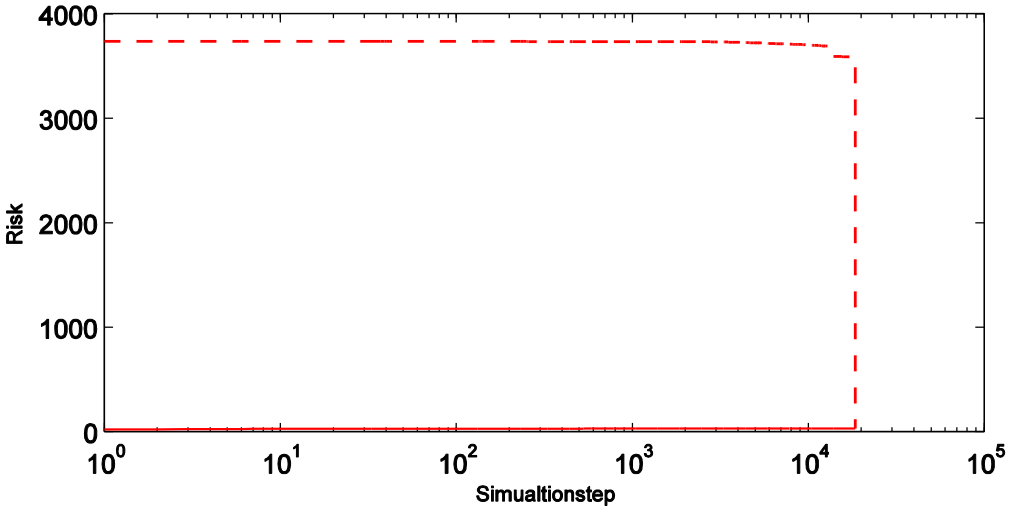

Figure 20: Evolution of the worst case and the fully determined risk measure.

Other outputs of interest are the cumulated risk per N-1-contingency, allowing a risk based comparison of different single element outages, or a list of the multi element outage combinations leading to high risk values.

4.2 Implementation of PFCCs

This section is about implementing PFCCs into the presented method. The selected PFCCs are HVDC lines, phase shifting transformers and as a FACTS device the TCSC.. They all have an effect on the active power flow, but they are modelled in different ways and so have a different influence on the risk of the power system.

4.2.1 HVDC lines

4.2.1.1 Integration of HVDC lines in the load flow calculation

HVDC lines are modelled in this work as active power injections. To account for the losses in active power they are modelled according to Eq. (4-10) consisting of load flow independent losses reflected by α_0 and load flow dependent ones modelled by the parameter α_1 as proposed in [13].

$$P_{HVDC,t} = P_{HVDC,f} - \left|P_{HVDC,f}\right| \cdot \alpha_1 - \alpha_0. \tag{4-10}$$

The HVDC lines power injections are added to the systems nodal power vector P_N as given in Eq. (4-11) resp. (4-12):

$$P_n = P_n + P_{HVDC,f} \forall n \in F, \tag{4-11}$$

$$P_n = P_n - P_{HVDC,t} \forall n \in T. \quad (4\text{-}12)$$

The parameterisation of the dataset is exactly the same as defined in the MATPOWER format [14].

4.2.1.2 Outage probability modelling of HVDC lines

HVDC lines consist of power electronics and conventional lines, so the outage probability of HVDC lines differs significantly from HVAC lines. This is taken into account by formulating the "HVDC branch-loading to branch-tripping-probability function" consisting of an offset value reflecting the outage probability of the line (β_0 in (4-13)) and a load dependent increasing part in tripping probability reflecting the power electronics part (α_1 in (4-13)). Facing the fact that the utilisation of HVDC lines is modelled here as deterministic values (the mean value is the set point of the HVDC and there is no variance in HVDC line loading) the outage probability is simply calculated by Eq. (4-13).

$$\overline{P_{trip\ hvdc,b}} = \alpha_0 + P_{hvdc,b} \cdot \alpha_1. \quad (4\text{-}13)$$

4.2.2 Phase shifting transformers

Phase shifting transformers (PSTs) are used to control mainly the active power flow in a line they are connected to and as a consequence of meshed grids also the lines surrounding it. Due to the increased transits in the pan European transmission system numerous PSTs were installed to on control load flows and so to account for the security of the overall power system. PSTs have become an important degree of freedom in today's transmission system operation.

4.2.2.1 PST variants

There are different kinds of phase shifting transformers, namely symmetrical and asymmetrical shifting transformers [15]. Their voltage phasor diagrams are shown in Figure 21 resp. Figure 22. The main difference between these two kinds of shifting transformers is that the magnitude of the primary and secondary terminal voltage is not equal. So the symmetrical PST introduces solely a shift in voltage angle, but the asymmetrical PST affects also the voltage magnitude. Assuming e.g., a perfect high voltage grid with reactive elements only, the symmetrical shifting transformer would only add an additional active power flow to the line it is connected to, while the asymmetrical one would also cause a reactive component.

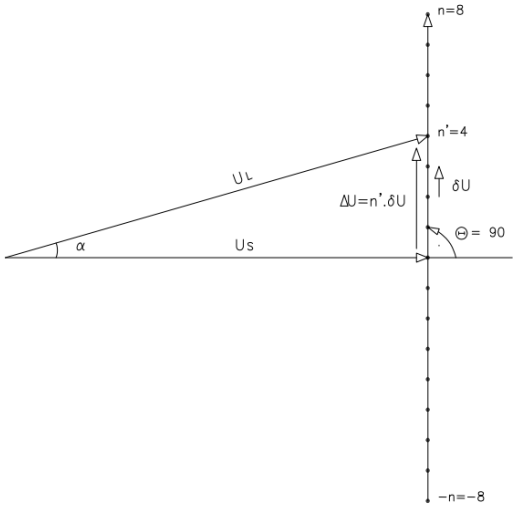

Figure 21: Asymmetrical shifting transformer with Θ = 90° [16].

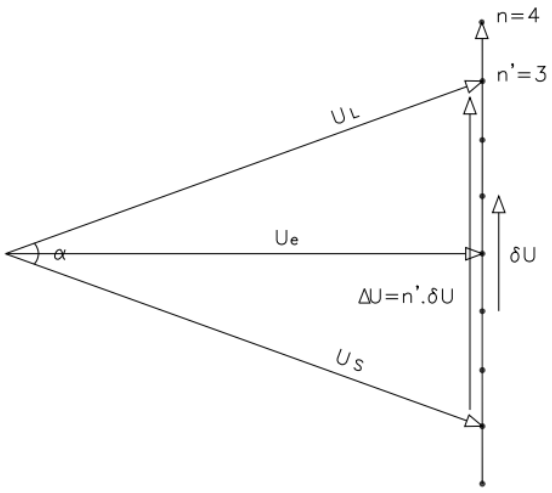

Figure 22: Symmetrical shifting transformer [16].

In the case of asymmetrical PSTs there are not exclusively those adding an additional voltage with a phase angle of 90° but also ones differing from 90°. The voltage phasors are visualised in Figure 23, showing the additional voltage with an angle $\theta \neq 90°$. For all variants the statement that the angle shift is influenced by the magnitude of the additional voltage is valid.

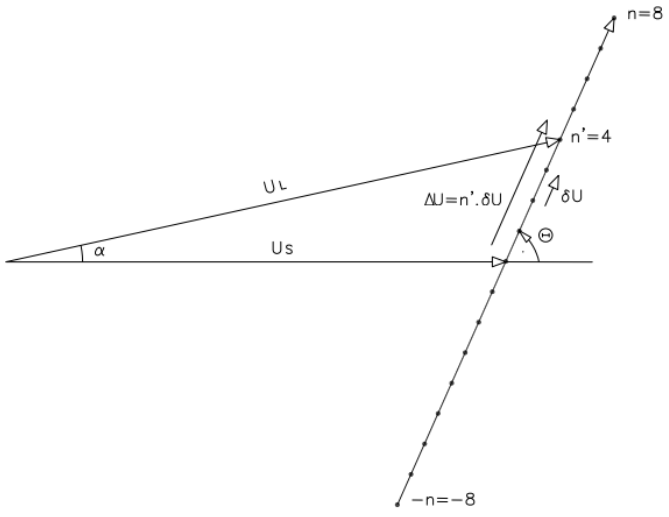

Figure 23: Asymmetrical shifting transformer with Θ ≠ 90° [16].

4.2.2.2 PST modelling

As already mentioned in the previous section, PSTs introduce an additional voltage angle spread and in some cases also influence the voltage magnitude. The DC-power flow

formulation used in this method is not accounting for voltage levels, so the only parameter of interest is the phase shift angle α of a particular PST.

The input data needed is stored according to the MATPOWER format given in [14]. The only input value needed is the shift angle α.

In Figure 24 the effect of introducing a PST in series to a line in the presented method is illustrated according to the work done in [17]. The first schematic shows a line modelled in DC-power flow simply by its reactance. In the second one a PST is placed in series to the line introducing an angle shift of α_{PST}. Due to the DC-power flow formulation this voltage angle shift can be expressed as a parallel active power source. The set-point of the equivalent parallel power source P_f is given by Eq. (4-14).

$$P_f = \frac{\alpha_{PST}}{X_{12}}. \tag{4-14}$$

Facing the fact that constant parallel power sources are hard to model it is replaced by nodal power injections on the beginning and the end of the line the PST is connected to which can be implemented in the equations of the DC-power flow by adding the injected power at the “from” node of the particular line and subtracting it at the “to” node of it.

$$P_n = P_n + P_f \forall n \in F, \tag{4-15}$$

$$P_n = P_n - P_f \forall n \in T. \tag{4-16}$$

In the “Simplification” subfigure in Figure 24 it can be seen that the injected power adds up to the power flow of the PST so the real power flow can be calculated by subtracting the injected power from the particular branch’s power flow.

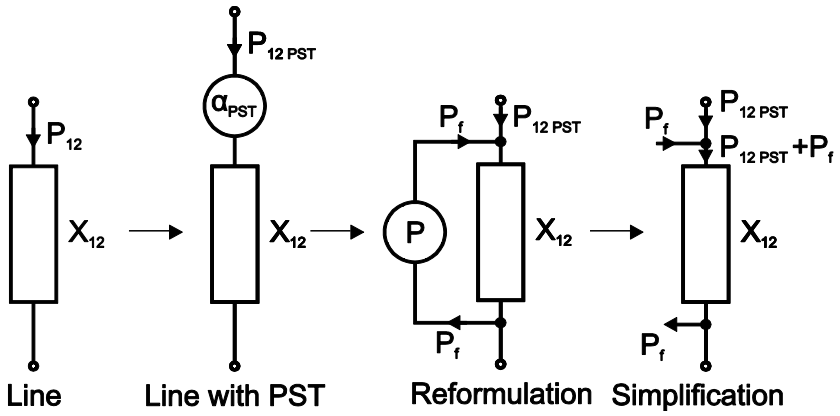

Figure 24: PST modelling [17] .

The PST influenced power flow over the line can be determined according to Eq. (4-17):

$$P_{12PST} = P_{12} - P_f. \tag{4-17}$$

4.2.3 FACTS

There are various types Flexible AC-Transmission Systems (FACTS) introducing controllability into transmission systems, either in terms of active or reactive power flows and with consequences for voltage angles and magnitudes. [18] gives a detailed view on each of the FACTS devices. The most important FACTS elements in real world power system operation are static compensators like e.g., SVC and STATCOM. They are able to provide or demand reactive power in the node they are connected to and change their set-points very quickly. Thus, they are ideal to locally compensate fluctuating demand in reactive power and account for the node voltage magnitude. In contrast to this the Thyristor Controlled Series Compensator (TCSC) introduces controllability in meshed grids by influencing the impedance of the branch they are connected in series with. They generally consist of a thyristor controlled capacitor parallel to an inductor. Optionally there can be a fixed compensation by another capacitor in series. So a TCSC is able to change its reactance during power system operation and so influence the power flow of both the line it connected to, as well as the power flow on parallel lines. By lowering the reactance of the TCSC the power flow can be attracted, and by increasing the reactance it can be suppressed. FACTS-devices also to be mentioned are the Unified Power Flow Controllers (UPFC) or the Static Synchronous Series Compensators (SSSCs) providing additional flexibility to the TSOs daily business.

Due to the limited use of FACTS in the pan-European power systems, in this work solely the TCSC FACTS element was selected for implementations, which can be modelled as a series reactance to the branch it is connected to according to the work done in [19]. The parameters of the TCSC element are a set-point X_{TCSC} and the maximum X_{TCSC}^{max} and minimum X_{TCSC}^{min} limits of the device which are used as constraints during an upstream optimisation. During the cascading risk assessment the set-point of the FACTs device is not changed but it's tested on plausibility by performing a check concerning the provided limits.

$$X_{TCSC}^{min} \leq X_{TCSC} \leq X_{TCSC}^{max}. \tag{4-18}$$

For each branch of the given power system a TCSC is connected to (B_{TCSC}) the branch reactance X_b is modified according to Eq. (4-19).

$$X_b = X_b + X_{TCSC} \; \forall b \in B_{TCSC}. \tag{4-19}$$

4.3 Case study

This section presents two different case studies to demonstrate the effect of PFCCs on system power flows and the over system risk using the modified IEEE 118 bus system extended by reliability numbers [20]. The first case study is about how different types of PFCCs affect the risk. The second case study is about controlling strategies of PFCCs being either central or de-central coordinated.

4.3.1 Influence of different PFCCs on system risk

This section is about demonstrating the effect of PFCCs in terms of system risk. The line where the PFCCs were placed is highlighted in yellow in Figure 25, where the IEEE 118 bus system is visualised. The color coding is in respect to the 97.5%-quantile of the line loading. Red lines mean a q97.5-utilisation of more than 100%, blue ones above 70% and green lines lower than 70%. The 97.5%-quantile was calculated by performing a probabilistic load flow during the optimisation giving the mean value and the standard deviation of the branch loadings. The 97.5%-quantile was determined according to Eq. (4-20):

$$P_{q97.5} = \left| \frac{P_B^{\mu} + 2 \cdot P_B^{\sigma}}{P_B^{max}} \right|. \tag{4-20}$$

This line where the PFCC is placed was found in an iterative process and shows a good potential for demonstrating the effect of PFCCs due to the fact that there are numerous lines in the surrounding neighborhood of the line and there is no single line in series to it constraining the optimisations as it would be the case for the red one in the lower left part of the power system. The set-point was determined by formulating and solving an optimisation problem.

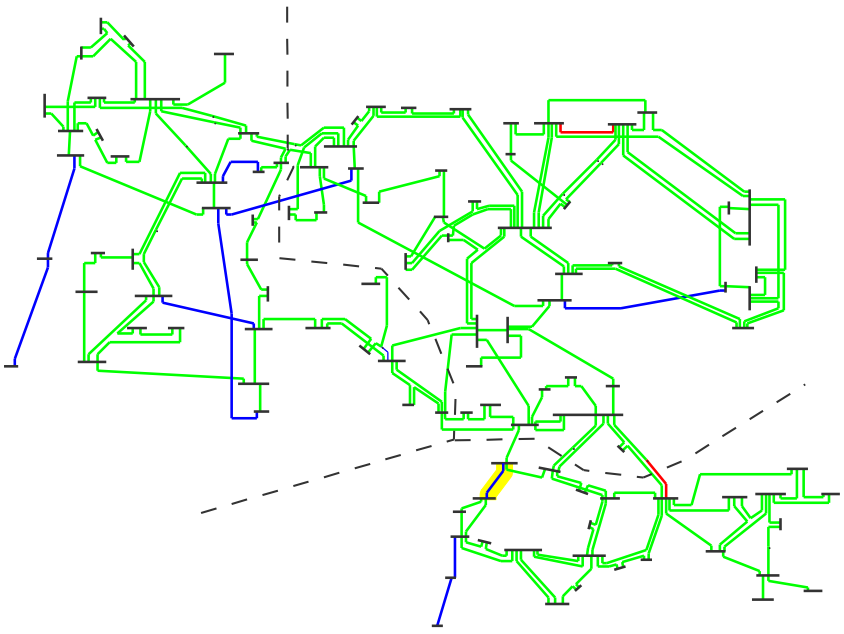

Figure 25: Initial case q97.5 loading (O = 65.9).

The optimisation objective which is shown in Eq. (4-21) highly penalises overloads and also accounts for the individual branch outage probability for not overloaded lines. This leads to an avoidance of overloaded lines and the smoothly utilised elements regarding their outage probabilities. To account for the uncertainty in branch loading the 97.5% -quantile value for the loading was chosen in the optimisation. The control variables of the

particular PFCC are given in Eq. (4-22). The optimisation is constrained by the limits of the PFCC according to (4-23).

$$\min_{x} \sum_{b \in B} \left(P_{q97.5,b(P_{q97.5,b} \leq 1)} \cdot p_{out,b(P_{q97.5,b} \leq 1)} + P_{q97.5,b(P_{q97.5,b} > 1)} \right). \tag{4-21}$$

where

$$x = \begin{bmatrix} \varphi_{PST} \\ P_{HVDC} \\ X_{TCSC} \end{bmatrix}, \tag{4-22}$$

such that

$$\begin{aligned} \varphi_{Pst,min} \leq \varphi_{Pst} \leq \varphi_{Pst,max}, \\ P_{HVDC,min} \leq P_{HVDC} \leq P_{HVDC,max}, \\ X_{TCSC,min} \leq X_{TCSC} \leq X_{TCSC,max}. \end{aligned} \tag{4-23}$$

4.3.1.1 HVDC

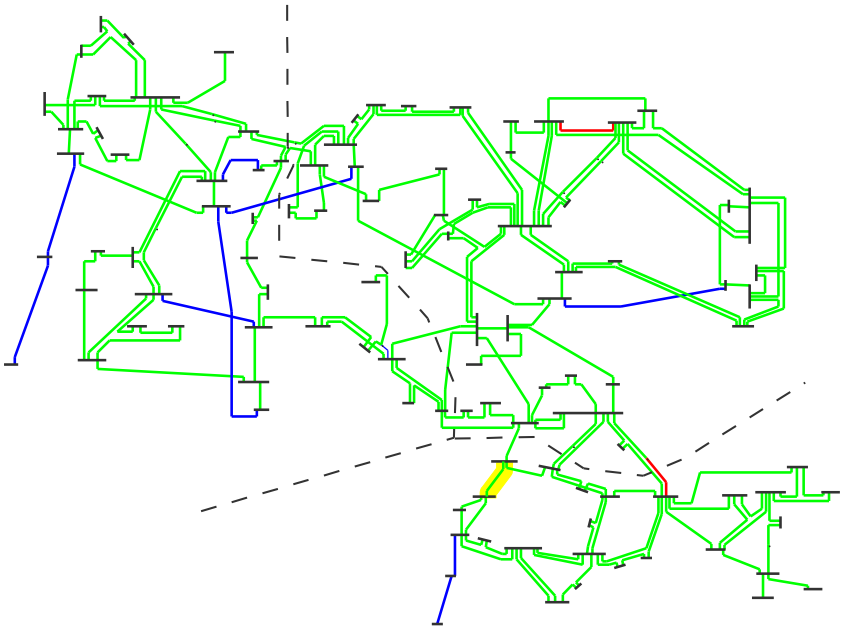

Figure 26: Initial case q97.5-loading with HVDC (O = 63.96 and P_{HVDC} = -41.1 MW).

4.3.1.2 PST

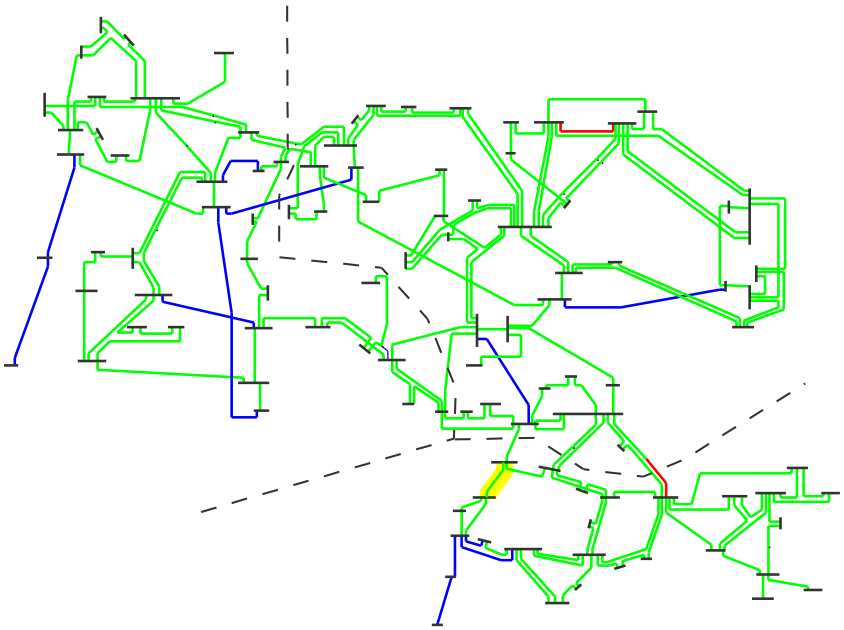

Figure 27: Initial case q97.5-loading with PST (O = 62.5and α=-20.7°).

4.3.1.3 TCSC

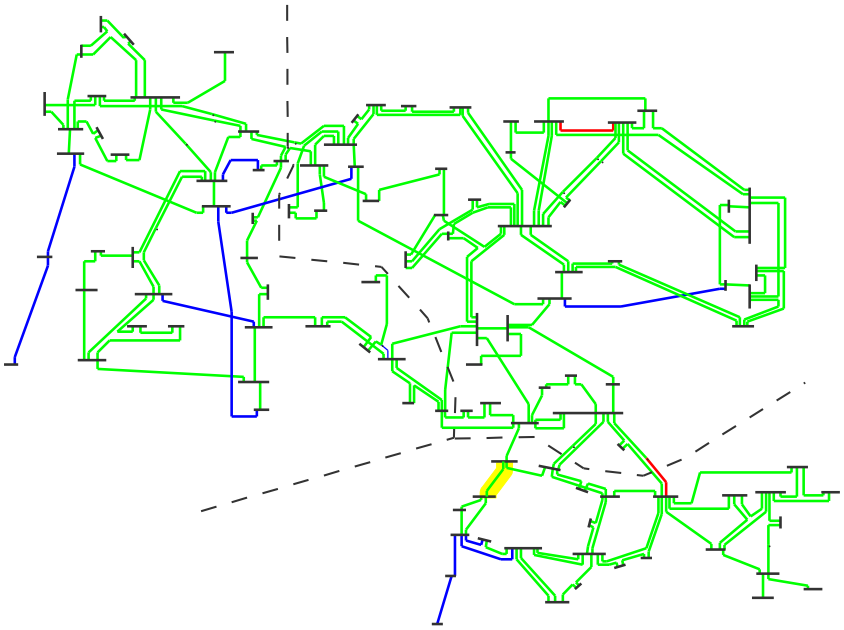

Figure 28: Initial case q97.5 loading with TCSC (O = 63.5 and X_{TCSC} = 160Ω).

4.3.2 Results and comparison

As can be seen in Figure 26 - Figure 28,the loading of the line the particular PFCC is in series with was reduced successfully in all PFCC case studies and no additional lines showed a significant increase in q97.5-loading. As seen in Figure 29, all single PFCC case studies led to a decrease in overall system risk, but there are differences among them. The simulation tool's lower limit as a stopping criterion for state probability was the same for all of the four simulations. The PST case study shows a need for much more simulation steps in Figure 29 than the other ones. This leads to the conclusion, that there are more likely outage combinations than in the other cases to be scanned. Nevertheless this case study shows the lowest system risk of all. This is due to the modelling of PSTs given in Section 4.2.2.2. The load flow over the PST is given by a system load flow dependent and independent part. The load flow dependent one is reflected by the reactance, and the load flow independent part by the nodal power injections. In the case of the TCSC, there is only a load flow dependent part. The TCSC itself as well as the branch it is in series to are both modelled as reactances. It is not generalisable that one technology is better in all scenarios, but the case study reflects that there is a significant difference in the devices' models and the way they influence the overall system risk.

The HVDC case study decreases the utilisation on one line in the southern part of the grid. Despite this decrease in utilisation, the HVDC has the lowest effect on lowering the overall system risk. This is because the set-point of the HVDC line stays unchanged over the

whole simulation, and leads to a heavy loading in the parallel branches after some simulation steps.

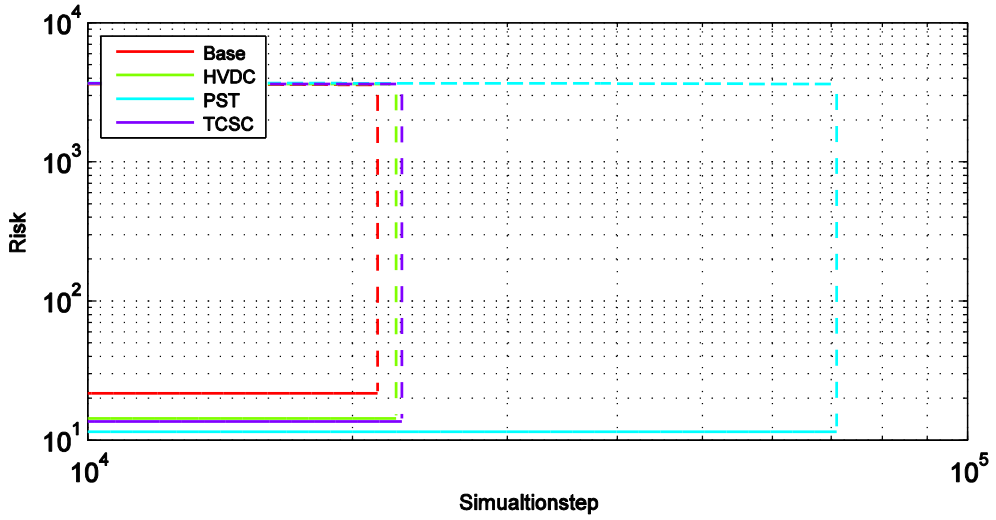

Figure 29: Risk evolution during the different PFCC case studies.

All PFCCs improve the overall system security in terms of Lost Load. The detailed results are given in Table 4, while the risk evolution during the simulation process is shown in Figure 29.

Table 4: Risk per PFCC case study.

	Set-point	w.c. risk in MW	b.c. risk. in MW	uncertainty in MW
Base	-	22.43	21.64	0.79
HVDC	-41.1 MW	15.08	14.32	0.76
PST	-20.7°	12.58	11.47	1.11
TCSC	160 Ω	14.33	13.57	0.76

4.3.3 Central vs. de-central coordination of PSTs

To evaluate the difference in risk between a central coordination of PFCC set-points and a de-central one, only accounting for the system risk of the particular grid area, two different scenarios were analyzed. In each network area one PFCC, in this case PST, is placed according to the highlighted branches in Figure 30 and their set-points were optimised by solving a minimisation problem given in the particular subsection.

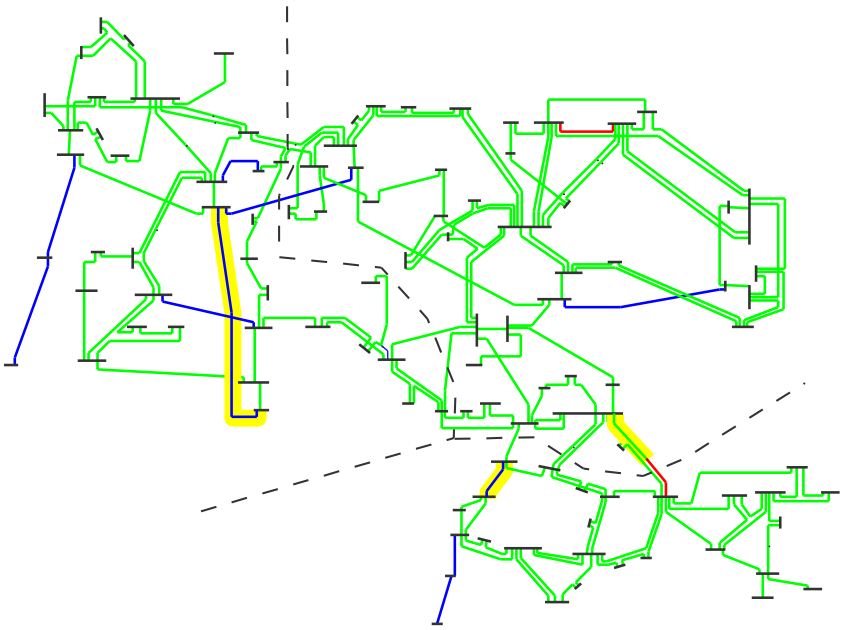

Figure 30: Initial case q97.5-branch-loading with PSTs (O = 65.9).

4.3.3.1 Central coordination

The optimisation's objective formulation for the central coordination approach is shown in Eq. (4-24) constrained by the PSTs limits given in Eq. (4-26). The terminology definition regarding $P_{q97.5}$ can be found in Eq. (4-25)

$$\min_{\alpha_{PST}} \sum_{b \in B} \left(P_{q97.5,b(P_{q97.5,b} \leq 1)} \cdot p_{out,b(P_{q97.5,b} \leq 1)} + P_{q97.5,b(P_{q97.5,b} > 1)} \right), \tag{4-24}$$

where

$$P_{q97.5} = \left| \frac{P_B^{\mu} + 2 \cdot P_B^{\sigma}}{P_B^{max}} \right|. \tag{4-25}$$

such that

$$\alpha_{Pst}^{min} \leq \alpha_{Pst} \leq \alpha_{Pst}^{max}. \tag{4-26}$$

By optimising the operation point of the PSTs in a central way the objective value could be decreased from 65.9 to 29.5. The set-points of each PST can be found in Table 5.

Table 5: PST set-points – central coordination.

PST #	Set-point in °
1	18.5
2	-11.5
3	18.5

Figure 31 holds the visualisation of the q97.5-line loading situation after the integration of the PST devices and the optimisation of their set-points. It can be seen, that the overload situation in the southern region could be eliminated but the utilisation in some other branches increased.

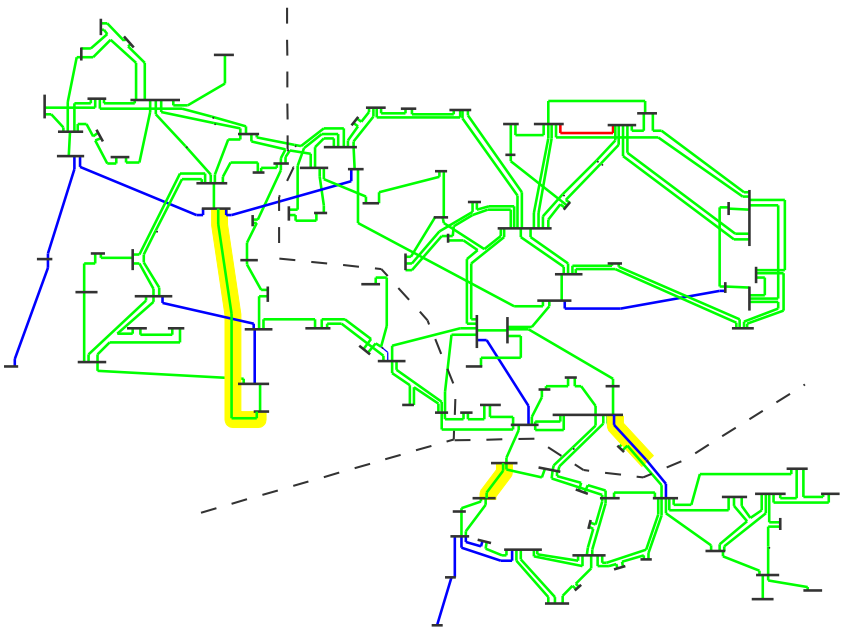

Figure 31: Central case q97.5-branch-loading with PSTs (O = 29.5).

4.3.3.2 De-central coordination

The optimisation's objective formulation for the central coordination approach is shown in Eq. (4-27) constrained by the PST limits already given in the section 4.3.

$$\min_{\alpha_{PST}} \sum_{b \in B_z} \left(P_{q97.5,b(P_{q97.5,b} \leq 1)} \cdot p_{out,b(P_{q97.5,b} \leq 1)} + P_{q97.5,b(P_{q97.5,b} > 1)} \right). \quad (4\text{-}27)$$

The solution of the de-central per zone optimisation of the PSTs is given in Table 6 in terms of set-points.

Table 6: PST set-points – de-central coordination.

PST #	Set-point in °
1	-8.9
2	-20.0
3	19.2

Figure 32 shows the q97.5 per branch utilisation in the test system. The value of the objective function exceeded even the initial case one.

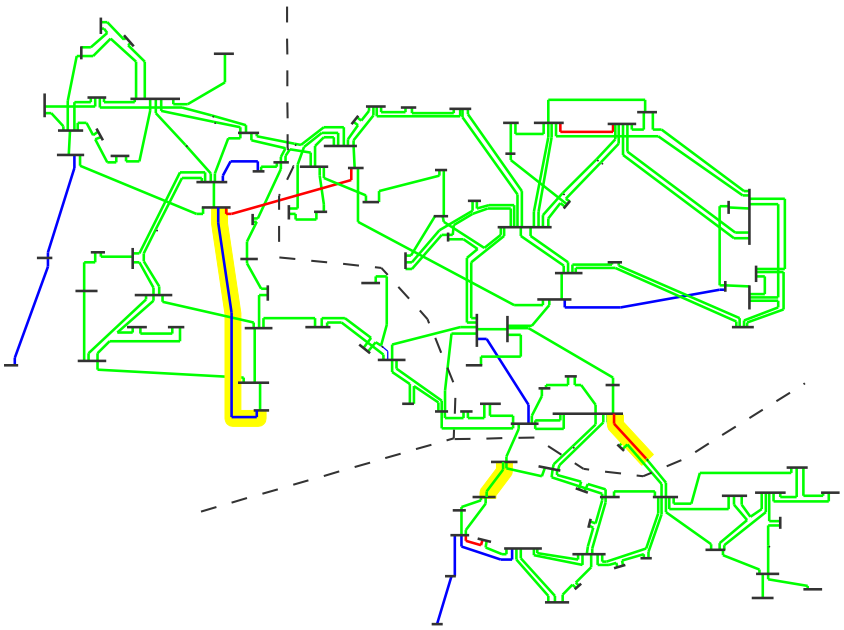

Figure 32: Central case q97.5-branch-loading with PSTs (O = 116.1).

4.3.3.3 Central vs. de-central coordination – comparison of results

As expected the central coordination approach leads to the best solution in terms of risk in this case study. Even though the de-central optimisation shows a higher objective function value than the base case it performs better in terms of risk. This leads to the conclusion, that an analysis of the initial state does not necessarily correctly reflect the risk of the overall system – a higher objective function coming from overloads and a high loading of likely outaged lines does not directly lead to a statement concerning the risk it holds.

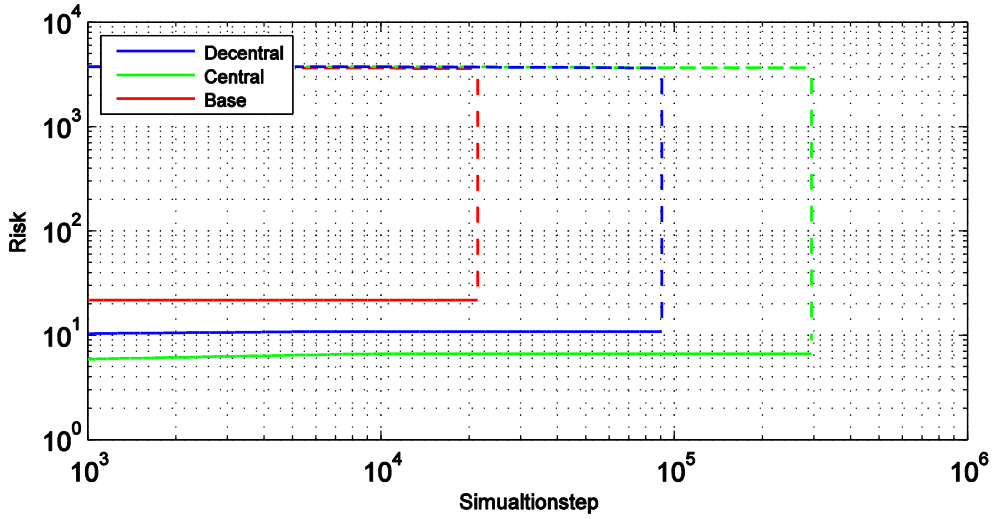

Figure 33: Risk evolution during the different cordination method case studies.

Table 7 gives an overview about the risk values and their uncertainties concerning different PFCC coordination strategy case studies.

Table 7: Risk per coordination method case study.

	w.c. risk in MW	b.c. risk. in MW	uncertainty in MW
Base	22.43	21.64	0.79
Central	8.90	6.63	2.27
De-central	12.56	10.78	1.78

4.4 Summary and conclusions

This chapter is about the implementation of PFCCs into the method developed during the work for Deliverable D4.2. Also some enhancements mainly concerning the quality of the results and the computational effort were implemented leading to a fast probabilistic cascading risk assessment tool.

The implemented PFCCs were tested and compared in terms of their effect on the overall system risk in one case study per component, leading to the conclusion that the different modelling of the particular components has a significant influence on the system security.

A second case study compared a central and de-central coordination of power flow controlling components, and it was shown that central coordination gives a better solution regarding the Lost Load. Another effect which is shown in the second case study is that a high loading of some lines and a non-optimal utilisation not necessarily leads to a higher risk than lower branch loadings and a smooth distribution of them. This implies that analyzing the initial state situation of a grid in terms of branch loadings does not immediately lead to a valid conclusion regarding the system risk - not even when taking account for the uncertainty in form of investigating the 97.5% quantiles of the line loadings.

5 Effect of Market Models on the System Risk

This chapter is about analyzing different market models in terms of their costs and the effect on the system risk. Market models differ in the way they handle congestion management, which is the aspect we will focus on in this part of the deliverable. For an ideal, fully competitive market with no congestion, there are no system related constraints limiting the trading activities in the whole overall trading zone. The market model based on this assumption is called uniform pricing. It does not account for any thermal limits of transmission system elements, so this kind of dispatching leads to the cheapest solution in terms of costs, but it's also likely to end up in a dispatch showing overloads of branches. A more sophisticated marked model is nodal pricing. This pricing method accounts for each single congestion of any branch in the underlying power system. This pricing method is used in the US, but has so far not been implemented in Europe. In order to account for congestion to some extent, simplified zonal pricing is used [21], which is a cross between nodal and uniform pricing accounting for network related constraints in terms of exchange powers on tie lines.

An additional method of interest is the N-1 secure dispatching method. This dispatch principle is similar to the nodal pricing dispatch, but ensures that there are no thermal violations of any branches in the case of an outage of any single branch (i.e., no N-1 overloads). The optimisation objective again is the overall cost in generation.

Market models were designed to account for the underlying power system and the limitation it brings to market activities. Since the nodal pricing method accounts for transmission constraints, it gives a more secure dispatch than e.g., uniform pricing in a deterministic view. Regarding the risk a given dispatch holds or the comparing two dispatches in terms of risk it is not that trivial to state any as simple statement. The aim of this work is to give a comparison of market models in terms of risk in a given test system.

This part of the present deliverable is structured as follows. Section 5.1 gives a short overview about the market models analyzed and a description of the way they were implemented. Section 5.1.1 holds two case studies concerning the risk evaluation of different market models in different scenarios and a comparison between them. A chapter summary can be found in Section 5.3.

5.1 Market models

5.1.1 Uniform pricing

The most simple market model is uniform pricing It is based on the assumption that there are no limits in transmitting power. The objective function for the optimisation is given in Eq. (4-24) and minimises the sum of the marginal costs c_g per generation multiplied with the unit's set-point P_g as a simplified implementation of the work done in [22].

$$\min_{P_G} \sum_{g \in G} (c_g \cdot P_g). \tag{5-1}$$

Even though the power system is assumed to be unlimited in terms of transmission power the output of the generation units is always limited by their lower and upper bounds. This leads to the constraints given in Eq. (5-2) and (5-3).

$$P_g \leq P_{g,max} \; \forall g \in G, \tag{5-2}$$

$$P_g \geq P_{g,min} \forall g \in G. \tag{5-3}$$

5.1.1 N-1 secure dispatch

The goal of N-1 secure dispatching is to ensure that there are no overloads after any single element contingency in a deterministic point of view. In this way, it can be ensured that one single outage does not immediately trigger a cascading event. It is prescribed in the ENTSO-E guidelines [23] that TSOs have to account for the N-1 security of their grids. Therefore, N-1 security is a central topic in daily grid operation and therefore the N-1 criterion is also part of principles in grid operation of TSOs like e.g.in the planning fundamentals of German TSOs [24].

The N-1 secure dispatching method again has as an objective function the overall generation cost. This optimisation's objective function is given in Eq. (5-4).

$$\min_{P_G} \sum_{g \in G} (c_g \cdot P_g). \tag{5-4}$$

The power output of each generation unit P_g is limited by its lower and upper boundaries as given in the section before in Eq. (5-2) and (5-3). Additionally the solution space is constrained by the maximum branch loading after each single line contingency mathematically formulated in Eq. (5-5). For a fast and computational efficient calculation of this post contingency flows the Line Outage Distribution Factors (LODF) already presented in Deliverable D4.2 are used and so the post contingency branch flow can easily be calculated according to [25].

$$|P_{B,i}| \leq |P_{B,i} + LODF_{i,o} \cdot P_{B,o}|. \tag{5-5}$$

As shown in Eq. (5-5) the post-contingency power flows are given as the base case load flow of the lines in operation $P_{B,i}$ plus a change in power flow due to the outage of a line calculated by weighting its pre-contingency power flow $P_{B,o}$ by the particular LODFs.

5.1.2 Nodal pricing (location marginal pricing - LMP)

Another market model presented here is nodal pricing or also referred to as Location Marginal Pricing (LMP). It is similar to the N-1 dispatching, but without consideration of security constraints. This method limits the power flow of each branch in a power system by its given thermal limit. The objective - minimising generation costs - stays the same for nodal pricing and is given in Eq. (5-6).

$$\min_{P_G} \sum_{g \in G} (c_g \cdot P_g). \tag{5-6}$$

The output of the generation units is always limited by their lower and upper bounds. This leads to the constraints given in Eq. (5-7) and (5-8).

$$P_g \leq P_{g,max} \; \forall g \in G, \tag{5-7}$$

$$P_g \geq P_{g,min} \forall g \in G, \tag{5-8}$$

$$|P_b| \leq \; |P_b^{max}| \forall b \in B. \tag{5-9}$$

To account for congestions in the grid, the list of optimisation constraints is extended by Eq. (5-9) limiting the maximum power flow in each branch of the power system. In this way, load flow situations violating any of the power flow related constraints are avoided. Any congestion leads to some kind of market splitting situation for affected nodes, where the cost differs between the nodes. For some nodes, the marginal costs in power supply will increase due to the fact that they cannot be supplied by the most cost efficient power plant according to the merit order caused by the congestion situation. This leads to an increase in overall generation cost but avoids the existence of overloads and so accounts for power system related limits.

5.1.1 Zonal pricing (market splitting)

Zonal pricing is a simplification of the nodal pricing method by reducing the number of constraints to cross boarder exchange flows among zones instead of each single branch's power flow. This zones are predefined and mostly represent geographical or organisational (e.g., TSO zones) connected areas. In this work the market splitting implementation of zonal pricing is considered. There is also a second method of zonal pricing called flow based market coupling [26].

The overall objective of zonal pricing is to minimise the generation cost. So the objective function stays unchanged and is given in Eq. (5-10):

$$\min_{P_G} \sum_{g \in G} (c_g \cdot P_g). \tag{5-10}$$

The power output of each generation unit is limited by its lower and upper boundaries reflected by Eq. (5-11) and Eq. (5-12).

$$P_g \leq P_{g,max} \; \forall g \in G, \tag{5-11}$$

$$P_g \geq P_{g,min} \forall g \in G, \tag{5-12}$$

$$\left| \sum_{b \in z} P_b \right| \leq \left| \sum_{b \in z} {P_b}^{max} \right| \forall z \in Z. \tag{5-13}$$

To account for the specialty of zonal pricing of limited exchange powers between zones the constraint list is extended by Eq. (5-13). The absolute value of the sum over all exchange powers crossing a given zonal-boarder z out of Z into a predefined positive direction is limited by the added constraint to not exceed the sum of given limits of border lines – the maximal exchange power beyond the neighboring zones to zone-border z.

5.2 Case study

In this section the solution of the previously presented different market models are presented for the IEEE 118 bus system in form of utilisation charts, risk measures as well as risk evolution charts followed by a discussion of results.

5.2.1 Uniform pricing

In Figure 34 the mean value branch loadings are shown for the solution obtained with the uniform pricing method, categorised by color. Red lines are on overload, blue lines exceed 70% of the thermal limit and green ones are below this limit. Due to the fact that this market model does not account for any branch loadings there are overloads. In this case one branch is overloaded and all others except six branches show a loading below 70%.

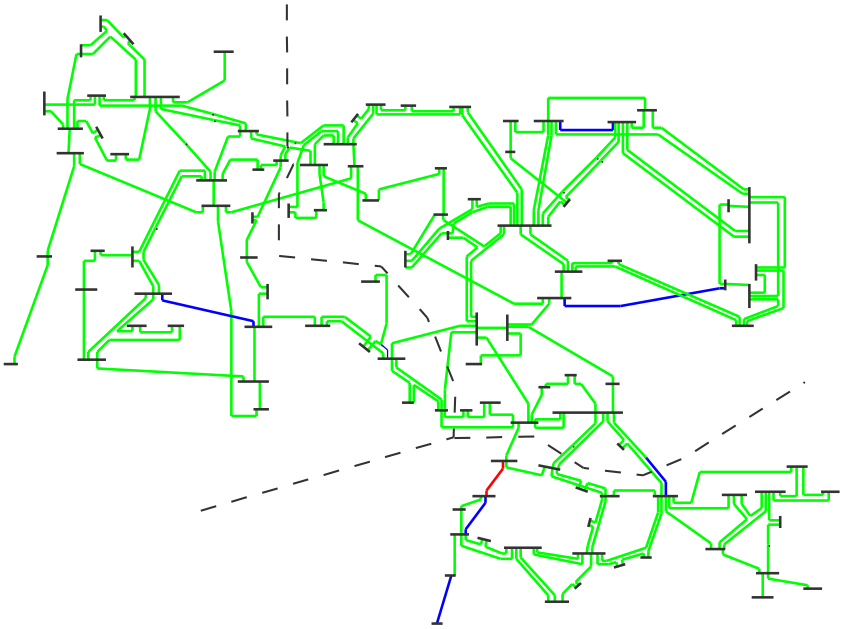

Figure 34: Uniform Pricing – line loading.

5.2.1 N-1 secure dispatch

The N-1 secure dispatch method leads to a low per element utilisation compared to the uniform pricing but it is also the most expensive dispatch as shown later on. There are no overloads present in the base case, and loadings above 70% (blue) show only up in highly meshed grid areas having numerous parallel paths, so the load flow is taken by those in case of an N-1 contingency.

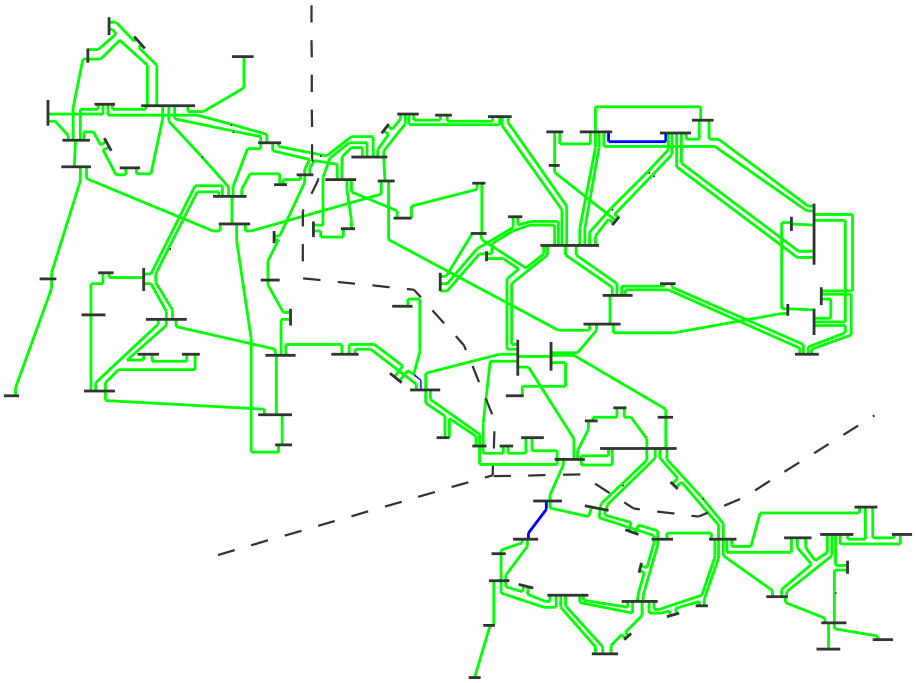

Figure 35: N-1 secure dispatch – line loading.

The share in risk per initially tripped branch regarding the uniform pricing dispatch and the N-1 secure dispatch is visualised in Figure 36 and Figure 37. These plots show staked bar charts giving the share in overall risk each initial contingency holds and it is uncertainty in risk, existing because of the infeasibility of a complete risk analysis. The risk per branch shows for the uniform pricing solution some highly valued lines compared with the N-1 secure case. A lineup of the two solutions leads to the result that the risk reduction from uniform pricing to N-1 secure dispatching comes from the branches between 130 and 140 and branch number 159. The risk could be lowered by minimising the tripping probability of those branches by minimising the branches' utilisation caused by a more secure dispatch.

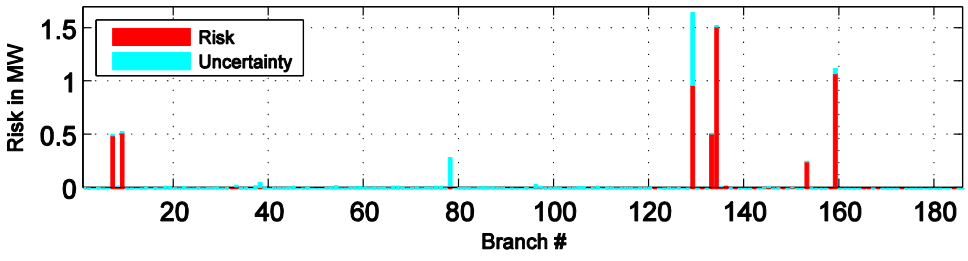

Figure 36: Risk per initial outaged branch (uniform).

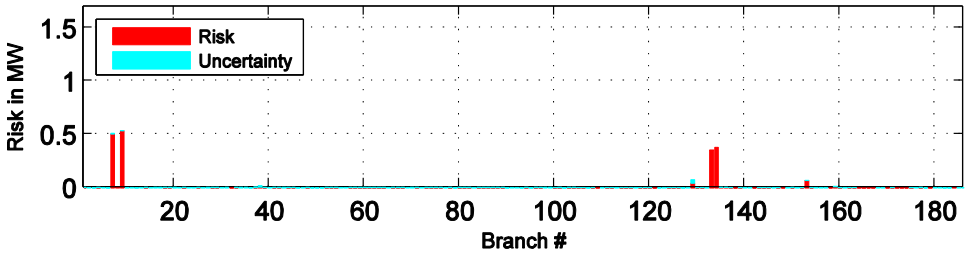

Figure 37: Risk per initial outaged branch (N-1).

5.2.1 Zonal pricing

Due to the relaxed loading situation in the base case of the IEEE 118 bus system, in terms of tie lines, the zonal pricing leads to the same dispatch as the uniform pricing, because of the missing congestions constraining the optimisation and finally leading to market splitting.

To be able to show the effect of zonal pricing the tie lines between the center region and the southern one of the test system were weakened to a maximum exchange power of 75 MW instead of 720 MW for the base case.

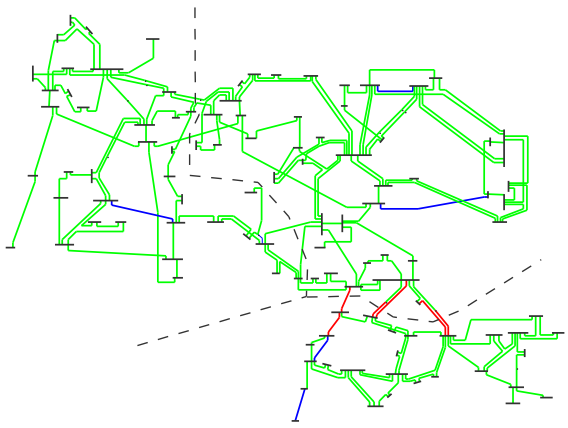

Figure 38: Uniform Pricing – line loading – weak tie lines

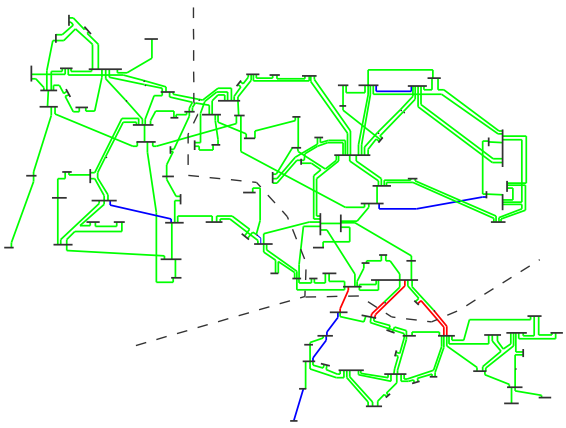

Figure 39: Zonal Pricing – line loading – weak tie lines

The result of this modified scenario is given in Figure 38 for the uniform pricing method and in Figure 39 for the zonal pricing to allow a comparison regarding the effect of market splitting on the utilisation of tie branches. It can be seen that the weakening of the tie lines led in the southern zone to an increase in line loading of nearly all tie lines. The uniform pricing dispatch exceeds the maximal exchange power between the central zone and the southern zone with a value of 90 MW at a rated exchange power of 75 MW and the zonal approach leads to an absolute inter zonal power exchange of 58 MW.

5.2.2 Nodal pricing (location marginal pricing - LMP)

The resulting per element utilisation of the nodal pricing method leading to a line flow based constrained optimisation is visualised in Figure 40. The solution leads for both scenarios to nearly the same picture in terms of color coded branch flows. Only a few branches show slightly differences. In both cases no lines are on overload (otherwise the nodal pricing methods optimisation would not have been feasible). A significant difference is noticeable concerning the overall dispatch costs of the LMP regarding the scenarios given in Table 8 for the base case resp. Table 9 for the weakened tie line scenario in the following section.

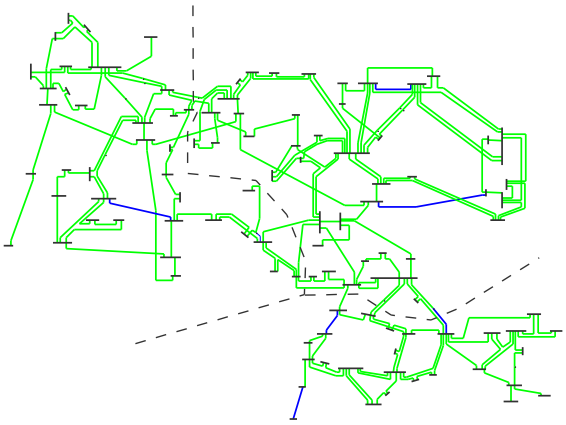

Figure 40: Nodal Pricing – line loading.

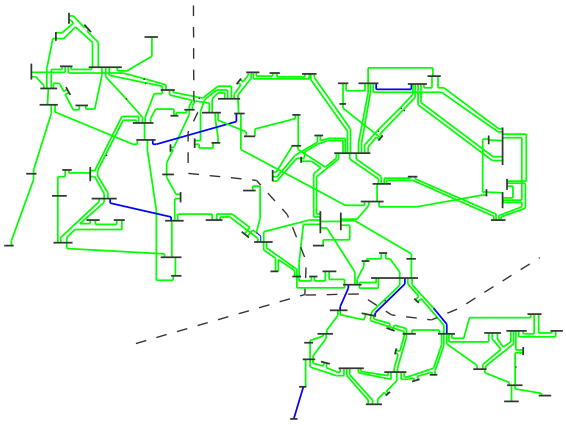

Figure 41: Nodal Pricing – line loading – weak tie lines.

5.2.3 Risk comparison of market models

In this section the results of the two scenarios and the different market models are presented and discussed.

5.2.3.1 Base scenario

The base scenario of the test system leads to a generation dispatch for the particular market models which shown in Figure 42. The uniform and zonal pricing method lead to exactly the same dispatch in terms of generation power due to the absence of congestions in terms of exchange power. The LMP method leads only to a slightly different dispatch utilising also more expensive units. The solution of the N-1 secure dispatch shows the need to use additional generation units for the sake of deterministic system security.

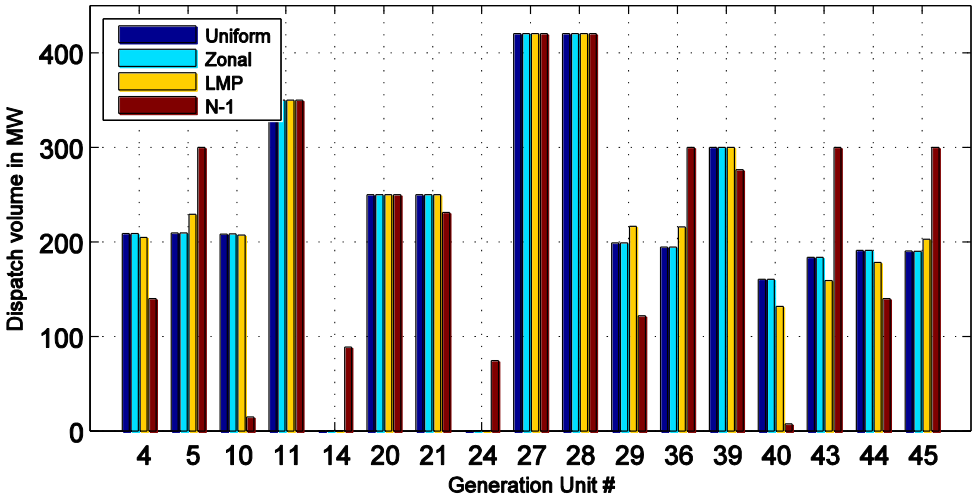

Figure 42: Generation unit dispatch per market model.

The discretised utilisation per branch is visualised in Figure 43. The uniforms as well as the zonal pricing methods show overloads whereas the N-1 secure dispatch and the LMP do not. The LMP leads to the lowest mean branch loading over all branches. In the case of the N-1 secure dispatch there is only a small number of elements exceeding a utilisation of 70%.

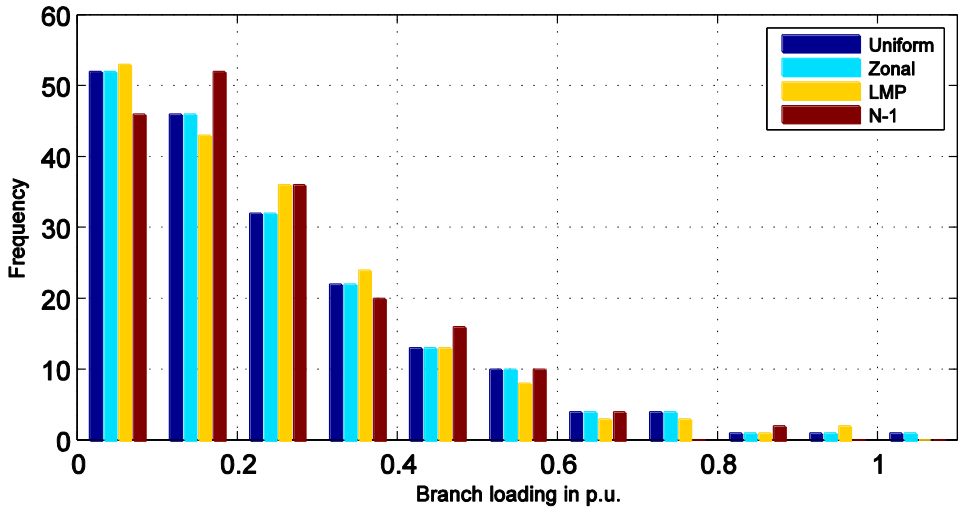

Figure 43: Frequency distribution of branch loadings.

The risk evolution during the probabilistic cascading risk assessment simulation is given in Figure 30. The dashed line reflects the worst case system risk determined by the assumption that all power is at risk for the first simulation step and the simulation lowering the value of risk by subtracting the certain load that is still supplied in this step multiplied with the simulation step's probability. The solid line reflects the best case risk estimate

calculated by summing up all simulation steps' Lost Load values in terms of risk, determined by the multiplication of the Lost Load in terms of power and the simulation step's probability.

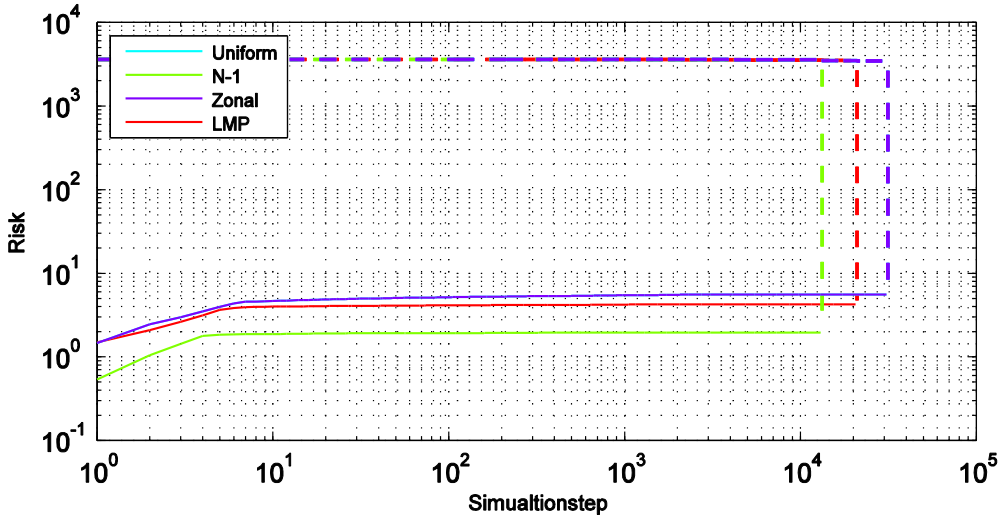

Figure 44: Overview of the risk evolution during simulation.

The exact numbers for the worst case risk, the best case risk and the uncertainty in risk are given in Table 8. The N-1 secure dispatch leads to the lowest risk, followed by the LMP approach with nearly double the risk and the uniform and zonal pricing method holding about 2.5 times the risk of the N-1 dispatch.

Table 8: Risk values of analyzed market models

	Price in p.u.	w.c. risk in MW	b.c. risk. in MW	uncertainty in MW
Uniform	42640	6.51	5.57	0.94
N-1	43483	2.54	1.96	0.58
Zonal	42640	6.51	5.57	0.94
LMP	42641	4.93	4.23	0.70

5.2.3.2 Scenario weak tie lines

In this scenario the effect of zonal pricing in comparison with uniform pricing is shown. The N-1 secure dispatch method did not lead to a solution due to infeasibility caused by the N-1 constraints of the optimisation problem especially for tie lines. In Figure 45 the generation dispatch is given. Different from the previous scenario, the solution of the

uniform pricing method and the zonal pricing are not equal anymore. This is due to the now active constraints of the zonal pricing optimisation problem formulation regarding exchange powers.

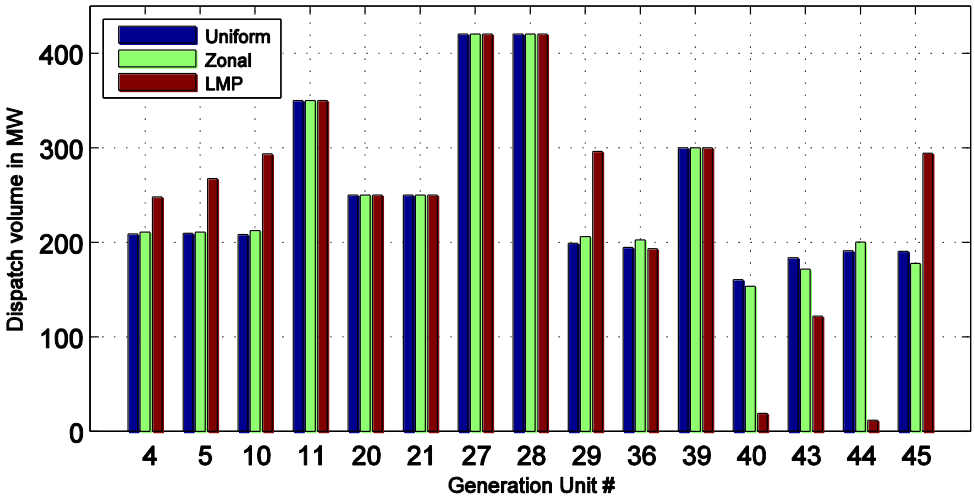

Figure 45: Generation unit dispatch per market model.

The histogram of the branch utilisation is given in Figure 46. The uniform and zonal pricing method both show two branches with a loading exceeding 200% which are tie lines with a low thermal limit compared to the other tie lines being parallel to them. Due to the feasibility of the LMP method there are no overloads present for this scenario.

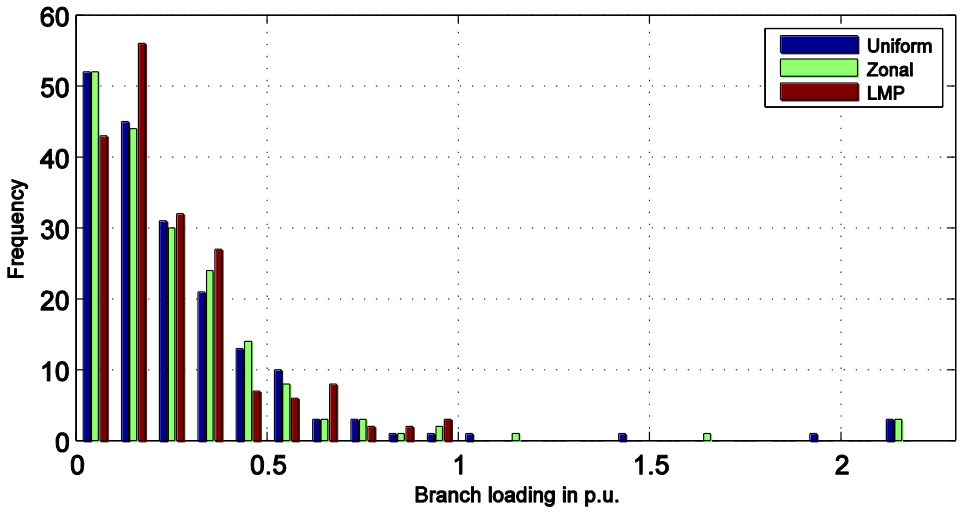

Figure 46: Branch loading.

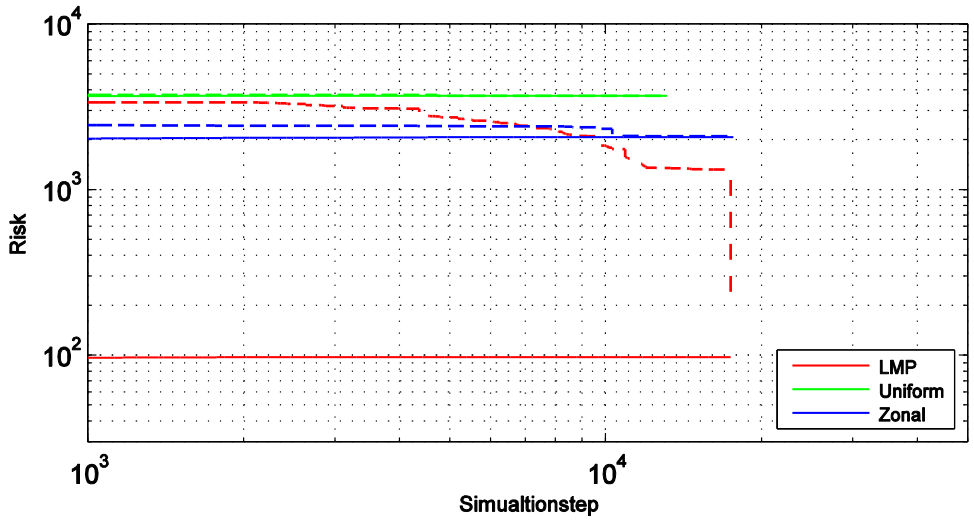

Figure 47: System risk of marker models.

The risk evolution in terms of worst and best case overall system risk estimate is given graphically in Figure 47 and in numerical in Table 9. The small difference in dispatch costs is due to the generation cost numbers of the IEEE-118 bus network. The uniform pricing method's dispatch shows the highest risk in this scenario. Nearly the whole system power in terms of load is lost. The zonal pricing method shows a power at risk of about half of the overall system's load at the same generation costs as the uniform pricing led to. The best solution in terms of risk gives the LMP method for this scenario.

Table 9: Risk values of analyzed market models - weaked tie lines.

	Price in p.u.	w.c. risk in MW	b.c. risk. in MW	uncertainty in MW
Uniform	42640	3684.73	3676.98	7.75
Zonal	42640	2094.11	2072	22.11
LMP	43084	193.08	97.07	96.01

5.3 Summary and conclusions

In this chapter the effect of selected marked rules on the overall system risk was presented. Section 5.1 gave a short description of the analyzed market models and the way they were calculated. Section 5.2 gave results in the form of case studies performed for two different scenarios. The first scenario was the base case of the IEEE 118 bus system reflecting a relatively relaxed utilisation of the power system. Dispatches were

generated, visualised in terms of generation unit utilisation and branch loadings and discussed. The outcome of this analysis was that the N-1 secure dispatching lead to the best dispatch in terms of risk, but also the most expensive one. The uniform and zonal pricing methods lead to the same solution due to the absence of active constraints. Zonal pricing disregards any congested lines, which leads to a low cost, but a high value in risk. The nodal pricing method's dispatch shows a low risk at low generation costs. The second case study was about showing the effect of zonal pricing on the overall system risk on a modified test system. Therefore the tie lines between two grid zones were weakened to artificially generate congestions in terms of exchange powers. The analysis lead to the result that the overall system risk could be decreased dramatically by using zonal pricing in comparison with uniform pricing at nearly the same generation costs. Nevertheless, compared to the base case scenario, the weak tie line scenario's dispatches show a significantly higher risk reflecting the virtue of a strong intermeshed power system in terms of tie lines.

6 Risk-based Security Assessment using AC Power Flow and Monte-Carlo Sampling

In this chapter a risk-based security assessment (RBSA) method is presented which allows to a) analyse and evaluate the risk of a power system's current state, b) predict the system's risk in a future state under varying scenarios and fluctuating inputs and c) propose remedial actions that can help to steer the power system into a risk averse state. The method obtains specific inputs from the tools presented in Chapters 2 and 3 (such as a set of contingencies) and assesses the system risk in two complementary implementations using different sets of risk metrics: a) fast screening, based on severity functions and b) detailed assessment of remedial actions, using an AC OPF framework based on Lost Load. In Section 6.1 we present the methodology explaining the implementation of both metrics in a stochastic AC power flow framework and we discuss explicitly how PFCCs can be incorporated (using as example HVDC lines). Section 6.2 presents the experimental setup, the test systems used and the testing hardware, while Section 6.3 shows the results of several case studies on a) the analysis of voltage security aspects of the system, b) the role of changing stochastic parameters, c) the impact of PFCCs on reducing system risk and d) computational aspects when applying the methodology to a realistic large-scale system.

The proposed methodology joins features of prominent state-of-the-art models by *Kirschen* and *McCalley*. In a comprehensive list of papers [27], [28], [29], [30] Kirschen *et al.* advocate the usage of a Monte-Carlo (MC) framework to adequately capture risk and uncertainty of random disturbances in power system operation. The MC approach uses AC power flow, includes heuristics for load shedding, and proposes corrective actions. Topics of research are: random contingencies, cascading events, sympathetic tripping, hidden failures using the notion of vulnerability regions (VRs) [28] and [30], and weather effects. The risk measure used is the notion of Lost Load, a very commonly used measure to quantify system risk. In particular, in [27] an interesting quantitative comparison between the proposed risk-based approach and a traditional, deterministic approach is provided, underlying how risk-based approaches provide a more complete picture on the system security. The paper also shows how these techniques can be used to improve TSO's insight into the system.

Another main stream of research is performed by McCalley and co-workers, presented in [31], [32], [33], [34] and [35]. In particular, in [32] and [33] Ni and McCalley propose an approach based on so-called risk indices which allows control room operators to assess the security levels of power systems in real-time. The method developed is referred to as online risk-based security assessment (OL-RBSA). In contrast to Kirschen's approach, the contingencies are not created at random but a predefined list of contingencies is used. So-called "*severity functions*" are used to quantify risk against several problems; i.e., severity against too low voltage, circuit overload, voltage instability and cascading. In their work cascading events are modelled with a looping mechanism based on hard limits on the maximum allowable power through the circuit.

Our methodology combines these two research streams in a tool with two complementary implementations/estimators, a) a fast system risk screening tool and b) a detailed assessment of remedial actions for steering the system in risk averse mode.

a) Inspired by McCalley we incorporated severity functions and included a mechanism based on hard limits to capture cascading overloads. This leads to the first estimator of our methodology, which is a fast screening tool used to get a quick first impression of what the risky states of the power system are.
b) Inspired by Kirschen we propose a methodology based on MC simulation and in which Lost Load is used as a first risk measure. An AC OPF optimisation formulation allows the assessment of a large set of remedial actions for reducing the system risk, based on different strategies, such as use of PFCC, redispatching actions or topology optimisation.

Since the focus of our work is on day or hour-ahead forecasting rather than on real-time operation, MC sampling is used to capture the uncertainty in system infeeds, resulting from load and variable renewables forecast errors (wind, solar) rather than for sampling of the contingencies. In the current setup, the list of contingencies is used as an input in the model, coming from the tools presented in Chapters 2 and 3. However, the flexibility of the methodology allows to readily sample contingencies as well. In order to adequately capture the complex stochasticity of wind/solar forecast errors, advanced stochastic simulation techniques are used (*copula theory)* that allow the simulation of stochastically dependent and non-Gaussian infeeds, see [36], [37], [38], [39]. This model provides a detailed assessment of remedial actions for the reduction of system risk and forms the first branch of the modelling methodology.

In the following sections we present in detail how the model is built up and how it is applied in a realistic setup.

6.1 Methodology description

In this section follows a brief description of the proposed AC RBSA method. The main features of the methodology are[1]:

- **Globally convergent AC computations.** In order to get the highest level of accuracy, full AC computations are used throughout the entire algorithm. AC methods allow to detect voltage problems, which are often the generating causes of system collapses. Approximate methods (e.g., based on DC computations) cannot detect such voltage problems which reduces their applicability in a realistic setup. Moreover, it is paramount that the AC power flow converges for every initial

[1] A first version of the method has been presented at PSCC2014 in Wroclaw, Poland, in August 2014, see [39].

guess. This is referred to as globally convergent computations. For this a robust solver is required based on advanced solution techniques.

- **Probabilistic load flow using Monte-Carlo sampling.** In order to capture the complex stochastic behaviour of the system resulting from fluctuating energy sources (wind, solar) and uncertainty in demand, MC sampling in combination with the copula theory (see below) is used.
- **Copula theory.** The copula theory allows modelling of non-normal distributions, whilst taking into account nodal stochastic dependency. These characteristics are typical characteristics for time and spatial correlation of forecast errors of load and variable renewables.
- **Deterministic security assessment (DSA) model.** For each sample of the MC simulation a detailed security assessment model is used, which integrates two risk metrics, leading to a fast screening tool and a tool that provides the remedial actions. The model is described in detail by a flowchart.
- **Cascading events.** It has been found that cascading events contribute heavily to system collapses. Therefore, a mechanism is incorporated which allows to simulate cascading events. In this implementation a cascading mechanism is used based on hard limits on the maximum allowable power through the circuits.
- **Remedial actions.** The methodology proposes automatically how to alleviate severe system states, i.e., voltage violations and circuits overloads. For this an AC OPF framework is used. Remedial actions that are currently implemented in our work include generation redispatching and load shedding. Other remedial actions, such as topology optimisation can readily be implemented. Our approach is as such highly flexible.
- **Fast screening vs. detailed analysis.** The methodology works with two measures of risk, namely severity (by McCalley) and Lost Load (see remedial actions). Since the severity risk measure is computationally cheap, hence very fast, it is proposed as a method for screening the system to look for severe system states. For these severe states a detailed analysis may be carried out using the Lost Load risk measure which costs more time but has higher accuracy. The concept of screening followed by a detailed analysis for the detected risky area is shown in Figure 48.

Below the listed key components are presented in more detail.

6.1.1 Globally convergent AC computations

A key building block in the methodology is the computation of a deterministic load flow (DLF), which is a load flow computation in which all inputs are fixed (known). Since voltage problems are often the cause of a system collapse, it is paramount to run a full AC power flow (or: load flow). Approximate methods, e.g., methods based on DC power flow, cannot detect voltage problems at all, or at least cannot capture them adequately. Furthermore, it is paramount that a globally convergent AC power solver is used, that is, a solver for which the AC power flow converges for every initial guess.

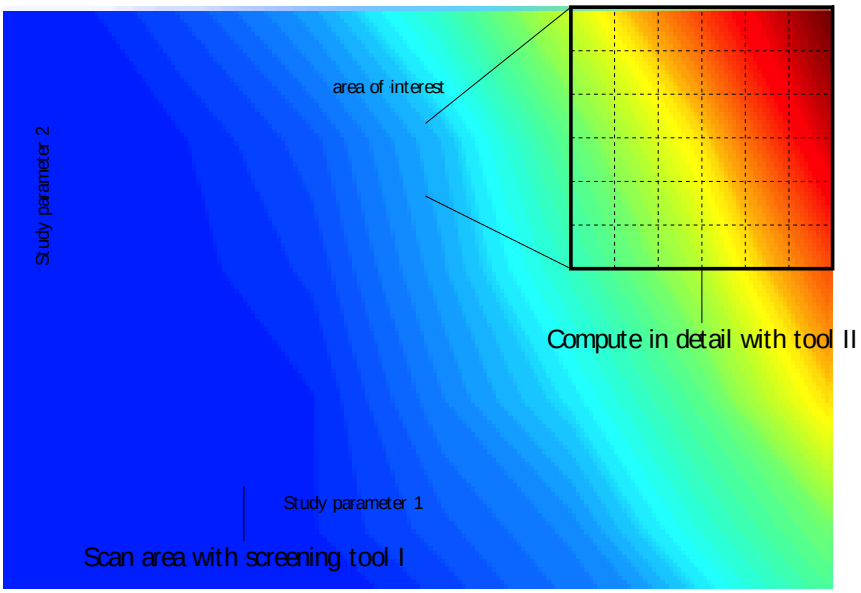

Figure 48: Example of how the screening tool (I) and the detailed analysis tool (II) can work together to speed up the risk assessment. Step 1) Screening the system with the fast tool based on severity. With the screening tool an area of interest is detected, typically risky system states. Step 2) The area of interest is computed thoroughly with the detailed analysis tool based on Lost Load.

6.1.2 Probabilistic load flow using Monte-Carlo sampling

A proficient framework to include uncertainty in power system steady-state analysis is the so-called probabilistic load flow (PLF). Mainly due to the limited computational power in the 1970s an analytical PLF was proposed by Borkowska [40]. The analytical approach was further developed by Allan and others [41], [42]. However, the analytical approach comes with the following key simplifying assumptions [43]:

1. The steady-state model is linearised around an operating point;
2. The system inputs are assumed to be normally distributed;
3. The system inputs are assumed to be statistically independent,

which result in a fast method; unfortunately, the accuracy of the method is reduced when the system infeeds are non-Gaussian and at the same time stochastically dependent. Note that although the classical analytical approaches assumed independent variables, the method can easily be extended to handle correlation, as shown in the approaches presented in Chapters 2-5.

The main alternative to analytical PLF is a PLF based on Monte-Carlo (MC) simulation. Such simulations avoid the above listed simplifications, and can therefore attain a much higher accuracy. Because of the rapid developments in computer technology and speed, day-ahead and real-time security assessment using methods based on MC sampling come within reach. Therefore, in the proposed methodology the MC PLF approach is followed.

6.1.2.1 Monte-Carlo framework

Probabilistic load flow (PLF) using Monte-Carlo (MC) simulation basically comes to computing a deterministic load flow (DLF) many times, typically in the order of 10s of thousands up to 1 million times. The MC framework allows for capturing the complex stochasticity of the system inputs, e.g., non-normal infeed distributions e.g. resulting from wind power forecast uncertainty, and it enables the mapping of specific (rare/high impact) events with possible catastrophic consequences.

As is usual in MC simulation the probability $\hat{p}$ of an event E is estimated by

$$\hat{p} = \frac{The\ number\ of\ occurences\ of\ event\ E}{N}, \tag{6-1}$$

where N is the number of MC samples. Accordingly, the 95% confidence interval is given by

$$\left(\hat{p} - 1.96\sqrt{\frac{\hat{p}(1-\hat{p})}{N}}, \hat{p} + 1.96\sqrt{\frac{\hat{p}(1-\hat{p})}{N}}\right). \tag{6-2}$$

Similarly, the 95% confidence interval for a quantity, e.g., Lost Load, redispatched generation, is given by

$$\left(\hat{\mu} - 1.96\frac{s}{\sqrt{N}}, \hat{\mu} + 1.96\frac{s}{\sqrt{N}}\right), \tag{6-3}$$

where $\hat{\mu}$ is the sample mean, s the sample standard deviation and N the number of MC samples.

6.1.2.2 Sampling of system infeeds

Essentially one can distinguish between two sources of uncertainty in power system analysis, namely:

1. Input uncertainty: variable load and generation;
2. Configuration uncertainty: changing topology due to outaged components.

The focus of the proposed implementation is on day- and hour-ahead risk assessment for systems with high levels of renewable energy sources (RES), hence focusing on forecast uncertainty. Therefore, we present case studies focusing on the sampling of the system infeeds, obtaining the set of contingencies as input from the two complementary tools presented in Chapters 2 and 4. However, due to the flexible and modular MC setup, the methodology allows to readily incorporate sampling of contingencies based on outage probabilities. The outage probabilities are considered stochastic parameters in the MC

setup and can be changed dynamically as a consequence of events such as moving weather fronts, etc.

The modelling of wind power has been studied extensively using the analytical PLF approach [44], [45,8,9], [46]. However, it is acknowledged that an MC framework based on the copula theory allows proper assessment of the complex spatial dependency between wind infeeds [36]. Important work on the implementation of copula theory for modelling power systems can be found in [37] and [38].

6.1.2.3 From snapshot data to probabilistic load flow

In order to model the forecast uncertainty, the system infeeds based on point forecasts (operational snapshots) are transformed to forecast error distributions. The different realisations are defined as samples of the forecast error distributions, around the point forecast value. The simulation is performed based on the following three steps:

1. Fixed load (point forecast) at each of the buses is replaced by a load distribution indicating the load forecast uncertainty. The dataset includes active load and reactive load at each of the buses (indicating point forecasts). Normal distributions are assumed around the point forecasts for modelling the load forecast uncertainty, e.g., the active load at Bus b, denoted $P_{D,b}$, is given by

$$P_{D,b} \sim N(\mu_b, \sigma_b), \tag{6-4}$$

   where μ_b is the mean and σ_b is the standard deviation. The standard deviation is defined by analysis of measurement data. The reactive load $Q_{D,b}$ at bus b is chosen such that the $tan\varphi = \frac{Q_{D,b}}{P_{D,b}}$ remains constant. For each MC sample k a number is drawn from this active power distribution $P_{D,b}$, and is matched to the respective reactive power sample $Q_{D,b}$. These P-Q values indicate a specific realisation of the respective forecast uncertainty. Figure 49 presents the resulting distributions for a specific implementation on the 5 bus system (see Powell [47]). At this point it is important to emphasise that the proposed methodology allows to choose any kind of distribution, such as normal, beta or empirical distributions, and to depict any other more complex relationships between active and reactive power, depending on data availability.

2. Next, one provides information about how the buses are correlated in the form of a correlation matrix R. Data analysis confirms that the power infeeds and forecast errors at different buses are stochastically dependent. Neglecting this stochastic dependence can lead to severe underestimation of the system risk as shown in [39]. In a real-time application this correlation matrix should be based on constant updates of historical power system measures or meteorological data and on geographic data such as distance and orography. In [38] it is discussed how this can be achieved. At this point it is important to emphasise that the proposed methodology can work with any correlation matrix, once available.
3. Using copula theory (see below), MC samples are generated consistent to the marginal distributions and the stochastic dependence.

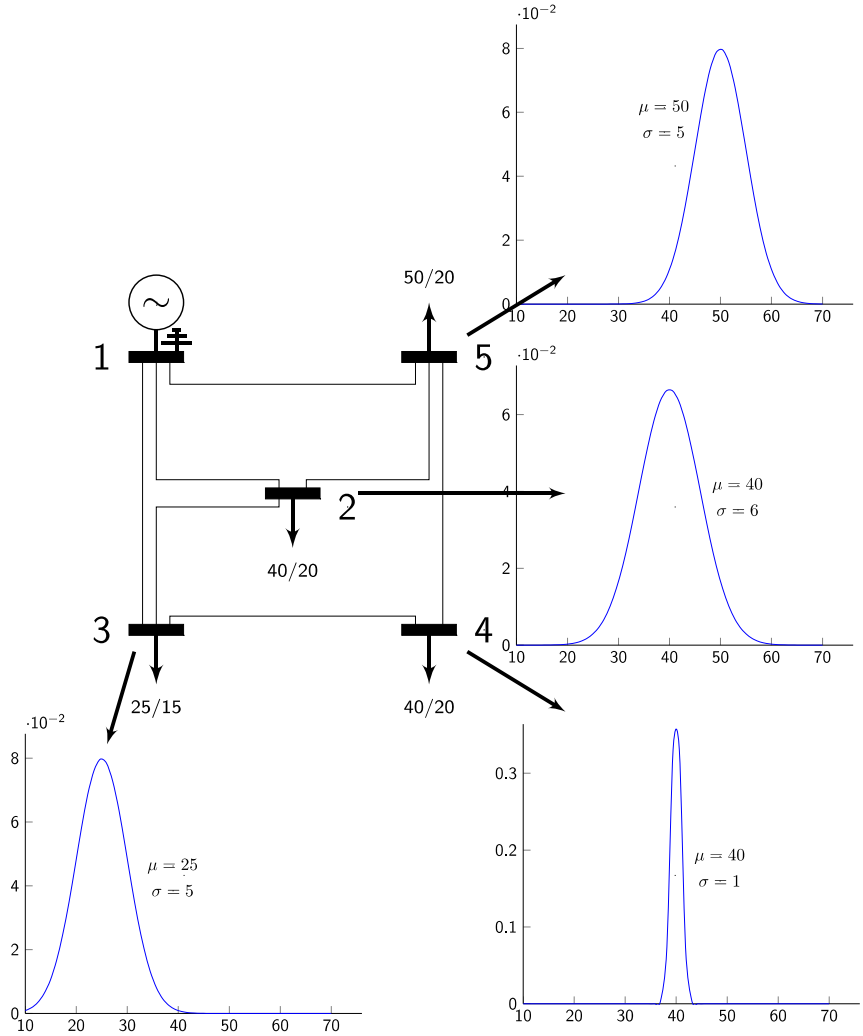

Figure 49: 5 bus system (Powell [47]).

6.1.3 Copula theory

Copulas are functions that "join together one-dimensional distribution functions to form multivariate distribution functions" and they were introduced by Sklar [48]. The multivariate distribution functions are such that the one-dimensional marginal distribution functions (marginals) are uniform on the interval $[0,1]$ [49]. For this reason in numerical simulation the copula theory is a powerful tool to generate MC samples based on the marginals whilst taking the dependency between the buses into account. In particular, they are very useful to capture stochastic phenomena of which the marginals are non-Gaussian [50].

6.1.3.1 Sklar's theorem

Sklar's theorem [48] states that for all cumulative distribution functions $F_{X_1 \dots X_n}(x_1, x_2, \dots, x_n)$ with one-dimensional marginals F_{X_i} $(i = 1, \dots, n)$ there exists a copula C such that

$$F_{X_1 \dots X_n}(x_1, \dots x_n) = C\big(F_{X_1}(x_1), \dots, F_{X_n}(x_n)\big). \quad (6\text{-}5)$$

Moreover, if all $F_{X_i}(i = 1, .. n)$ are continuous, then C is unique.

6.1.3.2 From marginals/data to uniforms/ranks

A random variable X is transformed into a uniform random variable U on $[0,1]$ by applying the cumulative distribution function (CDF) F_X. Similarly, by applying the inverse CDF F_X^{-1} (provided that the inverse exists) to a uniform random variable U on $[0,1]$ this random variable can be transformed into a random variable X, i.e.,

$$U = F(X) \Leftrightarrow X = F_X^{-1}(U). \quad (6\text{-}6)$$

In case F_X is not available, the empirical cdf may be used. To transform data from distributions to ranked variables (ranks) the data is sorted and the respective values are replaced by their positions in the sorted list.

6.1.3.3 Rank correlation

Since Pearson's well-known product-moment correlation coefficient, usually denoted by ρ, is not invariant under general cdfs, Spearman's rank correlation coefficient, denoted by ρ_r, is used instead. Spearman's correlation coefficient is defined as Pearson's correlation coefficient applied to the ranked variables, i.e., for random variables X_i with cdfs F_{X_i}, the rank correlation ρ_r is defined as

$$\rho_r(X_1, \dots X_n) = \rho\big(F_{X_1}(X_1), \dots, F_{X_n}(X_n)\big). \quad (6\text{-}7)$$

The rank correlation measures the monotonicity between random variables.

6.1.3.4 Sampling

The sampling of the system inputs is done as follows.

1. Analyse the stochastic dependence in the uniform/rank domain. From this analysis extract a correlation matrix R (see section 6.1.2);
2. Generate correlated ranks U_i $(i = 1, \dots, n)$ from the standard uniform distribution using a copula model and the provided correlation matrix R;
3. The correlated ranks U_i are transformed into marginal distributions by applying $F_{X_i}^{-1}$ to U_i $(i = 1, \dots,)$.

6.1.4 Deterministic security assessment model - flowchart

Figure 50 shows the DSA model flowchart. This process is followed for each MC sample of the system infeeds. The key components of the model are presented below.

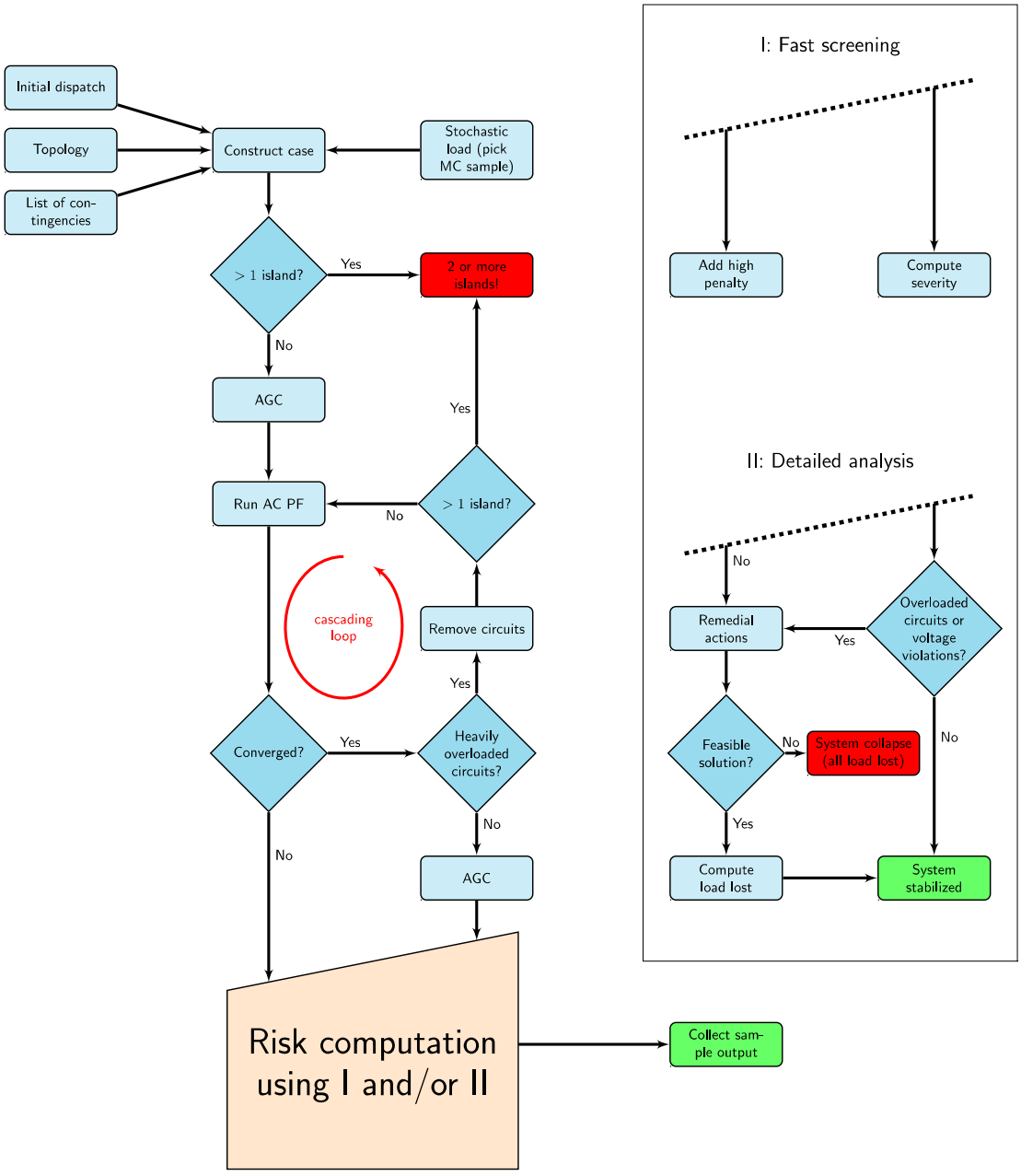

Figure 50: Flowchart for 1 MC sample.

6.1.4.1 DSA model inputs

The key inputs in the model are the system topology, the initial dispatch, the set of contingencies and the set of MC samples for the modelling of the uncertainty in the system infeeds. The set of contingencies are used to define the post-contingency state and in this implementation are coming from the preceding models presented in Chapters 2 and 4. Another implementation would allow to include them as stochastic variables and allow them to change for each MC sample, based on their outage probabilities. The initial

dispatch can be altered based on the different market regimes. For each MC sample the model assesses the system risk and allows capturing cascading events and system islanding.

6.1.4.2 Islanding

First, the algorithm verifies the existence of islanded networks and, if required, slack buses are added in order to enable the solution of the power flow (PF) equations. Next, a full AC PF computation is performed. If the AC PF does not converge, it is assumed that this indicates a severe system state and remedial actions such as redispatching and load shedding are needed to restabilise the system.

6.1.4.3 Cascading events

Since cascading overloads are often the generating causes of a system collapse, a mechanism is incorporated to capture cascading events. In our methodology we follow McCalley and use a mechanism based on hard limits, i.e., a circuit is outaged if the power flowing through it exceeds a predefined threshold. In particular, the following two assumptions are made:

- A circuit (transmission lines and transformers) is outaged if its complex power exceeds $1.50 \times$ the continuous rating;
- The circuit is outaged automatically and immediately; a TSO cannot perform any action.

If the AC PF does converge, it is checked whether there are heavily overloaded circuits, i.e., the flow through the circuit is at least $1.50 \times$ the continuous rating. If so, these circuits are removed from the system corresponding to immediate and automatic tripping. The process may repeat itself (as indicated by the red loop in Figure 50) until there are no heavily overloaded circuits anymore.

6.1.4.4 Automatic generation control (AGC)

After the cascading loop the power balance is restored using automatic generation control (AGC), see Section 6.1.6.3. If after AGC there are still overloaded circuits and/or voltage violations at the buses, remedial actions are required to restabilise the system. First it is verified if redispatching of generator power can resolve the problems; if not, redispatching in combination with load shedding is applied. To determine how to redispatch generation and how and where to shed load, an extended AC OPF is used, see Section 6.1.4.5. Herein load shedding is modelled with dispatchable loads. A clever usage of the AC OPF allows for finding a new economic dispatch which deviates minimally from the original dispatch and in which all voltage violations and circuit overloads are removed. The penalties for load shedding are set to high values such that load shedding is used only as a last resort.

6.1.4.5 Remedial actions

The methodology proposes automatically means to alleviate the system risk. The following remedial actions are incorporated:

1. Redispatching;
2. Load shedding.

However, it is important to notice that the methodology allows to incorporate other remedial actions as well, such as topology optimisation.

The methodology differentiates between four levels of risk:

1. No remedial actions are required; the system is stable
2. Redispatching: redispatching of generator power is necessary to alleviate circuits overloads and/or voltage violations at the buses
3. Redispatching + load shedding: redispatching is not enough to resolve the problems and in addition load must be shedded at 1 or more buses in order to restabilise the system.
4. System collapse: the system is under such a high level of stress that there are no means to restabilise the system anymore.

The methodology uses an extended AC optimal power flow framework to restabilise the system and to propose remedial actions.

AC optimal power flow framework

A major benefit of using an optimal power flow (OPF) framework for remedial actions is its great flexibility to model versatile correcting actions in an easy and proper manner. An obvious drawback of running an AC OPF problem is that it is considered to be computationally expensive (it is, say, 5 to 15 as expensive as a basic AC PF in case an interior point (IP) solver is used). Although heuristics may be much faster, (e.g., heuristics to alleviate circuit overloading, redispatching generation or load shedding), they do not guarantee optimality of the new operating point to any extent, and, which is worse, they may even detoriate the power system's overall stability. In contrast, by solving an AC OPF problem, a new operating state is found for which all constraints of the equipment (bus voltages, line ratings, generator power) are satisfied, in other words, the AC OPF guarantees a safe operating state, while, at the same, costs (e.g., costs for rescheduling of generation) are minimised.

Moreover, since computer processors become faster and faster each year, running an AC OPF problem in a real-time risk assessment program may actually become feasible in the very near future. For these reasons, in the proposed methodology, the AC OPF framework is adopted rather than heuristics.

The AC OPF takes the following form [14]. If we denote by

- N_B, N_G, N_L the number of buses, generators and circuits, respectively;
- θ, $|V|$ the voltage angle and voltage magnitude, respectively;

- $f_{P,g}$ and $f_{Q,g}$ the cost functions for active and reactive generation (which can be piecewise linear or polynomial functions);
- $P_{G,g}$, $Q_{G,g}$ the active and reactive power generated by generator g;
- P_D and Q_D the vectors of active and reactive demand at all buses (the vectors have size $N_B \times 1$);
- P_G and Q_G the vectors of active and reactive power injected at by the generators (the vectors have size $N_G \times 1$);
- $P_B(\theta, |V|)$ and $Q_B(\theta, |V|)$ the vectors of active and reactive injected power at the buses;
- C_G the generation connection matrix that shows for each bus which generators are connected (the matrix has size $N_B \times N_G$);
- $P_{line,ij}(\theta, |V|)$ and $P_{line,ji}(\theta, |V|)$ the vector of the circuit's power flows from bus i to j and from bus j to i (the vectors have size $N_L \times 1$); and
- X^{min} and X^{max} the safe lower and upper limit for a variable X, with X being a variable in $\{\theta_b, |V|_b, P_{line,ij}, P_{line,ji}, P_{G,g}, Q_{G,g}\}$,

then the default AC OPF problem is given by:

Minimise

$$\sum_{g=1}^{N_G} \left(f_{P,g}(P_{G,g}) + f_{Q,g}(Q_{G,g}) \right), \tag{6-8}$$

such that

$$P_B(\theta, |V|) + P_D - C_G P_G = 0, \tag{6-9}$$

$$Q_B(\theta, |V|) + Q_D - C_G Q_G = 0, \tag{6-10}$$

(Eq. (6-9) and (6-10) represent the PF equations, see Figure 51), and for all $l = 1,2,\ldots,N_L$:

$$|P_{line,ji}(\theta, |V|)| - P_{line,ji}^{max} \leq 0, \tag{6-11}$$

$$|P_{line,ij}(\theta, |V|)| - P_{line,ij}^{max} \leq 0, \tag{6-12}$$

and for all $b = 1,2,\ldots,N_B$:

$$\theta_b^{min} \leq \theta \leq \theta_b^{max}, \tag{6-13}$$

$$|V|^{min} \leq |V| \leq |V|^{max}, \tag{6-14}$$

and for all $g = 1,2,\ldots,N_G$:

$$P_{G,g}^{min} \leq P_{G,g} \leq P_{G,g}^{max}, \tag{6-15}$$

$$Q_{G,g}^{min} \leq Q_{G,g} \leq Q_{G,g}^{max}. \tag{6-16}$$

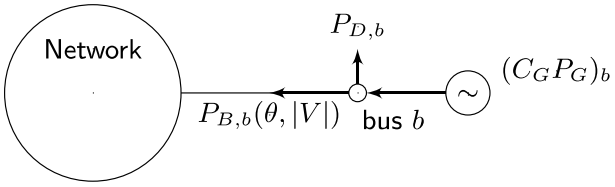

Figure 51: Power balance for active power.

Objective function alternative

In the default AC OPF formulation, the objective function f is the cost for active (and reactive) generation, see Eq. (6-8). In the context of remedial actions, however, it is more appropriate to minimise the shifted amount of generation as follows. If we denote by $P_{G,g}^{post}$ the active power from generator g after redispatching, and $P_{G,g}^{pre}$ is the active power from generator g before redispatching then instead we minimise the objective function

$$\sum_{g=1}^{N_G} w_g (P_{G,g}^{post} - P_{G,g}^{pre})^2 , \tag{6-17}$$

where w_g are weighting factors. This results in a new active generation profile (post) which is "closest" to the old generation profile (pre). The weighting factors can be used to influence which generators are used for redispatching.

6.1.5 Risk metrics: fast screening and detailed analysis

As discussed, the model incorporates a dual representation of system risk, by the combination of two complementary risk metrics:

I. Severity;
II. Lost Load.

The main advantage of the risk measure I is its computational speed whereas the main advantage of risk measure II is that it readily incorporates remedial actions for reduction of system risk.

6.1.5.1 Risk measure I: Severity

The first risk measure is based on the concept of severity functions [32,36]. This risk measure has been used in the AC risk assessment method in Deliverable D4.1. In this work severity functions are used for power flow through the circuits and voltages at the

buses. We follow an implementation of linear severity functions, as proposed in related literature. Other type of severity functions, such as exponential or quadratic functions, can be implemented for all or a set of the system circuits and buses to increase the sensitivity of the algorithm to specific system areas.

Severity function for overloaded circuits. Suppose that the continuous rating for circuit i is $P_{i,max}$ [pu]. Then, by computing the load factor

$$f = \frac{P_i}{P_{i,max}}, \tag{6-18}$$

where P_i is the actual power flowing through the circuit, the extent to which the circuit is loaded is obtained. In case the power flow through a circuit reaches its continuous rating, the severity starts to increase, see Figure 52; the higher the power flow through the circuit, the higher the severity. The severity is defined to be zero up to $f = 0.9$, grows linearly above this threshold and for $f = 1.0$ the severity is exactly 1.

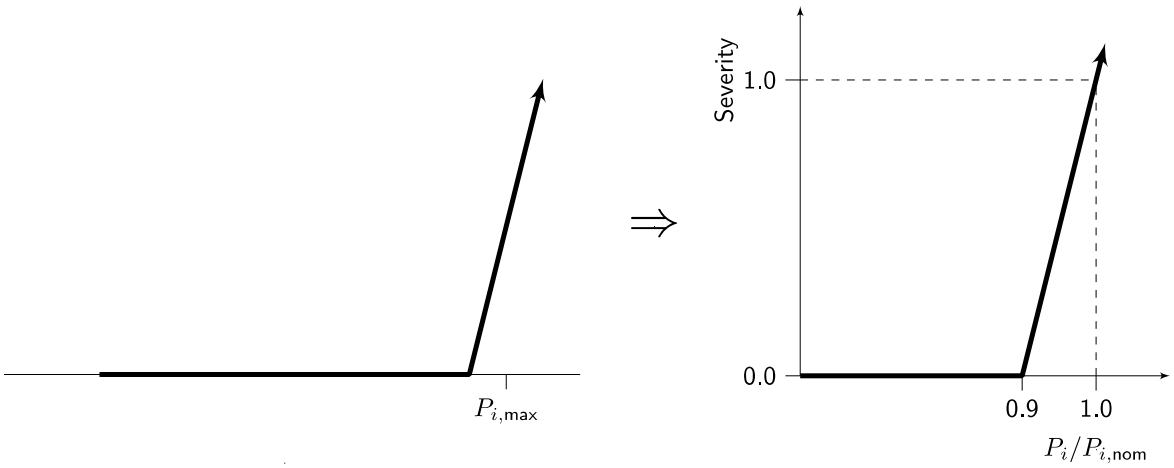

Figure 52: Severity function for overloaded circuits.

Severity function for voltage at the buses. Similarly, a severity function has been defined for the voltage magnitudes at the buses. Suppose that the safe operating range for a bus i is $[V_{i,min}, V_{i,max}]$ [pu] with a nominal voltage $V_{i,nom}$ right in between; $V_{i,nom} = (V_{i,min} + V_{i,max})/2$ [pu]. The width of the range is thus $w_i = (V_{i,max} - V_{i,min})/2$ [pu]. The voltage can either be too low or too high; by computing the number

$$f = \frac{V_i - V_{i,nom}}{w_i}, \tag{6-19}$$

where V_i is the actual voltage at the bus, it is found whether the voltage is too low or too high as follows. In case $f \epsilon [-1,1]$ the voltage is within the safe range; in case $f < -1$ the voltage is too low and in case $f > 1$ the voltage is too high. Accordingly, the severity for too high voltage is defined to be zero up to $f = 0.9$, grows linearly above this threshold and for $f = 1.0$ the severity is set to exactly 1, see Figure 53.

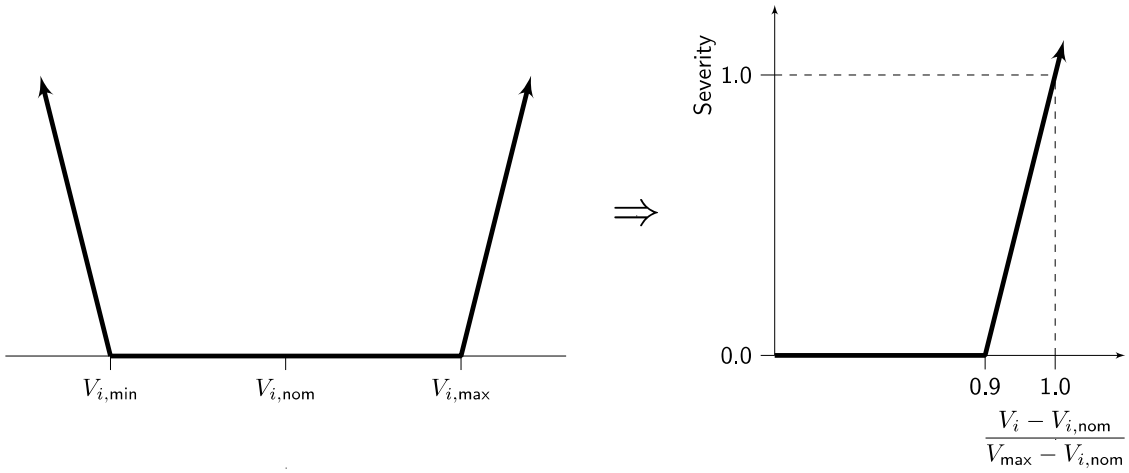

Figure 53: Severity function for too low and too high voltage.

6.1.5.2 Risk measure II: Lost Load

The second risk measure is based on the notion of Lost Load. This risk measure has been used in the AC risk assessment method in Deliverable D4.2. As can be seen in Section 6.1.4.5 the algorithm differentiates between four levels of risk:

1. No remedial actions;
2. Redispatching;
3. Redispatching + load shedding;
4. System collapse.

Samples with risk levels 2 or 3 contribute to the expected amount of shifted active power. For each sample k having either a risk level 2 or 3 the RMS value of shifted active power, denoted SP_k, is computed as follows:

$$SP_k = \sqrt{\frac{1}{N_G}\sum_{g=1}^{N_G}(P_{G,g}^{post} - P_{G,g}^{pre})^2}, \tag{6-20}$$

where N_G is the number of generators, $P_{G,g}^{post}$ is the active power from generator g after redispatching, and $P_{G,g}^{pre}$ is the active power from generator g before redispatching. Accordingly, the expected amount of shifted active power is then:

$$E[shifted\ active\ power] = \frac{1}{N}\sum_{k=1}^{N} SP_k, \tag{6-21}$$

where N is the number of MC samples. Similarly, samples with risk levels 3 or 4 contribute to the expected amount of Lost Load. For each sample k having a risk level 3 the amount of Lost Load, denoted LL_k is computed as follows:

$$LL_k = \sum_{b=1}^{N_B} (P_{D,b}^{post} - P_{D,b}^{pre}), \quad (6\text{-}22)$$

whereas for sample k having a risk level 4, i.e., a system collapse, this number LL_k is computed as:

$$LL_k = \sum_{b=1}^{N_B} P_{D,b}^{pre}, \quad (6\text{-}23)$$

i.e., all load is lost. In the formulas (6-22) and (6-23) above is N_B the number of buses, $P_{D,b}^{post}$ the active power demand at bus b after load shedding, and $P_{D,b}^{pre}$ the active power demand at bus b before load shedding. Accordingly, the expected amount of Lost Load is then:

$$E[Lost\ Load] = \frac{1}{N} \sum_{k=1}^{N} LL_k, \quad (6\text{-}24)$$

where N is the number of MC samples.

6.1.6 Implementation details

In this section follow details on the implementation of the methodology.

6.1.6.1 A globally convergent AC PF solver

It was found that the default AC PF solver in MATPOWER has difficulties to converge for system states that are severe. Since the proposed methodology relies heavily on a robust AC PF solver to work well, the AC PF solver in MATPOWER is replaced by an own, more robust, implementation based on MATLAB's routine fsolve(). This solver proved to be robust on an extended range of case studies as well as on large scale systems.

6.1.6.2 Load shedding using dispatchable loads

MATPOWER allows to model load shedding at the buses by incorporating so-called dispatchable loads in an extended AC OPF optimisation problem as follows:

1. One defines a list of buses at which it is allowed that load is shed.
2. The fixed load at these designated buses is replaced by generators having a negative output, hence taking power away from the network rather than injecting it, i.e., if the active and reactive load at a bus b is $P_{D,b}$ MW and $Q_{D,b}$ MVar, respectively, the newly introduced generator at bus b will operate default at $-P_{D,b}$ MW and $-Q_{D,b}$ MVar, just like if there were a load connected. Default these extra generators are switched "off".

3. Next one needs to also define generator cost functions for these extra generators. This can be done with a lot of freedom, but it is essential that the cost factors are set to large numbers, such that load shedding will be used as a last resort only.
4. One has obtained the exact same power system, however, with the big difference that it is now possible to adjust the amount of load demanded at each of the designated buses by: i) setting the appropriate cells in the list of loads, corresponding to active and reactive load, to zero, and, ii) choosing a dispatch for the newly introduced generators and switching them to "on", hence the name dispatchable loads.
5. The settings for the dispatchable loads are found by solving the extended AC OPF problem. Since it is expensive to adjust the dispatchable loads (see Step 3), the AC OPF will not touch upon them unless no feasible solution can be found without adjustment of these.

6.1.6.3 Automatic generator control

Some form of automatic generator control (AGC) is required to adjust the generators for stochastic load fluctuations. In our algorithm *zone-wise AGC* has been implemented (see also Figure 50): per zone the generators are adjusted by ratio to possible imbalances due to load changes. However, just like in reality, depending on how dramatically the overall load profile changes, AGC can or cannot follow the load properly; in the latter case manual redispatching of generation is required to avert higher risk.

Below three scenarios are given to illustrate this. In the first two scenarios, zone-wise AGC is sufficient to balance the system; in the third scenario generation redispatching is required in addition. The test system used is the IEEE 118 bus system, see Appendix A. The initial dispatch is determined by an AC OPF run. In Figure 54 the initial load profile is shown and in Figure 55 the redispatch based on AC OPF is shown.

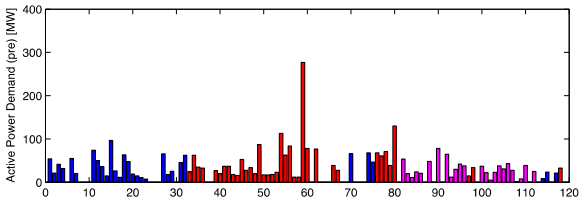

Figure 54: Initial load profile (blue = Zone 1, red = Zone 2, magenta = Zone 3).

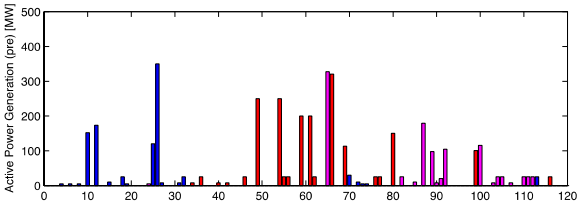

Figure 55: Initial generation profile (blue = Zone 1, red = Zone 2, magenta = Zone 3).

Scenario A: increase of load level per zone

In this first scenario the load level in Zone 2 (red) is increased by a factor 1.3, the load level in Zone 3 (magenta) is reduced by a factor 0.7, while the load level in Zone 1 (blue) is kept constant, see Figure 56 and Figure 57.

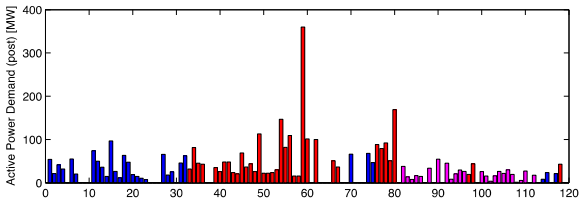

Figure 56: Changed load profile in Scenario A (blue = Zone 1, red = Zone 2, magenta = Zone 3).

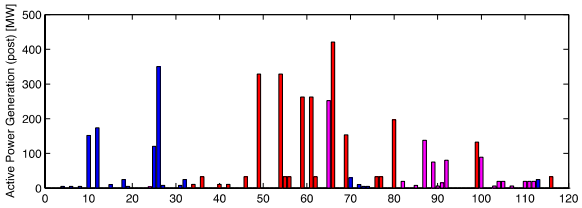

Figure 57: Changed generation profile in Scenario A (blue = Zone 1, red = Zone 2, magenta = Zone 3).

In Figure 58 the active power demand and in Figure 59 the active generation is shown per zone initially and after change of load profile and AGC. As it can be seen from the figure, the generators in Zone 2 deliver more power to provide for the local increase in load; in Zone 3 the generators are tuned a bit down because of the local decrease in load.

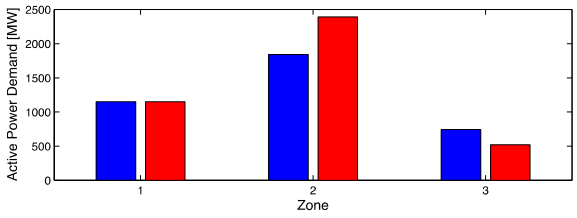

Figure 58: Zone-wise power demand in Scenario A (blue = pre, red = post).

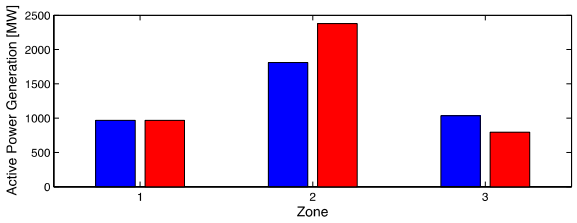

Figure 59: Zone-wise generation in Scenario A (blue = pre, red = post).

If we compare Figure 54 and Figure 56 we observe that in this first scenario the overall shape of the load profile did not change dramatically, which results in zero severity according to the screening tool; hence the generators are capable of following the load; the generator profile matches the load profile very well and, therefore, no redispatching is required.

Scenario B: stochastic load with low forecast error

In this scenario the load profile is changed as follows. From a multivariate normal distribution a new load profile is sampled using the copula theory. A correlation factor of $\rho_r = 0.5$ is taken for each zone. Further, $\sigma_b = 0.1\mu_b$ for buses $b = 1,2,\ldots,118$, where μ_b is the mean active load at bus b, just as it is provided in the data, see Appendix A, and σ_b is the corresponding standard deviation. In Figure 60 the changed load profile is shown and in Figure 61 the changed generator profile after AGC is shown.

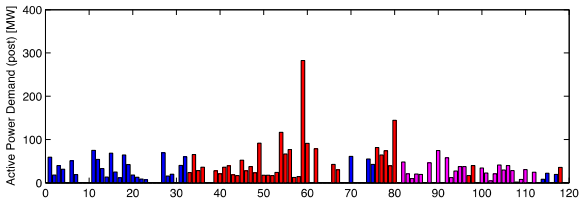

Figure 60: Changed load profile in Scenario B (blue = Zone 1, red = Zone 2, magenta = Zone 3).

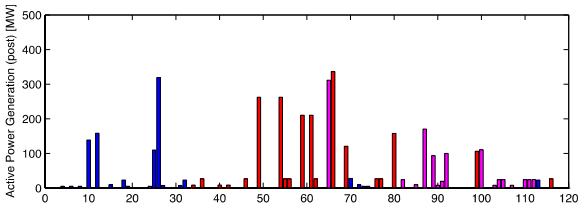

Figure 61: Changed generation profile in Scenario B (blue = Zone 1, red = Zone 2, magenta = Zone 3).

In Figure 61 the active power demand and in Figure 63 the active generation is shown per zone initially and after change of load profile and AGC. Again the generators can follow the load and the severity is low according to the screening tool: overload severity of 0.034 and voltage severity of 0.

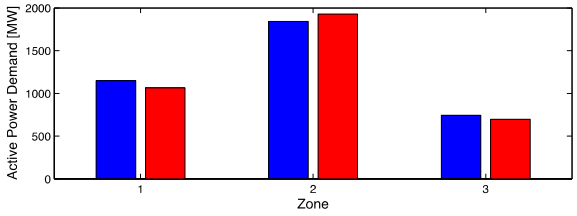

Figure 62: Zone-wise power demand in Scenario B (blue = pre, red = post).

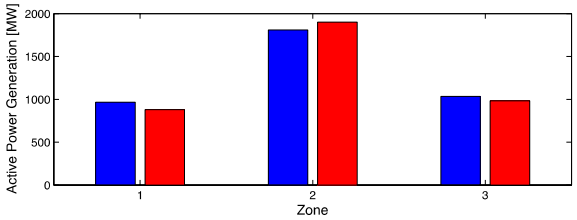

Figure 63: Zone-wise generation in Scenario B (blue = pre, red = post).

Scenario C: stochastic load with high forecast error

In this scenario the load profile is changed more dramatically due to a much higher forecast error; in this scenario $\sigma_b = \mu_b$ is taken for buses $b = 1,2,\ldots,118$. In this way a completely different load profile is obtained.

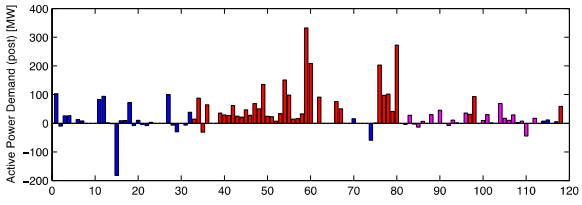

Figure 64: Changed load profile in Scenario C (blue = Zone 1, red = Zone 2, magenta = Zone 3).

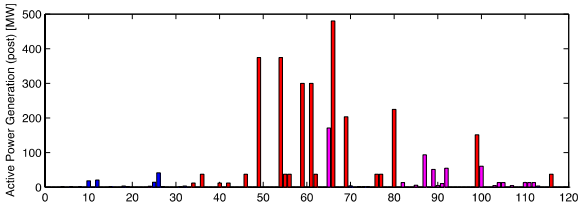

Figure 65: Changed generation profile in Scenario C (blue = Zone 1, red = Zone 2, magenta = Zone 3).

In Figure 64 the changed load profile can be seen and in Figure 65 the updated generator profile after AGC. If we compare Figure 54 and Figure 64 then we see that the shape of the load profile has changed a lot. In Figure 66 the power demand and in Figure 67 the generation is shown for each zone.

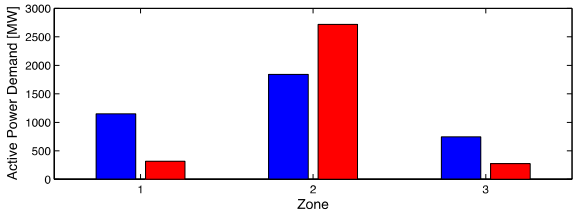

Figure 66: Zone-wise power demand in Scenario C (blue = pre, red = post).

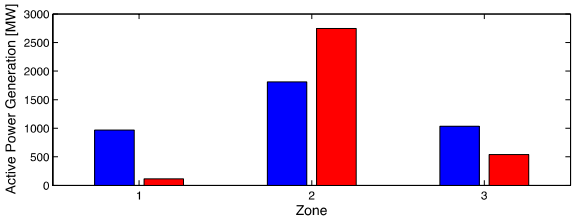

Figure 67: Zone-wise generation in Scenario C (blue = pre, red = post).

Because of the great difference in shape of the load profile, the generators cannot follow the load properly despite AGC. This can be seen from the severity computed by the screening tool: we find an overload severity of 0.3446 and a voltage severity of 0.0040. In addition generation redispatching is needed to obtain a system state with lower risk.

6.1.6.4 HVDC lines

Figure 68 shows a simplified model of the HVDC line as it is used in the methodology.

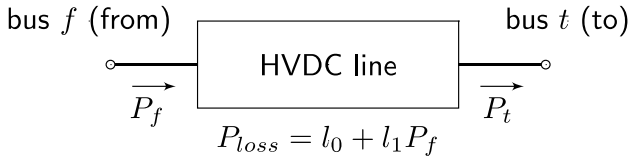

Figure 68: HVDC line model.

In this model, the power injected at the two buses f (from) and t (to) is known; the power losses are given by the formula

$$P_{loss} = l_0 + l_1 P_f \tag{6-25}$$

where P_f is the power injected at the f bus. Most commonly an HVDC line is modelled as the set of two generators with joined outputs, see Figure 69.

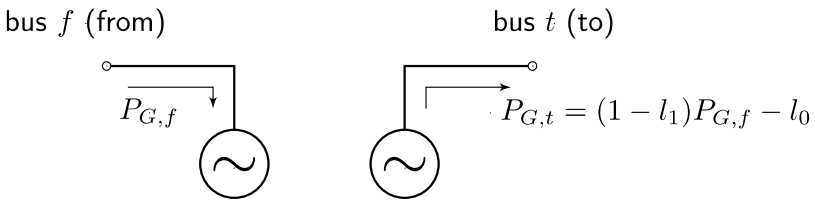

Figure 69: HVDC line equivalent generator model.

One of the generators is extracting power (negative injection) at bus f, and one of them is injecting power from the network at bus t, considering the existing losses. Using Eq. (6-25) the generator outputs are related as follows:

$$P_{G,t} = P_{G,f} - P_{loss} = (1 - l_1)P_{G,f} - l_0, \quad (6\text{-}26)$$

where $P_{G,t}$ is the generator at bus t (to) and $P_{G,f}$ the generator at bus f (from). For the generators the voltage magnitude and injected active power are specified, and the reactive power and voltage angle are computed by the PF equations (PV bus). Although an HVDC line cannot transmit reactive power, the equivalent generators may inject reactive power into the network.

In case of an HVDC lines it is necessary to provide the coefficient l_1 in Eq. (6-25) being the DC equivalent of the resistance in an HVAC line. Typically, l_1 is assumed to be very small ($l_1 \ll 1$).

6.2 Experimental setup

In this section the experimental setup is discussed. We first describe the test systems used for the experiments, followed by a description of the hardware and implementation environment and finally a presentation of how the approach adopted for the presentation of results.

6.2.1 Test systems

In this work two test systems were utilised:

1. The IEEE 118 bus system: a commonly used test system in power system studies; This well known test system is used to test the results of our methodology.
2. The UCTE 2713 bus system: a test system based on the UCTE country data as a result of combined efforts of all Umbrella partners. This large-scale realistic test system is used to test the applicability of our methodology on a real system.

6.2.1.1 IEEE 118 bus system

More information can be found in the Appendix.

6.2.1.2 UCTE 2713 bus system

The UCTE 2713 bus system is a reduced network equivalent of the UCTE system based on actual DACF data sets provided by the Umbrella partners. The UCTE 2713 bus system consists of 2713 buses (of which 1181 buses have active load connected), 458 generators and 4765 branches. Moreover, the test system consists of 14 zones of which Zone 1 are border nodes and the zones 2 to 14 represent different European countries.

Based on snapshots listed as critical by the TSOs, two cases were identified for detailed study, namely:

1. 08-02-2012 at 12:30: A moderately critical situation; the situation was considered to be critical by Amprion;
2. 22-08-2012 at 07:30: A very critical situation according to all TSOs. This test case is also used by the iTesla project.

In this report only the second test case is considered.

6.2.2 Testing hardware and software environment

The methodology proposed has been implemented in MATLAB using the package MATPOWER [14]. All experiments were performed on a desktop computer equipped with an Intel i7 3930K processor with 6 cores running at 3.2GHz and 16 GB DDR-3 RAM, running Ubuntu 14.04.

6.2.3 Visualisation of results

The main output of the RBSA method is the assessment of system risk. In order to allow this information to be efficiently used by TSOs, the following plots and graphs are generated:

- Iso-risk plots;
- Probability bar graphs.

6.2.3.1 Iso-risk plots

As the name reveals, *iso-risk* plots consist of curves along which the risk is constant. Using this information, the TSO can assess the current and expected risk level of the system at a specific point in time and plan the actions necessary to steer the system in a lower risk area. Iso-risk curves are constructed by a sensitivity analysis on main system control parameters, the so-called *study parameters*, such as forecast uncertainty, correlation and generator output. The iso-risk plots are generated as follows.

- A two-dimensional grid is defined consisting of $11 \times 11 = 121$ grid points. On the two axes are different study parameters, e.g., on the x-axis: forecast uncertainty and on the y-axis: correlation;
- For each of the 121 grid points an MC simulation is performed with N samples, hence in total $121N$ MC samples are computed. Each MC samples follows the flowchart as presented in Figure 50;
- For each grid point the mean, standard deviation and probabilities for the desired quantities are computed using Eq. (6-1) to (6-3);
- The mean values are stored for the 121 grid points and interpolation is used to compute a smooth iso-risk surface using these points. Probability bar graphs

6.2.3.2 Probability bar graphs

In order to visualise how the overall risk is composed, stacked bar graphs are constructed that show the probabilities of each of the four levels of risk, see Sections 6.1.4.5 and 6.1.5.2. Such a stacked bar graph can be generated for each of the 121 grid points in the iso-risk plot (or in between using interpolation). The grid points for which a bar graph is constructed are labelled, in most studies the grid points are selected along the xy-axis.

6.2.3.3 Example

Below in Figure 70 an example is presented of how the iso-risk plot and stacked bar graph are used together.

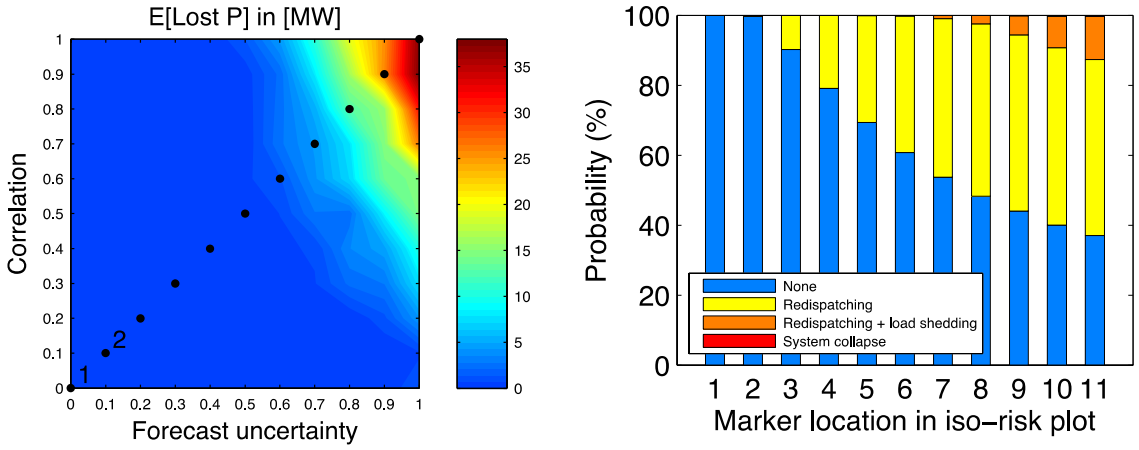

Figure 70: Example iso-risk plot (left) and stacked bar graph (right). The bars in the bar graph correspond with the markers in the iso-risk plot (1,2, ..., 11).

On the left is the iso-risk plot for lost active load (in [MW]). From the bar graph on the right it can be seen that the Lost Load is mainly caused by load shedding in the upper right corner which has high risk, i.e., high forecast uncertainty in combination with high correlation.

6.3 Case studies

In this section five case studies are presented, aiming in showing how the developed tool can be used for the assessment of power system security and focus in more detail on the following aspects:

a) Investigate the impact of forecast uncertainty in the assessment of the system risk focusing on the impact of forecast accuracy and the degree of spatial correlation between forecasts.
b) Investigate how different market models impact the system risk; how can market integration help with increasing the system operational security.

c) Investigate the role of PFCCs on enhancing the power system's robustness; under which conditions and operational framework can PFCCs be used to reduce system risk?
d) Investigate the role of cross-border flows on power system security: how can the proposed tool be used to trace the set points for cross-border flows that lead to a reduced overall system risk?
e) Investigate the applicability on a large-scale realistic network; can the method be applied in a realistic setup and how can the computational speed be reduced?

For the first four case studies we use the IEEE 118 bus system (see Appendix); for the case study 5 we utilise the UCT 2713 bus system (see Section 6.2.1.2 for more information).

The following five studies were performed:

1. **Central dispatch system (reference case).** This case study simulates a central dispatch system in presence of uncertainty. We investigate the impact of correlation between forecasts and/or forecast accuracy on the system risk. Moreover, this case will serve as a market reference for the following studies where different market designs are assessed.
2. **Self-dispatch system.** This case study assesses the risk for a self-dispatch system i.e., where the market is cleared without any consideration of intrazonal transmission constraints. We compare the results with the case of a central dispatch system (Case Study 1) to understand the possible benefits from a more integrated market setup.
3. **HVAC replaced by HVDC.** This case study investigates the role of PFCCs. In particular, one HVAC 345 kV line is replaced by a HVDC line of similar capacity. We choose this setup so we can isolate the impact of flow controllability to reduce the system risk.
4. **Generator study**. This case study shows how the proposed tool can be used to optimise cross-border exchanges for increasing system security. We shift generation between zones by adjusting the set points of different generators in each zone and show which set points reduce the system risk.
5. **Large system.** The primary goal of this study is to show how the proposed RBSA methodology can handle realistic scale systems. For this the UCT 2713 bus system developed by Umbrella partners is used. It is shown that the methodology is already fast, even run an a desktop computer and without any optimisations for speed and further discuss how further speed optimisations are feasible.

Note that the Case Studies 1, 2 and 3 are closely related. Therefore, the ranges for the iso-risk plots have been taken the same. In this way the reduction of risk translates to a plot which is "more blue"; the red zone (high risk) becomes smaller.

For Case Studies 1 to 4 the following correlation matrix is used, see Figure 71.

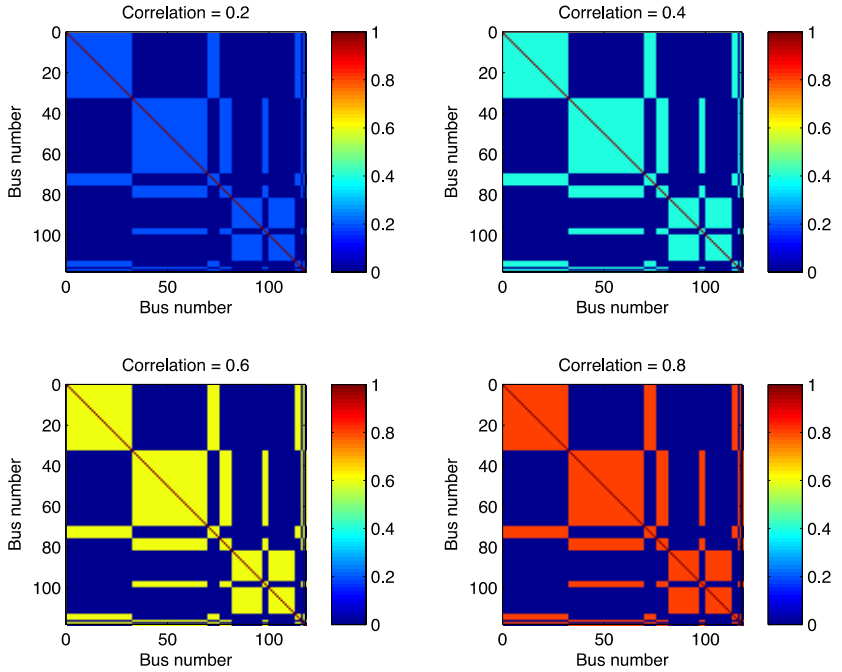

Figure 71: Correlation matrix for Case Studies 1 to 4 for different values of ρ_r.

For Case study 5 the correlation matrix shown in Figure 72 is used. This correlation matrix is based on the distances between the capitals of the European countries; countries that are close to each other (e.g., Netherlands and Belgium) are considered to be strongly dependent and countries that are further away from each other (e.g., Netherlands and Poland) are considered to be weakly dependent.

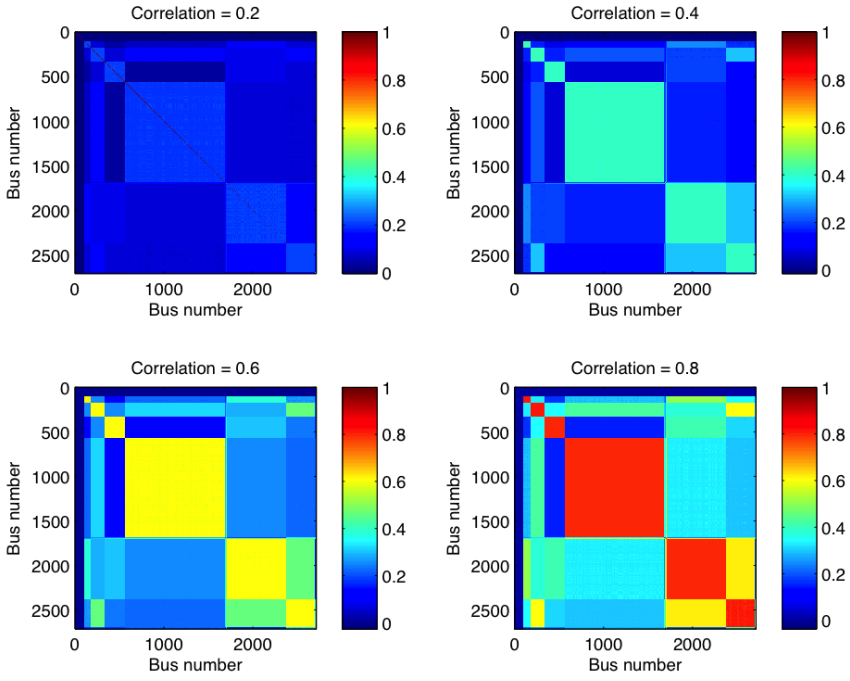

Figure 72: Correlation matrix for Case Study 5 for different values of ρ_r.

The correlation matrices are designed in order to a be able to perform the case studies and to easily monitor the impact of correlation on the system risk. It must be emphasised however that the proposed RBSA methodology can work with *any realistic* correlation matrix once available.

In a real-time application the correlation matrices should be build up based on constant updates of historical meteorological data in order to capture phenomena as wind direction and wind speed, and on geographic data such as distance and orography. In [38] it is discussed how this can be done.

6.3.1 Case study 1: Central dispatch system (reference case) and investigation of impact of uncertainty

In this case study we simulate a central dispatch system in presence of uncertainty. Our starting point is an operational snapshot where significant cross-border flows appear in the system. For this case we investigate how forecast uncertainty impacts system risk, by making a series of experiments for different levels of forecast uncertainty and for different degrees of spatial correlation between the forecasts. This case study moreover serves as a reference for the following studies.

6.3.1.1 Simulation setup

We consider the IEEE 118 bus system, as described in the Appendix. The following modifications are made:

i) The system is divided into three zones as seen in Figure 73;
ii) The load in Zone 2 is multiplied by a factor 2;
iii) The generator capacity in Zone 2 is limited to $0.8 \times$ the original capacity;
iv) The continuous ratings of the transmission lines from Zone 1 to Zone 2 and from Zone 3 to Zone 2 are increased by a factor 2;
v) The initial dispatch P_0 is obtained by a solution of an AC OPF problem with global cost minimisation, representing an optimal central dispatch system.

By these changes, an operational snapshot with increased cross-border flows is obtained. In particular, due to the limited generation capacity in Zone 2, the demand in Zone 2 is served by generators from Zone 1 and Zone 3.

The key characteristics of the deterministic security assessment (DSA) algorithm implementation are:

i) A zone-wise AGC is implemented in the 3 zones considered;
ii) Redispatch is based on a AC OPF, with main objective objective to minimise the deviation from the initial dispatch P_0;
iii) Load shedding is allowed at all buses, with a cost penalty of 10000 per MW.

Finally, the forecast uncertainty is modelled in the Monte-Carlo simulation as follows:

i) All loads are considered to be uncertain and correspond to a mix between load and renewables connected at a lower voltage levels. We assume that the forecast

errors are normally distributed, and that the standard deviation σ_b of each load is ranging as a percentage of the point forecast μ_b; i.e., σ_b ranges in steps of $\frac{1}{100}\mu_b$ within the range $0 \leq \sigma_b \leq \frac{1}{10}\mu_b$;

ii) Loads are considered to be correlated, assuming that loads in each zone are correlated while loads across different zones are not correlated. A zone-wise correlation matrix is therefore assumed and the degree of correlation is considered a parameter which is changed in different simulations from 0 (independent infeeds) to 1 (comonotonic infeeds) with a step of 0.1, see Figure 71.

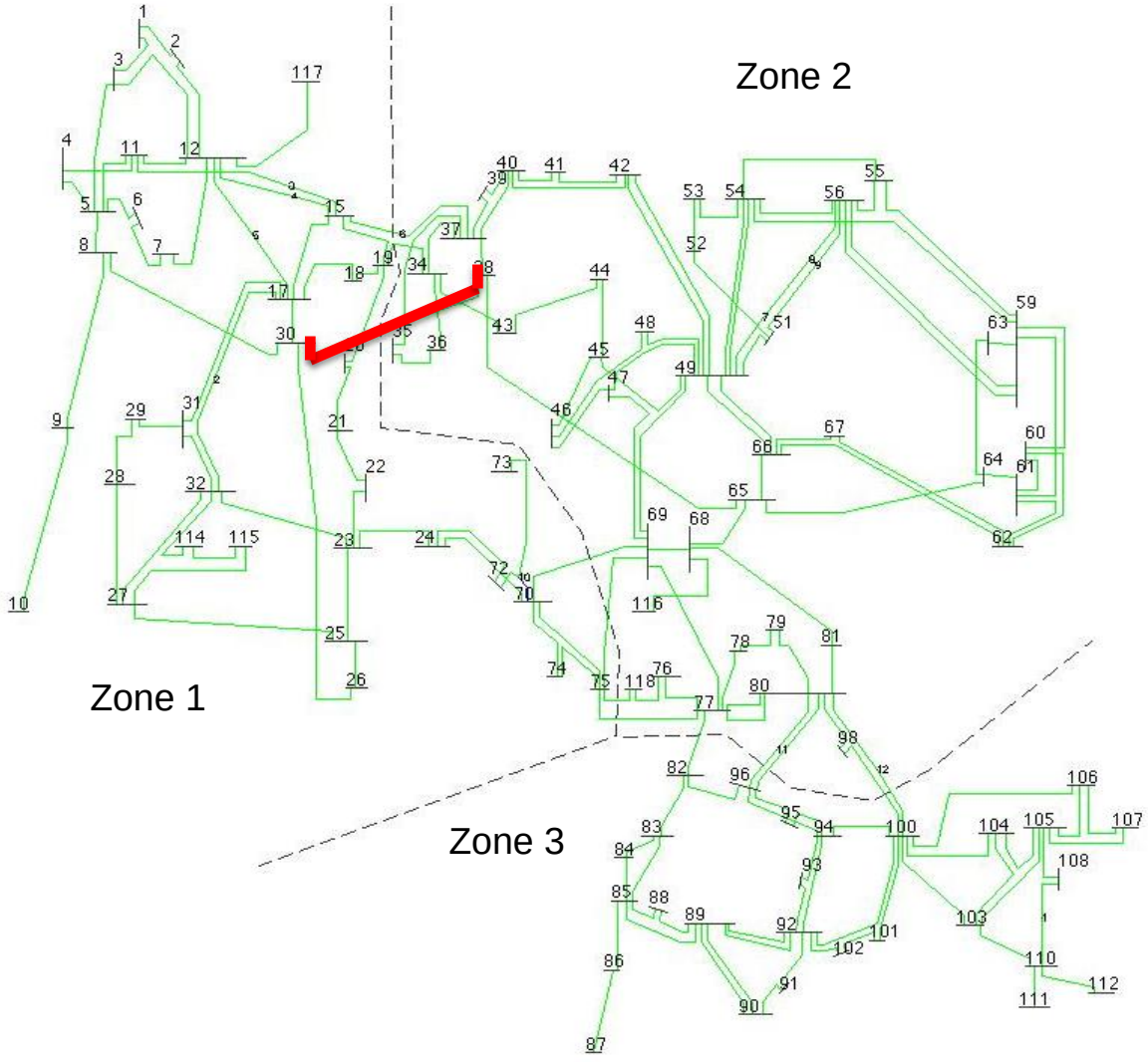

Figure 73: The 3-zone 118 bus test system. Highlighted in red: In Case Study 3 the 345 kV HVAC line connecting buses 30 and 38 is replaced by an HVDC link with the same capacity to improve the robustness of the power system .

In Table 10 an overview of the simulation settings for this case study is provided.

Table 10: Simulation settings for Case Study 1.

Test system	IEEE 118 bus	
	Adjustments:	
	Load	Zone 2: $2.0\times$ more active and reactive load.
	Generator capacity	Zone 2: reduced to $0.8\times$ original capacity.
	Transmission lines	Continuous rating of the transmission lines from Zone 1 to Zone 2 and from Zone 3 to Zone 2 are increased by a factor 2.
	Dispatch (P_0)	AC OPF (objective: minimal costs)
DSA setup	Type of AGC	Zone-wise, 3 zones
	Redispatch	AC OPF (objective: minimal deviation from P_0)
	Load shedding	At all load buses, cost penalty: 10,000 per MW.
Monte-Carlo setup	Uncertainty range modelling:	Forecast uncertainty, range: $0 \leq \sigma_b \leq \frac{1}{10}\mu_b$ (x-axis iso-risk plots).
		Correlation, range: $0 \leq \rho_r \leq 1$ for each zone (y-axis iso-risk plots).
	Correlation matrix	Zone-wise, 3 zones, zones are independent, see Figure 71.
	Nr. MC samples	10,000
Runtime	Fast screening (I)	4480 seconds (= 1 hour 15 minutes)
	Detailed analysis (II)	17560 seconds (= 4 hours 52 minutes)

6.3.1.2 Results

As discussed in section 6.2.3.1, in total 121 Monte-Carlo Simulations were performed in order to estimate the impact of changing parameters (11 values of forecast uncertainty x 11 values of degree of correlation). Each simulation involves the estimation of 10000 samples of the RBSA model. The results are depicted in a 11x11 grid in the form of iso-risk plots. The total simulation time is 4480 seconds (= 1 hour 15 minutes) for the screening tool and 17560 seconds (= 4 hours 52 minutes) for the detailed analysis tool.

Figure 74 and Figure 75 present the iso-risk plots for voltage and overload severity respectively as they are obtained by the screening tool. Figure 76 and Figure 77 present the iso-risk plots for lost active load in [MW] for lost reactive load in [Mvar] respectively based on the detailed analysis. In Figure 78 the iso-risk plot is shown for shifted active generator power in [MW] and in Figure 79 the iso-risk plot is shown for lost shifted reactive generator power in [Mvar]. The shifted generation indicates to what degree the current dispatch needs to be changed in order to alleviate circuit overloads and voltage violations, see Eq. (6-21).

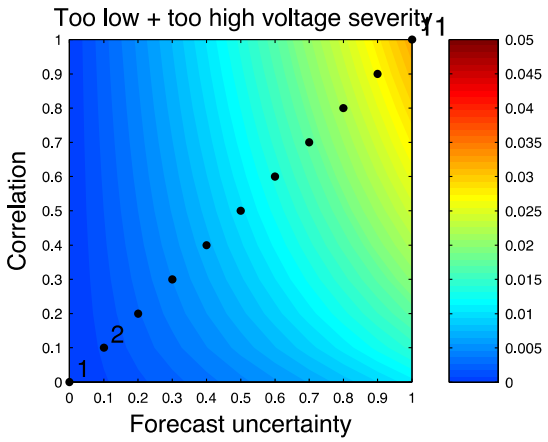

Figure 74: Voltage severity for Study Case 1 (output screening tool).

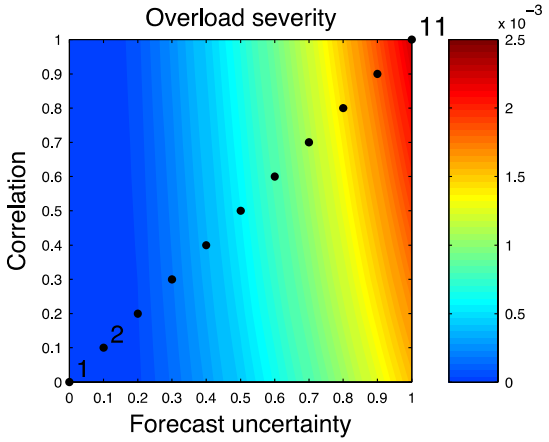

Figure 75: Overload severity for Study Case 1 (output screening tool).

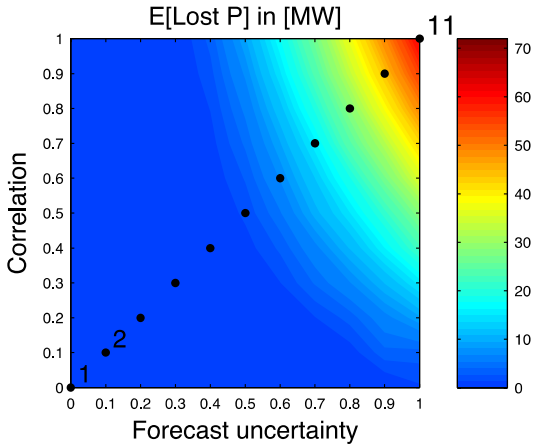

Figure 76: Lost active load for Study Case 1 (output detailed analysis).

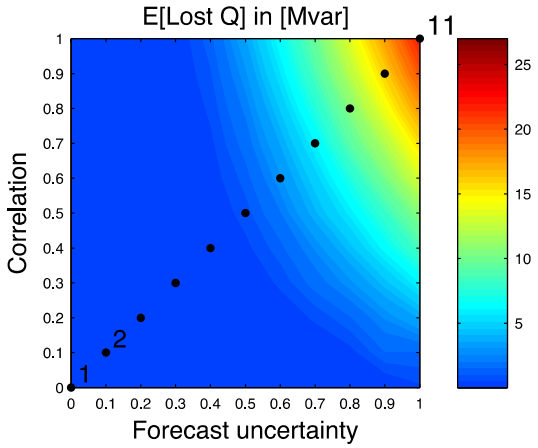

Figure 77: Lost reactive load for Study Case 1 (output detailed analysis).

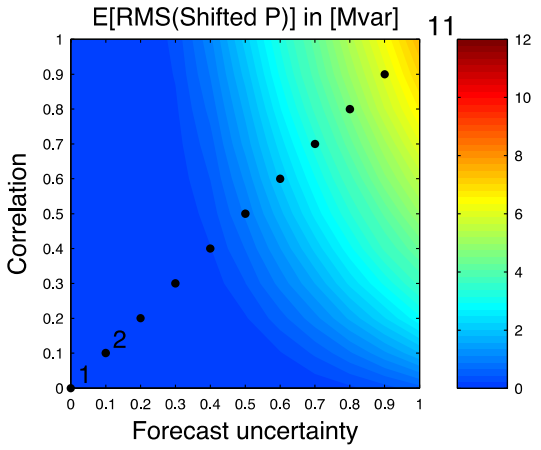

Figure 78: Shifted active generator power for Study Case 1 (output detailed analysis).

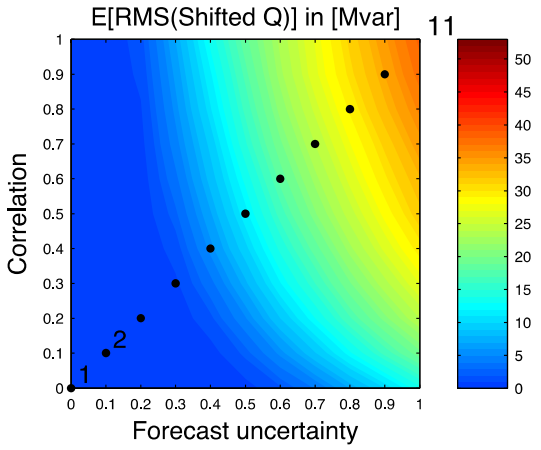

Figure 79: Shifted reactive generator power for Study Case 1 (output detailed analysis).

In Figure 80 the four levels of risk and their corresponding probabilities are presented. In Figure 81 the probability of cascading events, overloaded circuits and voltage violations are shown.

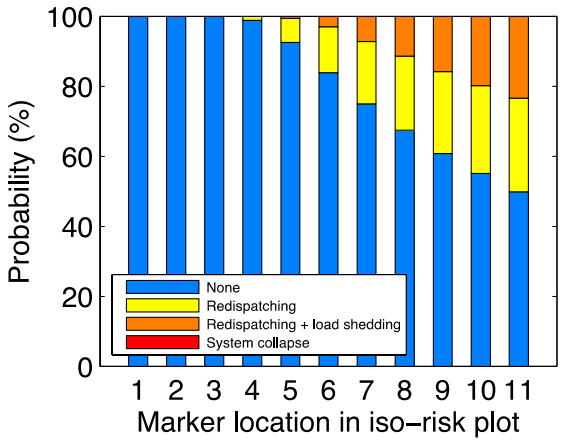

Figure 80: Four levels of risk and their corresponding probabilities for Study Case 1 (output detailed analysis).

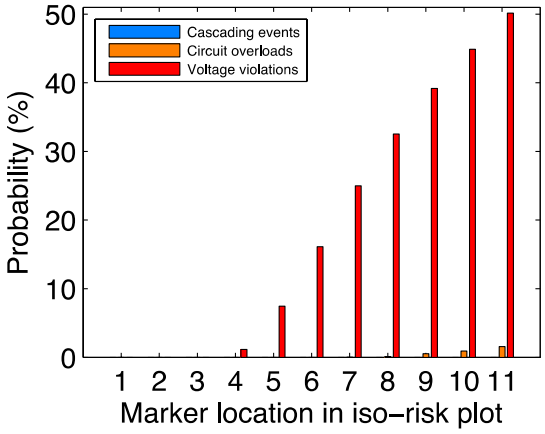

Figure 81: Probability of cascading events, overloaded circuits and voltage violations for Study Case 2 (output screening tool).

The following observations can be made:

- Neglection of correlation and/or forecast uncertainty can lead to severe underestimation of the system risk. This follows from all figures: if we move along the x-axis to the right (low to high forecast uncertainty) the risk increases; and if we move along the y-axis (low to high correlation) the risk also increases; it is therefore necessary that the forecast uncertainty is modelled in detail, and that the possible spatial correlation between forecast errors is depicted in the tool used for the assessment of the system risk;

- The results concerning the impact of forecast uncertainty clearly underline the necessity of enforcing the link between market and system operation. In particular, pushing gate closure times closer to real time operation of the system translates into a direct improvement of forecast accuracy. The results show that reducing this forecast uncertainty will lead to a reduction of the overall system risk and will in some cases suffice to bring the system in safe operating zones;
- Both the fast screening tool and the detailed analysis tool trace the same high risk region in all results, showing that the tools are indeed complementary and that the results are in line;
- The probability that redispatching (Risk level 2) or redispatching in combination with load shedding is needed (Risk level 3) increases gradually from the Marker 1 to Marker 11, see Figure 80; Thus, increasing forecast uncertainty and the correlation between the system infeeds leads to an increased probability of redispatching and load shedding;
- The probability of a system collapse is very low, see Figure 80;
- The probability of a cascading event is negligible, see Figure 81;
- As shown in Figure 81, voltage violations contribute the heaviest to the system risk, while line overloads occur less often. Since only AC methods can trace the voltage risk, one can conclude that methods that rely on DC approximations may severely underestimate the system risk. AC based methods should be used as a last part of the risk assessment tool, as proposed in this implementation.

6.3.2 Case study 2: Self-dispatch system

In this case study a self-dispatch system is considered, i.e., the market is cleared without any consideration of transmission constraints in each zone; transmission constraints are only considered between zones, corresponding to the market capacity across international borders.

6.3.2.1 Simulation setup

We consider the IEEE 118 bus system with the same modifications, and the same DSA and MC setup as in the Case Study 1. The key difference is that the initial dispatch in the DSA setup corresponds to a self-dispatch system. In particular, an AC OPF implementation is adopted where all inter-area line constraints are removed.

A two-step approach is used to compute the initial self-dispatch:

i) A first dispatch P_0 is obtained by a solution of an AC OPF problem with local cost minimisation, representing the self-dispatch system;

ii) This market dispatch P_0 cannot be used directly since this dispatch would immediately lead to violations. Therefore, a second AC OPF problem is solved, namely a safe dispatch P_1 is computed which deviates minimally from P_0 but is such that there are no violations initially.

In Table 11 an overview of the simulation settings for this case study is provided.

Table 11: Simulation settings for Case Study 2.

Test system	IEEE 118 bus	
	Adjustments:	
	Load	Zone 2: $2.0 \times$ more active and reactive load.
	Generator capacity	Zone 2: reduced to $0.8 \times$ original capacity.
	Transmission lines	Continuous rating of the transmission lines from Zone 1 to Zone 2 and from Zone 3 to Zone 2 are increased by a factor 2.
	Dispatch (P_0)	AC OPF (objective: minimal costs) This is the market dispatch not taking into account the power system's physical constraints, leading to violations.
	Dispatch (P_1)	AC OPF (objective: minimal deviation from P_0) This is the dispatch without violations computed by TSOs.
DSA setup	Type of AGC	Zone-wise, 3 zones
	Redispatch	AC OPF (objective: minimal deviation from P_1)
	Load shedding	At all load buses, cost penalty: 10,000 per MW.
Monte-Carlo setup	Uncertainty range modelling:	Forecast uncertainty, range: $0 \leq \sigma_b \leq \frac{1}{10}\mu_b$ (x-axis iso-risk plots).
		Correlation, range: $0 \leq \rho_r \leq 1$ for each zone (y-axis iso-risk plots).
	Correlation matrix	Zone-wise, 3 zones, zones are independent, see Figure 71.
	Nr. MC samples	10,000
Runtime	Fast screening (I)	n/a
	Detailed analysis (II)	27920 seconds (= 7 hours 45 minutes)

6.3.2.2 Results

As in the Case Study 1, 121 Monte-Carlo simulations were performed (10000 samples each) with the same parameter settings, and the results are presented in the same form of iso-risk plots. The total simulation time is 27920 seconds (= 7 hours and 45 minutes) for the detailed analysis tool.

In Figure 82 and Figure 83 the iso-risk plots based on the screening tool for voltage and overload severity are shown. The results from the detailed analysis tool are presented in Figure 84 and in Figure 85 in the form of iso-risk plots of lost active load in [MW] and lost reactive load in [Mvar] respectively. In Figure 86 and in Figure 87 the iso-risk plots for shifted active generator power in [MW] and for shifted reactive generator power in [Mvar] are shown. The shifted generation indicates to what degree the current dispatch needs to be changed in order to alleviate circuit overloads and voltage violations, see Eq. (6-21).

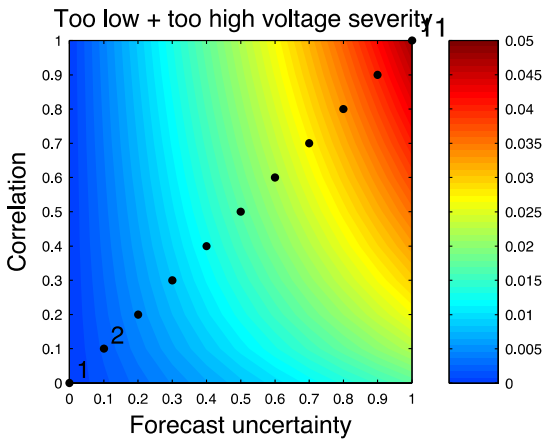

Figure 82: Voltage severity for Study Case 2 (output screening tool).

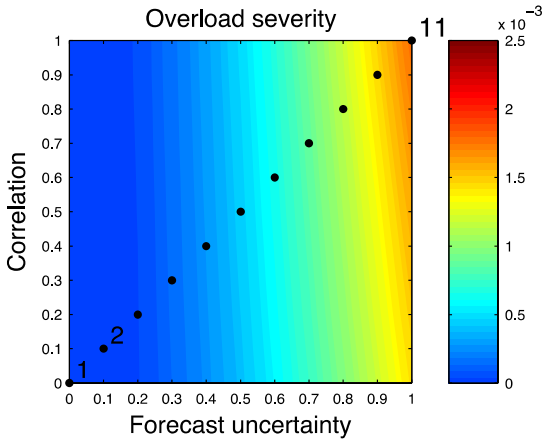

Figure 83: Overload severity for Study Case 2 (output screening tool).

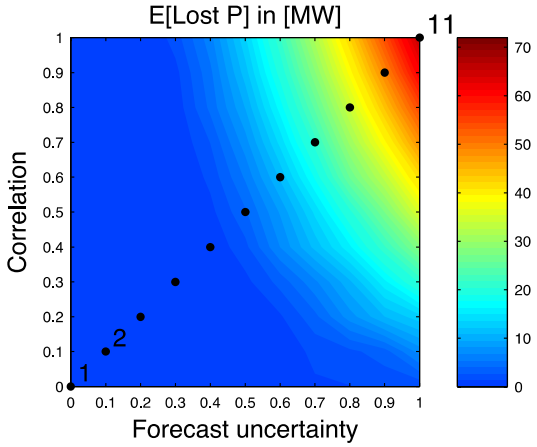

Figure 84: Lost active load for Study Case 2 (output detailed analysis).

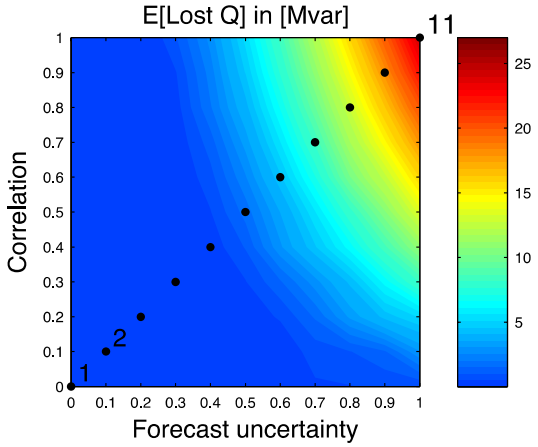

Figure 85: Lost reactive load for Study Case 2 (output detailed analysis).

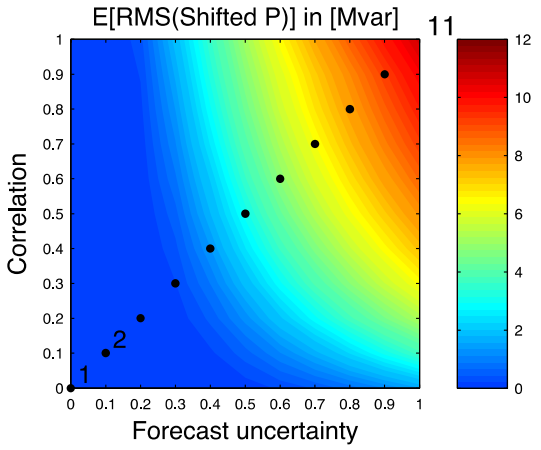

Figure 86: Shifted active generator power for Study Case 2 (output detailed analysis).

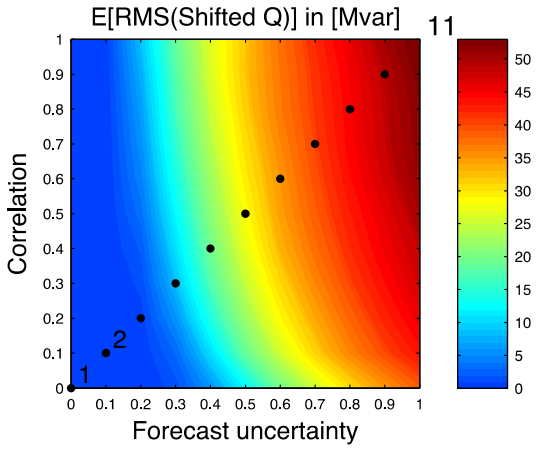

Figure 87: Shifted reactive generator power for Study Case 2 (output detailed analysis).

In Figure 88 the four levels of risk and their corresponding probabilities are shown while Figure 89 presents the probability of cascading events, overloaded circuits and voltage violations.

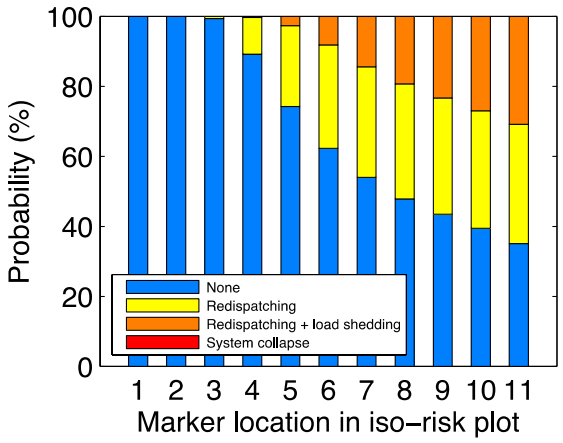

Figure 88: Four levels of risk and their corresponding probabilities for Study Case 2 (output detailed analysis).

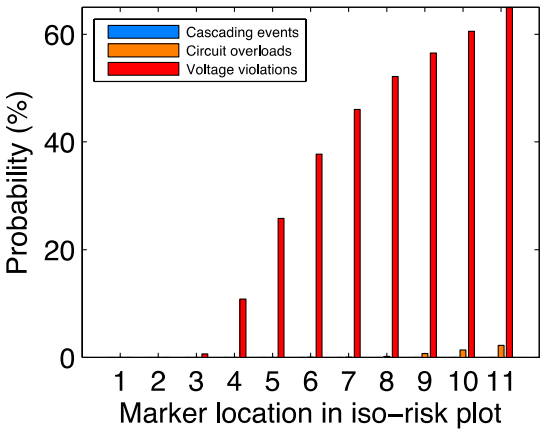

Figure 89: Probability of cascading events, overloaded circuits and voltage violations for Study Case 2 (output screening tool).

The following observations can be made:

- The self-dispatch system results in higher risk. By comparing the respective risk plots for the two systems, (e.g., the amount of Lost Load, compare Figure 76 and Figure 84), one can see that the expected amount of Lost Load for the self-dispatch system is higher than for the central dispatch system. This is to be expected since the self-dispatch does not take into account the physical constraints of the system and TSOs have to adjust the dispatch in order to alleviate line overloads. This can for example be seen from Figure 90 which shows the overload

severity if the market dispatch P_0 would be used rather than the safe dispatch P_1 computed by TSOs.

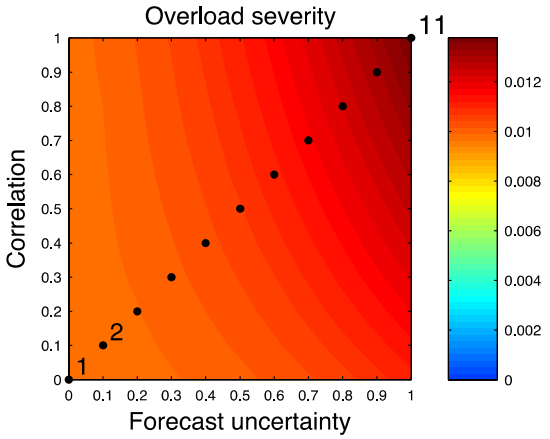

Figure 90: Initial overload severity for the market self-dispatch resulting from not taking into account transmission constraints within the zones.

6.3.3 Study 3: HVAC line replaced by HVDC line

The primary goal of this study is to investigate the impact of PFCC on the system. In particular, we assess the impact of replacement of specific lines in the system with HVDC lines on the system risk and show how the proposed RBSA methodology can be used to investigate optimal placement of HVDC lines for reducing the system risk. Since the cross-border flows are substantial, see Case Study 1, incorporating HVDC is used to solidify the power system.

6.3.3.1 Simulation setup

We consider the IEEE 118 bus system with the same modifications, and the same DSA and MC setup as in the Case Study 1. The key difference is that the HVAC 345 kV line from bus 30 to 38 with continuous rating of 350 MW is replaced by an HVDC line with the same capacity transporting 300 MW of active power, see Figure 73.

By choosing an HVDC link of the same capacity we isolate the effect of power flow controllability on system security with respect to the base case. The set-point of the HVDC line is also allowed to change during the simulation.

In Table 12 an overview of the simulation settings for this case study is provided.

Table 12: Simulation settings for Case Study 3.

Test system	IEEE 118 bus	
	Adjustments:	
	Load	Zone 2: $2.0 \times$ more active and reactive load.
	Generator capacity	Zone 2: reduced to $0.8 \times$ original capacity.
	Transmission lines	Continuous rating transmission lines from Zone 1 to Zone 2 and from Zone 3 to Zone 2 increased by a factor 2. HVAC line from bus 30 to bus 38 (cap. 350 MW) replaced by HVDC 345 kV line transporting 300 MW.
	Dispatch (P_0)	AC OPF (objective: minimal costs)
DSA setup	Type of AGC	Zone-wise, 3 zones
	Redispatch	AC OPF (objective: minimal deviation from P_1)
	Load shedding	At all load buses, cost penalty: 10,000 per MW.
Monte-Carlo setup	Uncertainty range modelling:	Forecast uncertainty, range: $0 \leq \sigma_b \leq \frac{1}{10}\mu_b$ (x-axis iso-risk plots).
		Correlation, range: $0 \leq \rho_r \leq 1$ for each zone (y-axis iso-risk plots).
	Correlation matrix	Zone-wise, 3 zones, zones are independent, see Figure 71.
	Nr. MC samples	10,000
Runtime	Fast screening (I)	n/a
	Detailed analysis (II)	13790 seconds (= 3 hours 50 minutes)

6.3.3.2 Results

As in the Case Study 1, 121 Monte-Carlo simulations were performed (10000 samples each) with the same parameter settings, and the results are presented in the same form of

iso-risk plots. The total simulation time is 13790 seconds (= 3 hours 50 minutes) for the detailed analysis tool.

Figure 91 and Figure 92 present the iso-risk plots for voltage and overload severity respectively as they are obtained by the screening tool. Figure 93 and Figure 94 present the iso-risk plots for lost active load in [MW] for lost reactive load in [Mvar] respectively based on the detailed analysis. In Figure 95 the iso-risk plot is shown for shifted active generator power in [MW] and in Figure 96 the iso-risk plot is shown for lost shifted reactive generator power in [Mvar]. The shifted generation indicates to what degree the current dispatch needs to be changed in order to alleviate circuit overloads and voltage violations, see Eq. (6-21).

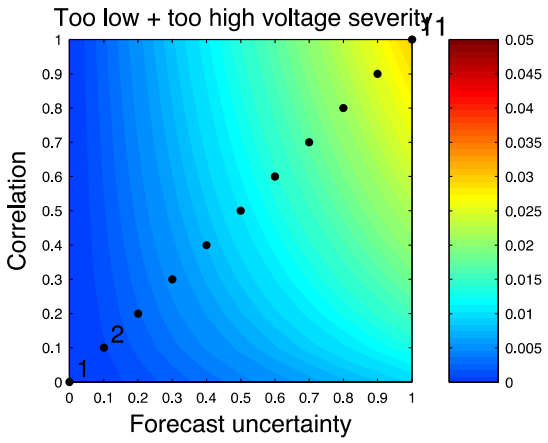

Figure 91: Voltage severity for Study Case 3 (output screening tool).

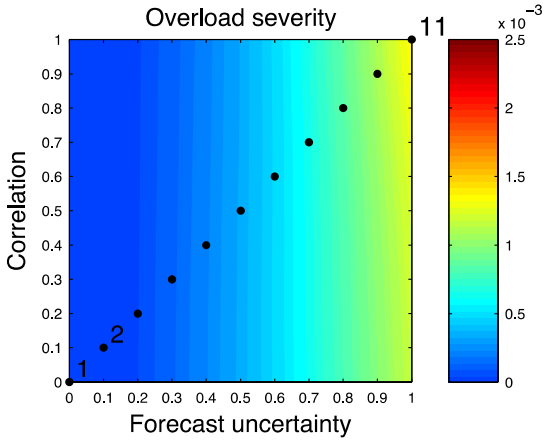

Figure 92: Overload severity for Study Case 3 (output screening tool).

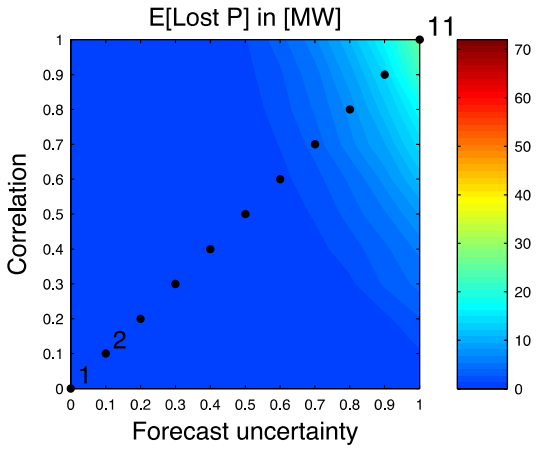

Figure 93: Lost active load for Study Case 3 (output detailed analysis).

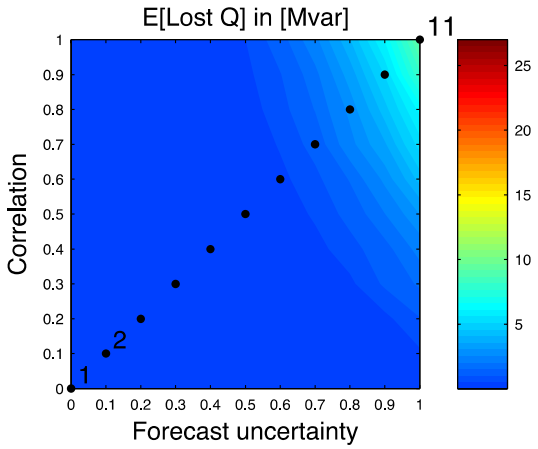

Figure 94: Lost reactive load for Study Case 3 (output detailed analysis).

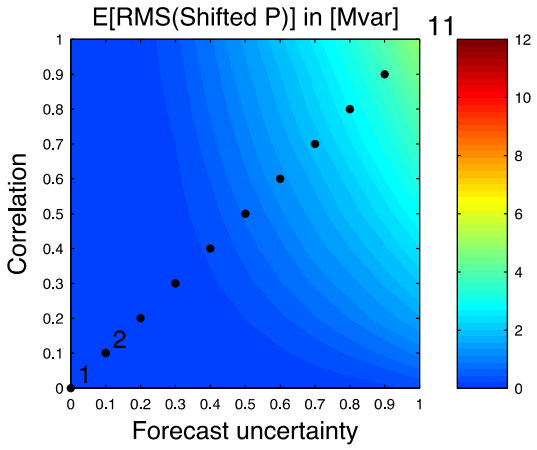

Figure 95: Shifted active generator power for Study Case 3 (output detailed analysis).

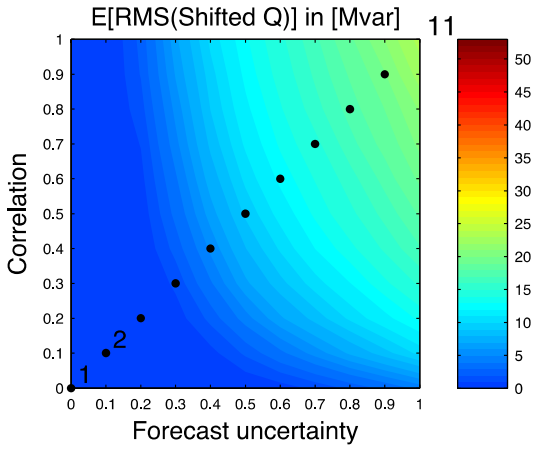

Figure 96: Shifted reactive generator power for Study Case 3 (output detailed analysis).

In Figure 97 the four levels of risk and their corresponding probabilities are shown and in Figure 98 the probability of cascading events, overloaded circuits and voltage violations are shown.

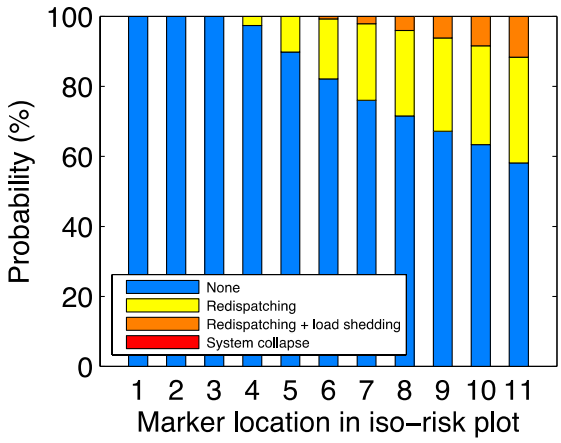

Figure 97: Four levels of risk and their corresponding probabilities for Study Case 2 (output detailed analysis).

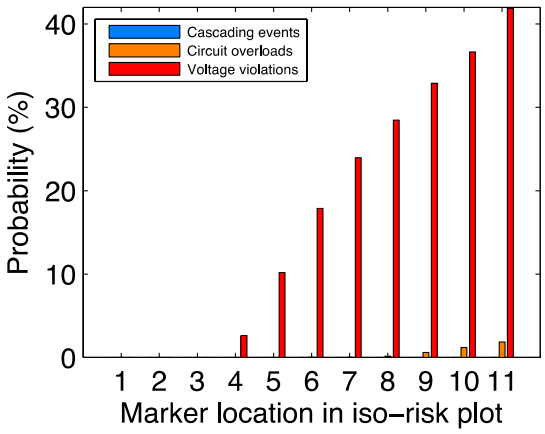

Figure 98: Probability of cascading events, overloaded circuits and voltage violations for Study Case 2 (output screening tool).

The following observations can be made:

- Incorporating HVDC in the system reduces the overall risk by a great amount. The screening tool shows a strong reduction in voltage severity and overload severity, see Figure 91 and Figure 92 in comparison with the reference (Case Study 1), see Figure 74 and Figure 75. Also the detailed analysis shows a great reduction in expected amount of Lost Load and shifted generation; all iso-risk plots are no far less red; actually, they show blue and green only;

- Thanks to the HVDC connection between Zone 1 and Zone 2 the expected amount of Lost Load has been reduced from 70 MW to just over 20 MW.

6.3.4 Case study 4: Generator study IEEE 118 bus system

The primary goal of this study is to show how the proposed RBSA methodology can be used to trace the impact of cross-zonal flows on system security. In particular, we show that shifting generation from one zone to another can have an positive effect on the system risk and that the proposed methodology can help to analyse this effect.

6.3.4.1 Simulation setup

We consider the IEEE 118 bus system with the same modifications, and the same DSA and MC setup as in the Case Study 1. The key difference is that we choose a fixed degree of correlation for the MC setup and instead we use cross-border flows as parameter.

To vary the cross-border flow, the output of two generators is changed: the output of generator at bus 26 in Zone 1 is varied between 350 and 300 MW, and at the same time the generator at bus 87 in Zone 3 is varied between 222 and 272 MW in steps of 5 MW. Hence generation of power is slightly shifted from Zone 1 to Zone 3. The generator at bus 26 is on the y-axis of the iso-risk plot. In this study the rank correlation ρ_r is kept constant, namely: $\rho_r = 0.5$.

In Table 13 an overview of the simulation settings for this case study is provided.

Table 13: Simulation settings for Case Study 4.

<table>
<tr><td>Test system</td><td colspan="2">IEEE 118 bus</td></tr>
<tr><td></td><td colspan="2">Adjustments:</td></tr>
<tr><td></td><td>Load</td><td>Zone 2: $2.0\times$ more active and reactive load.</td></tr>
<tr><td></td><td>Generator capacity</td><td>Zone 2: reduced to $0.8\times$ original capacity.</td></tr>
<tr><td></td><td>Transmission lines</td><td>Continuous rating of the transmission lines from Zone 1 to Zone 2 and from Zone 3 to Zone 2 are increased by a factor 2.</td></tr>
<tr><td></td><td>Dispatch (P_0)</td><td>AC OPF (objective: minimal costs)</td></tr>
</table>

DSA setup	Type of AGC	Zone-wise, 3 zones
	Redispatch	AC OPF (objective: minimal deviation from P_0)
	Load shedding	At all load buses, cost penalty: 10,000 per MW.
Monte-Carlo setup	Uncertainty range modelling:	Forecast uncertainty, range: $0 \leq \sigma_b \leq \frac{1}{10}\mu_b$ (x-axis iso-risk plots).
	Second study parameter:	Generator output at bus 26 (in Zone 1), range: $300 \leq P_{G,26} \leq 350$ MW, versus generator at bus 87 (in Zone 3). (y-axis iso-risk plots).
	Correlation matrix	Zone-wise, 3 zones, zones are independent, see Figure 71. Rank correlation is fixed: $\rho_r = 0.5$.
	Nr. MC samples	10,000
Runtime	Fast screening (I)	6580 seconds (= 1 hour 50 minutes)
	Detailed analysis (II)	25590 seconds (= 7 hours 6 minutes)

6.3.4.2 Results

As in the Case Study 1, 121 Monte-Carlo simulations were performed (10000 samples each) with the same parameter settings, and the results are presented in the same form of iso-risk plots. The total simulation time is 6580 seconds (= 1 hour 50 minutes) for the screening tool and 25590 seconds (= 7 hours and 6 minutes) for the detailed analysis tool.

Figure 99 and Figure 100 present the iso-risk plots for voltage and overload severity respectively as they are obtained by the screening tool. Figure 101 and Figure 102 present the iso-risk plots for lost active load in [MW] for lost reactive load in [Mvar] respectively based on the detailed analysis. In Figure 103 the iso-risk plot is shown for shifted active generator power in [MW] and in Figure 104 the iso-risk plot is shown for lost shifted reactive generator power in [Mvar]. The shifted generation indicates to what degree the current dispatch needs to be changed in order to alleviate circuit overloads and voltage violations, see Eq. (6-21).

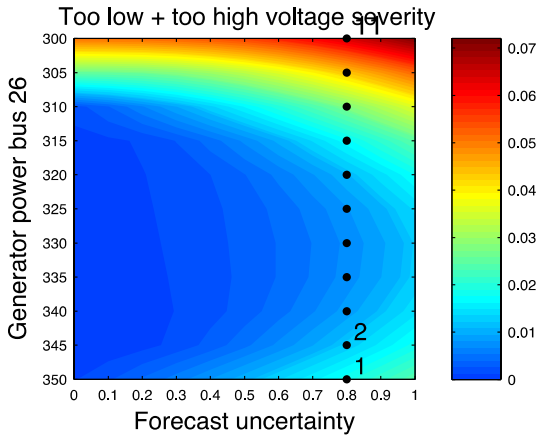

Figure 99: Voltage severity for Study Case 4 (output screening tool).

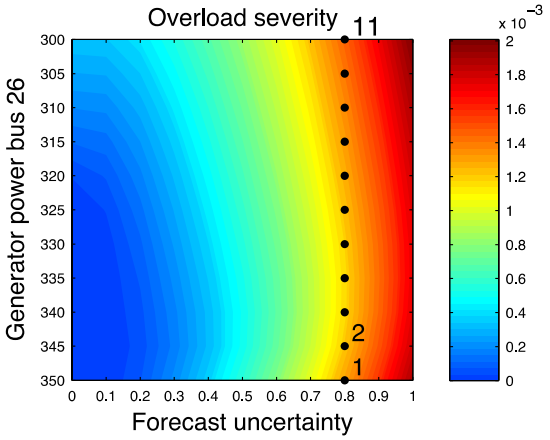

Figure 100: Overload severity for Study Case 4 (output screening tool).

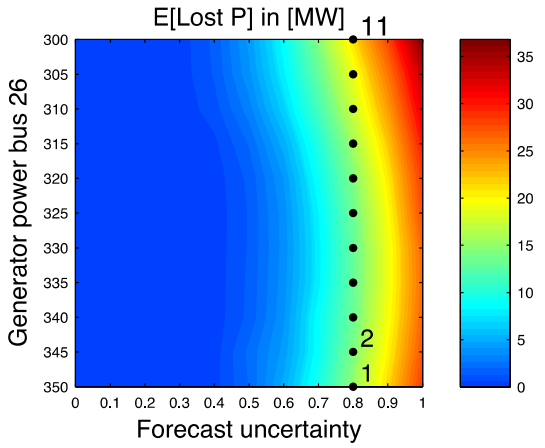

Figure 101: Lost active load for Study Case 4 (output detailed analysis).

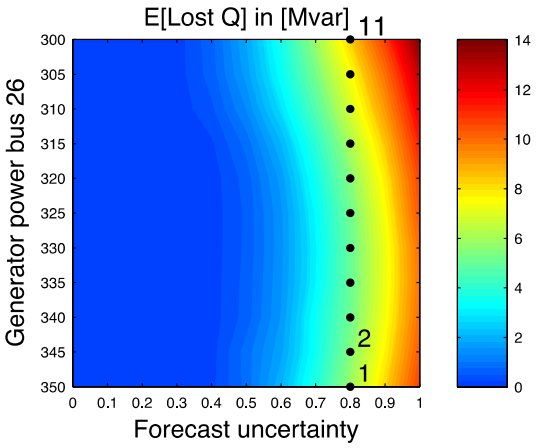

Figure 102: Lost reactive load for Study Case 4 (output detailed analysis).

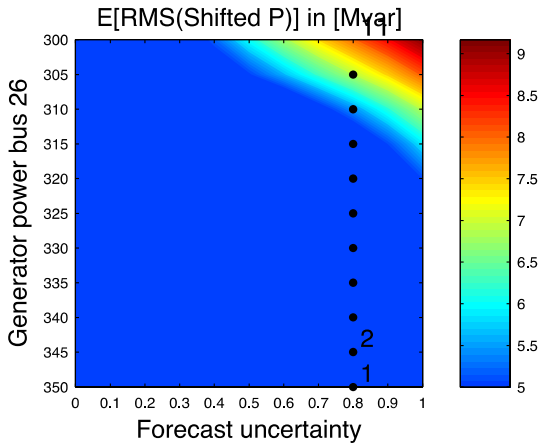

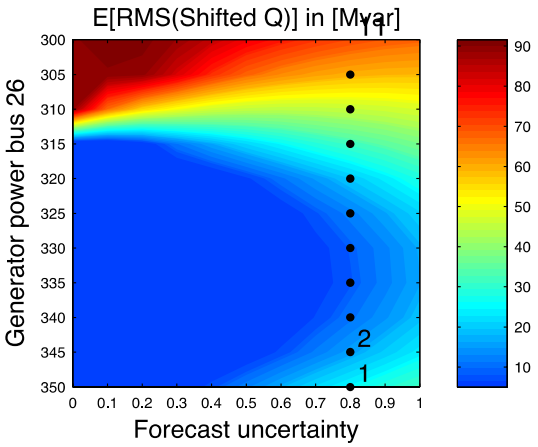

Figure 103: Shifted active generator power for Study Case 4 (output detailed analysis).

Figure 104: Shifted reactive generator power for Study Case 4 (output detailed analysis).

In Figure 105 the four levels of risk and their corresponding probabilities are shown and in Figure 108 the probability of cascading events, overloaded circuits and voltage violations are shown.

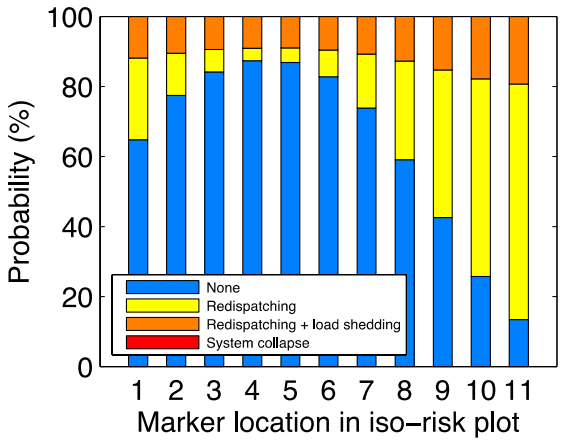

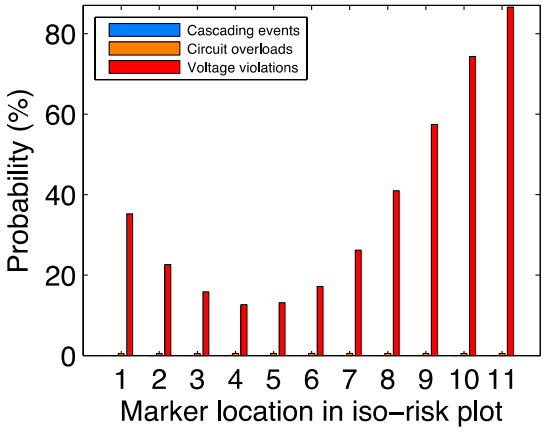

Figure 105: Four levels of risk and their corresponding probabilities for Study Case 4 (output detailed analysis).

Figure 106: Probability of cascading events, overloaded circuits and voltage violations for Study Case 4 (output screening tool).

The following observations can be made:

- It is seen that shifting generation from Zone 1 to Zone 3 has a great impact on the system risk: along the indicated Markers 1 to 11, the risk (e.g., the expected amount of Lost Load) first decreases gradually and then increases gradually. This can be observed best from Figure 105 and Figure 106;
- From the figures it follows that the most optimal setting is to decrease the output of the generator at bus 26 in Zone 1 from 350 MW to 335 MW and to increase the output of the generator at bus 87 in Zone 3 from 222 MW to 237 MW (Marker 4); in that case the risk is the lowest.

6.3.5 Study 5: Large system

The primary goal of this study is to show that the proposed RBSA methodology can handle realistic scale systems. In this study the UCTE 2713 bus system developed by Umbrella partners is used. The system consists of a total of 2713 buses (of which 1181 are load buses) and 458 generators divided over 14 zones, see also Section 6.2.1.2.

6.3.5.1 Simulation setup

Due to issues with data (the provided dispatch led to severe voltage violations and an unrealistic voltage profile), a new dispatch is computed using AC OPF with objective function the minimisation of shifted power, see Eq. (6-17). The new dispatch is computed such that it deviates minimally from the original provided dispatch but is such that voltages are within safe limits (between 0.9 and 1.1 p.u.) and circuit overloads are alleviated.

In this study also a more detailed correlation matrix is used, namely the one shown in Figure 72. In Table 14 an overview of the simulation settings for this case study is provided.

Table 14: Simulation settings for Case Study 5.

Test system	IEEE 118 bus	
	Adjustments:	
	Load	None
	Generator capacity	None
	Transmission lines	None
	Dispatch (P_0)	AC OPF (objective: minimal deviation from dispatch provided with data set but such that voltages and circuit flows are within safe ranges)
DSA setup	Type of AGC	Zone-wise, 14 zones
	Redispatch	AC OPF (objective: minimal deviation from P_0)
	Load shedding	At all load buses, cost penalty: 10,000 per MW.
Monte-Carlo setup	Uncertainty range modelling:	Forecast uncertainty, range: $0 \leq \sigma_b \leq \frac{1}{10}\mu_b$ (x-axis iso-risk plots).
		Correlation, range: $0 \leq \rho_r \leq 1$ for each zone (y-axis iso-risk plots).
	Correlation matrix	Zone-wise, 14 zones, zones are dependent, see Figure 72.
	Nr. MC samples	1,000

Runtime	Fast screening (I)	n/a
	Detailed analysis (II)	10990 seconds (= 3 hours 20 minutes)

6.3.5.2 Results

To generate the iso-risk plots 121 Monte-Carlo simulations were performed (1000 samples each). The total simulation time is 10990 seconds (= 3 hours 20 minutes) for the detailed analysis tool.

Figure 104 and Figure 108 present the iso-risk plots for voltage and overload severity respectively as they are obtained by the screening tool. Figure 109 and Figure 110 present the iso-risk plots for lost active load in [MW] for lost reactive load in [Mvar] respectively based on the detailed analysis. In Figure 111 the iso-risk plot is shown for shifted active generator power in [MW] and in Figure 112 the iso-risk plot is shown for lost shifted reactive generator power in [Mvar]. The shifted generation indicates to what degree the current dispatch needs to be changed in order to alleviate circuit overloads and voltage violations, see Eq. (6-21).

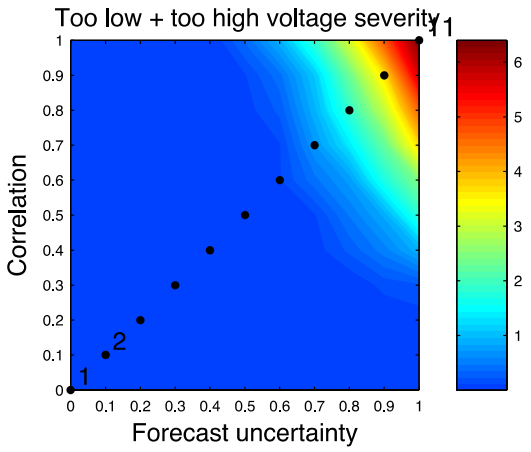

Figure 107: Voltage severity for Study Case 5 (output screening tool).

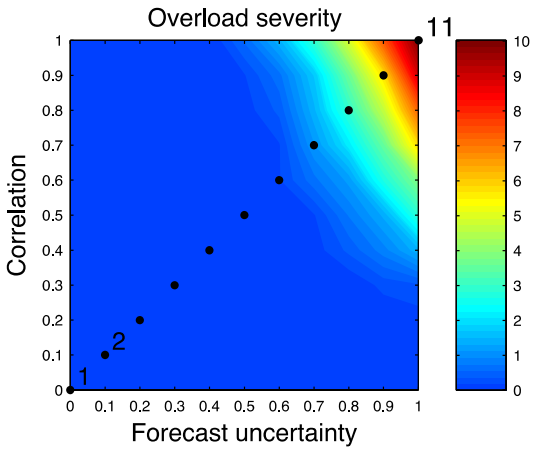

Figure 108: Overload severity for Study Case 5 (output screening tool).

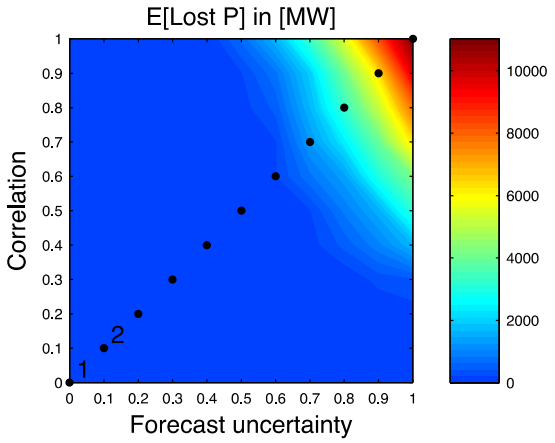

Figure 109: Lost active load for Study Case 5 (output detailed analysis).

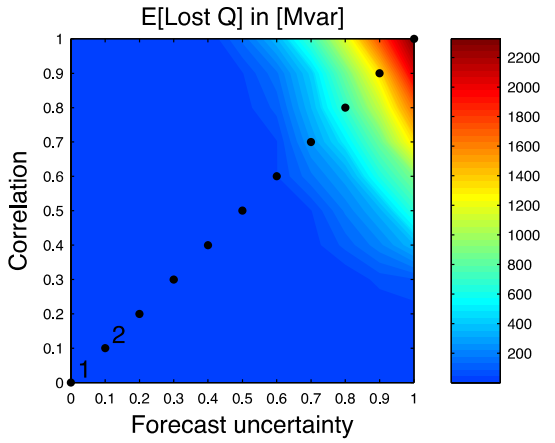

Figure 110: Lost reactive load for Study Case 5 (output detailed analysis).

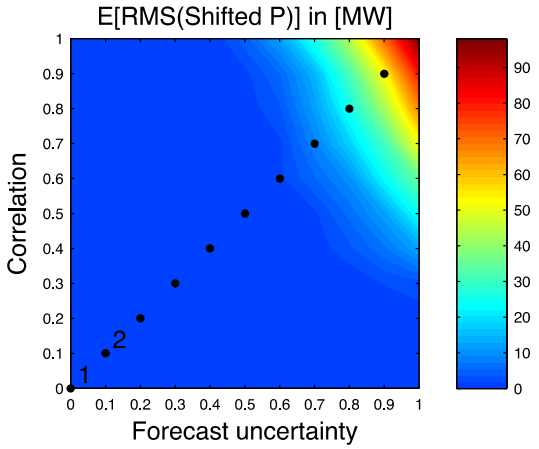

Figure 111: Shifted active generator power for Study Case 5 (output detailed analysis).

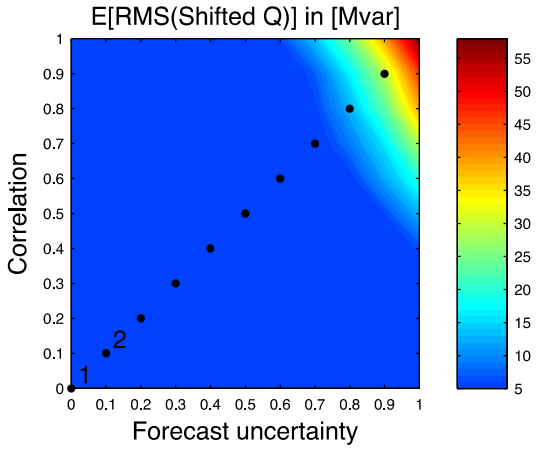

Figure 112: Shifted reactive generator power for Study Case 5 (output detailed analysis).

In Figure 113 the four levels of risk and their corresponding probabilities are shown and in Figure 114 the probability of cascading events, overloaded circuits and voltage violations are shown.

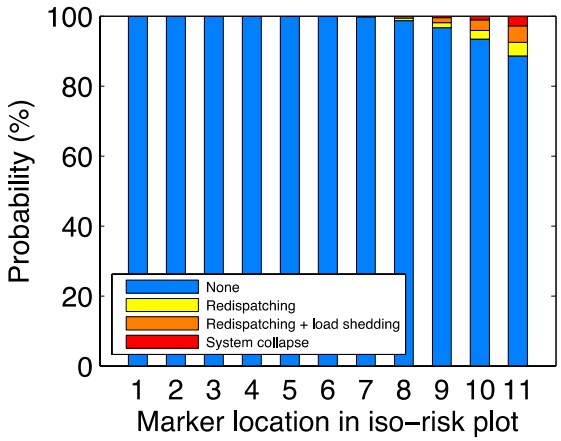

Figure 113: Four levels of risk and their corresponding probabilities for Study Case 5 (output detailed analysis).

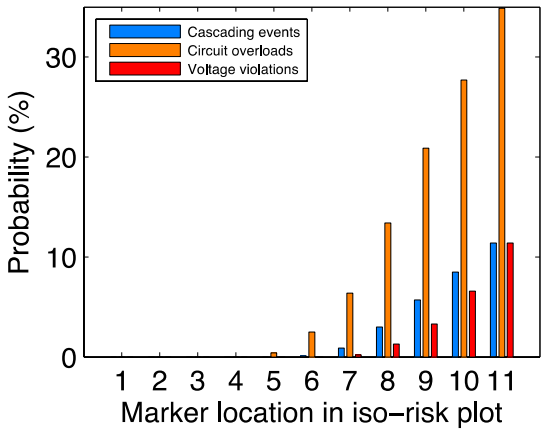

Figure 114: Probability of cascading events, overloaded circuits and voltage violations for Study Case 5 (output screening tool).

The following observations can be made:

- Both circuit overloads and voltage violations contribute to the system risk. Therefore, methods that rely on DC approximations, would severily underestimate the risk;
- For the UCTE 2713 bus system, the probability of cascading events is significant: in case of high correlation and high forecast uncertainty in 10% of the cases a cascading event occurs, see Figure 114. This may be the result of taking an AC OPF dispatch as initial dispatch rather than an AC SCOPF dispatch. The initial dispatch was changed due to data issues, see Section 6.3.5.1.

6.3.6 A note on accuracy

The accuracy that the proposed methodology can obtain depends on N, the number of MC samples that is used in the simulations. This follows directly from Eq. (6-2) and Eq. (6-3). In Table 15 the obtained accuracy is listed for four quantities in Case Study 1.

Table 15: Estimated quantities and accuracy for Case Study 1 with $N = 10.000$ MC samples.

Quantity	**Marker location**	**Sample mean ($\hat{\mu}$)**	**Sample standard deviation (s)**	**95% confidence interval (see Eq.** (6-3) **)**	**Width / $2\hat{\mu}$**
Lost active load	6 (safe)	2.15	16.03	2.15 ± 0.30	0.14
Lost active load	11 (severe)	61.58	141.49	61.6 ± 2.77	0.05
Shifted active power	6 (safe)	1.00	3.64	1.00 ± 0.07	0.07
Shifted active power	11 (severe)	7.47	11.13	7.47 ± 0.21	0.03

In Table 16 the obtained accuracy is listed for six probabilities in Case Study 1.

Table 16: Estimated probabilities and accuracy for Case Study 1 with $N = 10.000$ MC samples.

Event	**Marker location**	**Probability p (%)**	**95% confidence interval (see Eq.** (6-2) **)**	**Width / $2p$**
Risk level 2 (redispatching)	6 (safe)	13	13 ± 0.66	0.05
Risk level 2 (redispatching)	11 (severe)	27	27 ± 0.87	0.03
Overload problems occur	11 (severe)	1.6	1.6 ± 0.24	0.15
Voltage problems occur	6 (safe)	16	16 ± 0.72	0.05
Voltage problems occur	11 (severe)	50	50 ± 0.98	0.02
Risk level 3 (redispatching + load shedding required)	6 (safe)	3	3 ± 0.33	0.11

Generally, it holds that the accuracy is high for large probabilities and that for small probabilities (rare events) the accuracy is lower. This can be seen from the last column of the tables.

It is found that the proposed RBSA methodology delivers already a good level of accuracy with a relatively small amount of MC samples.

From Eq. (6-3) it follows that one can do two things to further increase the level of accuracy:

- Increase N, the number of MC samples. For example, if N is increased by a factor 100, the width of the 95% confidence decreases by a factor $\sqrt{100} = 10$, hence we gain an order of accuracy;
- Incorporate variance reduction techniques. Basically, these techniques provide a sample space with a smaller sample standard deviation s.

The first solution is straightforward, but expensive since the computation time also increases by the same factor, e.g., by a factor 100 in the example above. The second solution is computationally cheap, but this requires further research since typically variance reduction techniques are difficult to implement.

6.3.7 A note on runtime

The computation time of the RBSA methodology depends on:

1. The number of grid points in the iso-risk plot;
2. N, the number of MC samples;
3. The actual risk level: in case of high transmission flows, there is the risk of a cascading event. In that case an AC PF is computed multiple times, namely 1 AC PF per cascading iteration, see the flowchart in Figure 50;
4. Whether the fast screening tool (I) or the detailed analysis tool (II) is used: the fast screening tool (I) costs hardly anything extra; the computation time for the fast screening tool is determined by points 1 to 3 listed above (Applying the severity functions comes down to interpolation which is very cheap). However, recall that the detailed analysis tool (II) proposes remedial actions using an AC OPF framework. Hence, in case of a severe system state, the power system needs to be restabilised and hence for each sample which represents a severe system state an AC OPF problem is solved. This is quite expensive (as costly as 5 - 15 AC PFs).
5. The number of available processors. Since MC is embarrassingly parallel, the overall computation time can be reduced by a factor p, the number of available processors.

In Table 17 the runtime is listed for Case Studies 1 and 4 for each of the two tools. It is observed that the detailed analysis tool (II) is four times as expensive as the screening tool (I). This is due to computation of remedial actions using an AC OPF framework.

Table 17: Runtime for entire case studies using the screening tool (I) and/or the detailed analysis tool (II). Time in seconds.

Experiment	**Fast screening tool (I)**	**Detailed analysis tool (II)**
Case Study 1	4476	17562
Case Study 4	6577	25592

In Table 18 the runtime is shown for computation of 1 grid point in the iso-risk plot using 10.000 MC samples for both the IEEE 118 bus system and the UCTE 2713 bus system.

Table 18: Runtime to compute 1 grid point in the iso-risk plot using 10.000 MC samples. Time in seconds.

	Safe system state (Marker 1 in iso-risk plot)		**Severe system state (Marker 10 in iso-risk plot)**	
Test system	*Fast screening tool (I)*	*Detailed analysis tool (II)*	*Fast screening tool (I)*	*Detailed analysis tool (II)*
IEEE 118 bus	38	45	43	210
UCTE 2713 bus	3305	10435	3408	19448

It can be seen that:

- Computing a severe system state (Marker 10) with the detailed analysis tool (II) is more expensive than computing a safe system state (Marker 1). This is due to the fact that in a severe system state more often remedial actions are needed to stabilise the system, hence more often an AC OPF problem is solved;
- Computing a severe system state (Marker 10) with the screening tool (I) is as expensive as computing a safe system state (Marker 1). This is because the screening tool (I) only performs interpolation to compute the severity which costs in both cases the same amount of computations;
- Computing 1 grid point for the UCTE 2713 bus system is about 100 times more expensive than computing 1 grid point for the IEEE 118 bus system, although the number of buses differs only a factor 25.

6.4 Summary and conclusions

In this chapter a RBSA method was presented which enables the analysis and evaluation of the risk of a power system in a future state, relying on the current estimation of uncertainty, under varying scenarios and stochastic inputs. The method further proposes the optimal set of remedial actions that can be used by TSOs to steer the system into a risk averse state. This dual output of the method is achieved by the use of two complementary risk metrics, namely a fast screening tool based on severity functions and a detailed assessment of remedial actions using Lost Load as a second risk metric in an AC OPF framework. In order to get the highest level of accuracy, the method combines a copula-theory based MC simulation framework for the stochastic part, and a full AC PF based part as core of the deterministic security assessment algorithm.

A set of detailed case studies were investigated using the IEEE 118 bus system and the UCTE 2713 bus system, where the developed tool was used to assess different aspects of power system security. Key takeaways from the analysis are summarised as follows:

- The combination of a fast screening approach based on severity functions and a detailed approach based on Lost Load provides a complete tool for power system security assessment. In a real-life setup the tools work together: the screening tool is constantly monitoring where the system lies on the risk map, while the remedial actions tool provides indications on operational adjustments for steering the system in a risk-averse mode.
- The proposed setup is very versatile and specific parts can be easily extended for real-life applicability, e.g., extended remedial actions module with branch switching and topology optimisation (see Umbrella Work Package 3) or wind-forecast module (see Umbrella Work Package 2)
- The proposed methodology can handle different assessments, related to forecast uncertainty (marginal distributions and correlation), generator studies, economic dispatching, particular post-contingency states, etc.
- The analysis shows that not taking forecast uncertainly into account can lead to a severe underestimation of system risk. It was shown that by increasing the variability or the degree of correlation of the system inputs leads to a totally different system risk. In other words, a tool that underestimates these factors would make a much lower estimation of the security risk of the system.
- An AC PF framework is necessary for online security assessment of the system, since voltage problems contribute heavily on the system risk.
  PFCCs can play an important role on system stabilisation. A proper control and operation of these devices provides degrees of freedom to the TSO that are invaluable for steering the system in low-risk areas. Strategic placement and operation of the devices can allow them being a counteraction against uncertainty.
- Computational time: although it is often argued that the higher computational burden of a MC framework with full AC PF computations, our results on the realistic UCTE 2713 bus system show that the application of the proposed methodology in a real-time environment becomes within reach. In particular, the overall runtime of the method to produce an iso-risk plot was in the order of hours on a single desktop computer.

Realising the importance of solution speed for the application of the tool in a real-time environment, we discuss below key considerations for speeding up the computations.

1. Parallelisation: MC simulation is massively parallelisable. One may think of MPI to address multiple computers, or, more recently, CUDA to take advantage of GPU computing. Basically it holds that using k times more computers yields k times faster results;
2. Software Implementation: For the experiments the methodology was implemented in MATLAB in combination with the MATPOWER package, which is by default not optimised in speed. By implementing the method in a programming language which supports high performance computing (HPC) the overall computation time can strongly be reduced;
3. Deterministic algorithm boosting: the AC PF computations can be speed up by deploying modern Newton-Krylov methods since the use of iterative solution techniques is very suitable for data reuse of the repeated PF computations in MC and for contingency analysis, see e.g., [51], independent from the size of the analysed system.
4. Stochastic algorithm boosting: To reduce the required number of MC samples to get a predefined level of accuracy, one can apply variance reduction techniques based on rare event simulation.

These aspects are key subjects for future research towards a real-life application of this tool.

7 Conclusions

Deliverable D4.3 presents a range of risk-based methods for power system operational planning and real-time operation. The methods aim at reducing the risk in power system operation, with particular focus on incorporating uncertainty from renewables and intra-day trading in operational planning and risk assessment for cascading events. While the methods presented in this deliverable are based on previous work in Deliverable D4.1 and D4.2, the methods have been extended to consider the role of power flow control devices (such as HVDC and PSTs) and different market design to reduce system operational risk.

The deliverable consists of three parts which can be read as stand-alone method descriptions or as a complete risk assessment method, similar to the set-up in Deliverable D4.2.

7.1 Probabilistic security constrained optimal power flow with corrective control

The first part (Chapters 2 and 3) considers the integration of uncertain in-feeds in the dispatching process of the TSOs, using chance constrained optimisation and the probability of N-1 violations as a risk measure. In chapter 2, flexibility from HVDC and PSTs are included in the optimisation, while chapter 3 investigates how central dispatch and self-dispatch markets perform under uncertainty.

The method presented in Chapter 2 is an extension to the probabilistic security constrained optimal power flow (pSCOPF) presented in [1], [2]. The original formulation used chance constrained optimisation to guarantee that the system will remain secure with a given probability, even in presence of uncertain in-feeds. The current method extends this formulation by incorporating *corrective control* actions from HVDC and PSTs, as well as a more flexible activation of balancing reserves (i.e., based on their location in the system). The goal of the method is to better represent how uncertainty can be handled in real-time operation, by modelling corrective control actions not only related to contingencies, but also corrective actions handle deviations from the planned generation schedule due to RES fluctuations or intra-day trading. Using corrective control actions related to forecast deviations is in common use in grid operation today (i.e., switching actions and redispatch performed in real-time), but are hard to model within the OPF problem since the random variables should be handled as continuous variables. To implement the reaction of HVDC, PSTs and reserves within the existing modelling framework, it was assumed that they change their set-points according to an affine control policy (i.e., proportional to the deviation from forecasted values). The new formulation allows for corrective actions based on the local forecast deviations, not only the overall power mismatch.

The new formulation is demonstrated in a case study for the IEEE 118 bus system, where the effect of corrective control from HVDC, PSTs and reserves are demonstrated separately. It is found that by planning reactions to the forecast deviations that can be performed in real-time, it is possible to reduce cost. This effect is particularly strong when

the actions are taken based on local forecast deviations. Activating reserves based on the local forecast deviations decreased the cost of uncertainty almost to zero, and was found to be the most effective way of lowering the cost of handling uncertain in-feeds. Corrective control from HVDC and PSTs showed almost no effect when only the overall power mismatch is considered, but led to a significant decrease in the cost when the devices react based on local forecast deviations. In this case, it was found that the system performs better when a large part of the HVDC capacity or the PST angle range is allocated to handling forecast deviations.

In chapter 3, two versions of the above OPF formulations representing two different market designs are presented, a central dispatch market and a self-dispatch market. In addition, it is assumed that the TSO is able to perform real-time redispatch as a reaction to forecast deviations. This option is incorporated in both the central dispatch OPF and the self-dispatch OPF.
The two market designs were tested on the IEEE 118 bus system. First, the two markets were compared to each other in the deterministic case to highlight their characteristics. The central dispatch market clearing leads to a generation dispatch with higher cost than the initial generation dispatch obtained in the self-dispatch market, since the market clearing of the central dispatch market accounts for transmission constraints (thus being more constrained). However, the generation dispatch obtained from the self-dispatch market requires a large amount of redispatch to obtain a N-1 safe dispatch. Therefore, the overall operation cost (market clearing + redispatch) is lower for the central dispatch market design. In the second part of the market evaluation, different redispatch policies were investigated. In the first redispatch policy, all redispatch measures had to be defined in the day-ahead planning. In the second policy, additional real-time redispatch measures which are modelled as a reaction to the uncertain in-feeds, can be introduced in the optimisation to model how congestion can be handled in real-time. For both the central and the self-dispatch markets, it was found that consideration of real-time redispatch in the planning phase (i.e., integration of real-time redispatch in the optimisation problem) significantly reduces the cost of handling uncertain in-feeds.

7.2 Probabilistic risk assessment

The second part (Chapters 4 and 5) estimates the overall system risk, considering uncertain in-feeds, the effect of cascading events and using lost load as a risk measure. Chapter 4 describes the extensions to the previously developed method and demonstrates how power flow controlling devices can be used to decrease system risk, while chapter 5 investigates the effect of a set of different market designs.

Chapter 4 presents an extension to the method developed during the work for Deliverable 4.2. Power flow controlling devices (i.e., HVDC, PSTs and TCSC) are modelled and incorporated in the risk assessment. Their set-points are defined through an optimisation which minimises the probability of line outages and line overloads, and is kept constant during the entire risk simulation. Further enhancements, mainly concerning the quality of results and the computational effort, were implemented leading to a fast probabilistic

cascading risk assessment tool.
The implemented PFCCs were tested and compared in terms of their effect on the overall system risk in a case study for the IEEE 118 bus system. Incorporating the flexibility of the power flow controlling devices has a significant influence on the system security, in the sense that they can both reduce the risk and the amount of congestion in the initial state. A second case study compared central and de-central coordination of the power flow controlling components. In the central coordination, the set-points were found based on a simultaneous optimisation of all PST angles, considering all line loadings in the system. In the de-central coordination, each PST optimised separately, considering only the line loadings in the zone where it is located. It was found that when the devices are coordinated through a central optimisation, the risk (measured in terms of the lost load) is lower. Further, it was observed that a high loading of some lines not necessarily leads to higher risk than when the branch loadings are more smoothly distributed among the lines. Thus, looking at the branch loadings in the base case (without outages) does not immediately lead to a conclusion regarding the system risk - not even when accounting for the influence of uncertainty on the line loading. To gain knowledge of the system risk, a cascade simulation (or at least a simulation incorporating N-1 cases) is necessary.

In Chapter 5, the effect of different market designs on the overall system risk was presented, including a short description of the analyzed market models and compared in a case study for the 118 bus system. The analyzed market designs included uniform pricing (no transmission constraints), zonal pricing (constraints on the tie line flows), nodal pricing (constraints on the power flows in the base case scenario) and N-1 security (constraints on the power flows in the base case and the outage scenarios). The market outcomes where then compared by the risk analysis tool (without further consideration of remedial actions like redispatch or power flow control devices).
It was found that an N-1 secure dispatch is the most expensive, but least risky dispatch. Uniform and zonal pricing lead to the same solution, since the tie line constraints are not binding (i.e., there is no congestion on the tie lines). The zonal pricing leads to a low cost, high risk dispatch, while nodal pricing leads to low risk at low generation costs. In a second case study, the tie lines between two grid zones were weakened to artificially generate tie line congestions such that the effect of zonal pricing can be assessed. It was found that the overall system risk decreased dramatically by using zonal pricing in comparison with uniform pricing at nearly the same generation costs. However, zonal pricing can still be considered risky compared to the nodal and N-1 dispatches. Weakening the tie lines generally leads to higher risk, which shows the importance of strong interconnections.

7.3 Risk-based security assessment using AC power flow and Monte-Carlo sampling

The third part (Chapter 6) presents a method to both visualise and control system risk for a given operating state. Through a Monte-Carlo (MC) simulation setup for the uncertain in-feeds, the method considers a range of possible future operating states. The method

provides a risk map based on a fast screening method to visualise system risk, as well as control actions to steer the system into low risk operation.

Chapter 6 presented an RBSA method which enables a probabilistic analysis and evaluation of the risk of a power system in a future state, based on AC power flow and considering varying scenarios of the stochastic inputs. The method provides two outputs. First, a fast screening tool based on N-1 analysis and severity functions is used to monitor the system risk level, visualised through a risk map. Second, a detailed analysis of specific, particularly risky situations can be provided. For those cases, the risk is measured in terms of Lost Load and an AC OPF is used to propose specific actions which can be used by TSOs to steer the system into a risk averse state. In order to get the highest level of accuracy, the method combines a MC simulation framework based on copula theory for generation of stochastic inputs, and a full AC power flow as the core of the deterministic security assessment algorithm. Although the more detailed analysis setup in this chapter (compared to Chapters 2-5) leads to a higher computational burden, the computational time can be kept within limits. This is shown through the implementation on the full scale UCTE system, for which a risk map could be produced within a few hours on a single desktop computer. Additional improvements to reduce the computational time even further are proposed, including parallelisation and enhanced algorithms for both the deterministic and stochastic parts of the simulation.
The method is demonstrated through two case studies for both the IEEE 118 bus system and the full UCTE system with 2713 buses. It was found that an appropriate assessment of uncertainty is a key factor to assess system risk. In particular, it was shown that correlation between different uncertainties plays an important role. Further, it was found that voltage problems significantly contribute to system risk, and should thus not be neglected in the risk assessment. Finally, it was seen that power flow control devices can significantly contribute to low risk operation.

7.4 Conclusions

The three methods above deal with different aspects of the risk assessment, ranging from stochastic optimal power flow to risk assessment for cascading events in presence of uncertain in-feeds. While Chapter 2 and 3 show that a probabilistically secure dispatch is more expensive than a deterministic dispatch, Chapter 4 – 6 show that it is important to consider uncertainty in the operational planning phase to avoid high risk in real time operation. This indicates that the additional cost of considering uncertainty in the planning process might lead to overall lower cost, due to a lower need for remedial actions and lower risk of lost load in real time operation. Market designs that account for transmission constraints in the market clearing are found to lead to a lower overall operational cost and lower risk, which means an increase in expected social welfare.

Further, all methods show that power flow controlling devices are valuable for lowering cost and reducing risk in power system operation. It is found that the power flow controlling devices (HVDC, PSTs, FACTSs) can be effectively used to counteract possible negative impacts of uncertainty. In some cases, it might even be more effective to use HVDC

capacity and PST flexibility to handle uncertainty in real time than to use this flexibility to maximise power transits in the forecasted system state. Thus, we predict that handling of uncertainties might be an important objective for the operation (and even installation) of power flow control devices in the future.

8 Bibliography

[1] UMBRELLA Workpackage 4, "Deliverable 4.1 Risk-based assessment concepts for system security," 2012.

[2] L. Roald, F. Oldewurtel, T. Krause, and G. Andersson, "Analytical reformulation of security constrained optimal power flow with probabilistic constraints," in *IEEE PowerTech*, Grenoble, 2013.

[3] S. Chatzivasileaiadis, T. Krause, and G. Andersson, "Flexible AC transmission systems (FACTS) and power system security — a valuation framework,".

[4] UMBRELLA Workpackage 3, "Deliverable 3.2 Report on EOPF considering uncertainties," 2014.

[5] C. Muller et al., "The impact of forecasting errors and remedial actions on operational security and eficiency in classical and probabilisitc market coupling," in *Power Systems Computation Conference (PSCC)*, Wroclaw, 2014.

[6] M. Vrakopoulou, K. Margellos, J. Lygeros, and G. Andersson, "Probabilistic guarantees for the N-1 security of systems with wind power generation," in *PMAPS 2012*, Istanbul, 2012.

[7] D. Bienstock, M. Chertkov, and S. Harnett, "Chance-constrained optimal power flow: risk-aware network eontrol under uncertainty," *SIAM Review*, vol. 56, no. 3, pp. 383-574, 2014.

[8] Z. Han, "Phase shifter and power flow control," *IEEE Transactions on Power Apparatus and Systems*, vol. PAS-101, no. 10, pp. 3790-3795, October 1982.

[9] J. Verboomen, D. Van Hertem, P. Schavemaker, W. Kling, and R. Belmans, "Analytical approach to grid operation with phase shifting transformers," *IEEE Transactions on Power Systems*, vol. 23, no. 1, pp. 41-46, February 2008.

[10] S. Vandenberghe and S. Boyd, *Convex optimization*. Cambridge: Cambridge University Press, 2004.

[11] E. Kreyszig, *Statistische methoden und ihre anwendungen*., 1975.

[12] B. Danforth, *Variance-covariance matrix*., 2009.

[13] D. Shi. (2012) Power system network reduction for engineering and economic analysis.

[14] R. Zimmerman, C. Murillo-Sanchez, and R. Thomas, "MATPOWER: steady-state operations, planning and analysis tools for power systems research and education," *IEEE Transactions on Power Systems*, vol. 26, no. 1, pp. 12-19, 2011.

[15] ENTSO-E. (2014) Phase shift transformers modelling.

[16] UCTE - Subgroup "Network models and forecast tools“. (2007) UCTE data exchange format for load flow and three phase short circuit studies.

[17] T. Dietrichsteiner. (2012) Lastflussregelung in vermaschten netzen.

[18] N. Hingorani and L. Gyugyi, *Understanding FACTS-concepts and technology of flexible AC transmission systems*., 2000.

[19] G. Fujita, P. Goswami, R. Yokoyama, and G. Shirai, "Local power flow based decentralized TCSC Controller," in *International Conference on Power System Technology, POWERCON '98*, 1998.

[20] Markus Obergünner et al. (2001) Ermittlung von Eingangsdaten für Zuverlässigkeitsberechnungen aus der VDN-Störungsstatistik.

[21] E. Bjørndal, M. Bjørndal, and V. Gribkovskaia, *Congestion management in the nordic power market – nodal pricing versus zonal pricing*. Bergen: Institute for research in economics and business administration, 2013.

[22] K. Cheung, P. Shamsollahi, D. Sun, J. Milligan, and M. Potishnak, "Energy and ancillary service dispatch for the interim ISO New England electricity market," *IEEE Transactions on Power Systems*, vol. 15, no. 3, pp. 968-974, 2000.

[23] ENTSO-E, *Draft network code for operational security*.

[24] 50Hertz Transmission GmbH, Amprion GmbH, TenneT TSO GmbH, TransnetBW GmbH, *Grundsätze für die planung des Deutschen ubertragungsnetzes*., 2012.

[25] G. Jiachun, F. Yong, L. Zuyi, and S. Mohammad, "Direct calculation of line outage distribution factors," *IEEE Transactions on Power Systems*, vol. 24, 2009.

[26] T. Krause, "Evaluating congestion management schemes in liberalized electricity markets applying agent-based computational economics," Zurich, PhD Thesis 2006.

[27] D. Kirschen and D. Jayaweera, "Comparison of risk-based and deterministic security assessments," *IET Generation, Transmission and Distribution*, vol. 1, no. 4, pp. 527-533, 2007.

[28] D. Kirschen and D. Nedic, "Consideration of hidden failures in security analysis," in *Power Systems Computation Conference*, 2002.

[29] D. Kirschen, K. Bell, D. Nedic, D. Jayaweera, and R. Allan, "Computing the value of security," in *IEE Proceedings Generation, Transmission and Distribution*, vol. 150, 2003, pp. 673-678.

[30] M. Rios, D. Kirschen, D. Jayaweera, D. Nedic, and R. Allan, "Value of security: modeling time-dependent phenomena and weather conditions," *IEEE Transactions on Power Systems*, vol. 17, no. 3, pp. 543-548, 2002.

[31] Y. Dai, J. McCalley, N. Abi-Samra, and V. Vittal, "Annual risk assessment for overload security," *IEEE Transactions on Power Systems*, vol. 16, no. 4, pp. 616-623, 2001.

[32] M. Ni, J. McCalley, V. Vittal, and T. Tayyib, "Online risk-based security assessment," *IEEE Transactions on Power Systems*, vol. 18, no. 1, pp. 258-265, 2003.

[33] M. Ni et al., "Software implementation of online risk-based security assessment," *IEEE Transactions on Power Systems*, vol. 18, no. 3, pp. 1165-1172, 2003.

[34] H. Wan, J. McCalley, and V. Vittal, "Risk-based voltage security assessment," *IEEE Transactions on Power Systems*, vol. 15, no. 4, pp. 1247-1254, 2000.

[35] F. Xiao and J. McCalley, "Power system risk assessment and control in a multiobjective framework," *IEEE Transactions on Power Systems*, vol. 24, no. 1, pp. 78-85, 2009.

[36] G. Papaefthymiou, "Integration of stochastic generation in power systems," Delft University of Technology, PhD thesis 2006.

[37] G. Papaefthymiou and D. Kurowicka, "Using copulas for modeling stochastic dependence in power system security analysis," *Applied Energy*, vol. 24, no. 1, pp. 40-49, 2009.

[38] G. Papaefthymiou and P. Pinson, "Modeling of spatial dependence in wind power forecast uncertainty," in *Proceedings of the 10th International Conference on Probabilistic Methods Applied to Power Systems*, 2008.

[39] M. De Jong, G. Papaefthymiou, D. Lahaye, K. Vuik, and L. Van der Sluis, "Impact of correlated infeeds on risk-based power system security assessment," in *PSCC2014*, Wroclaw, 2014.

[40] B. Borkowska, "Probabilistic load flow," *IEEE Transactions on Power Apparatus and Systems*, vol. 93, pp. 752-759, 1974.

[41] R. Allan and M. Alshakarchi, "Probabilistic AC load flow," *Proceedings of the Institution of Electrical Engineers*, vol. 123, no. 6, pp. 531-536, 1976.

[42] R. Allan and M. Alshakarchi, "Probabilistic techniques in AC load flow analysis," *Proceedings of the Institution of Electrical Engineers*, vol. 124, no. 2, pp. 154-160, 1977.

[43] P. Chen, Z. Chen, and B. Bak-Jensen, "Probabilistic load flow: a review," in *Proceedings of the Third International Conference on Electric Utility Deregulation and Restructuring and Power Technologies*, 2008.

[44] P. Jorgensen, J. Christensen, and J. Tande, "Probabilistic load flow calculation using Monte Carlo techniques for distribution network with wind turbines," in *Proceedings of the 8th International Conference on Harmonics and Quality of Power*, vol. 2, 1998, pp. 1146-1151.

[45] J. Usaola, "Probabilistic load flow in systems with wind generation," *IET Generation, Transmisson and Distribution*, vol. 3, pp. 1031-1041, 2009.

[46] D. Villanueva, A. Feijo, and J. Pazos, "Probabilistic load flow considering correlation between generation, loads, and wind power," *Smart Grid and Renewable Energy*, vol. 2, pp. 12-20, 2011.

[47] L. Powell, *Power system load flow analysis*.: McGraw-Hill, 2005.

[48] A. Sklar, "Functions de repartition a n dimensions et leur marges," *Publ. Inst. Statis. Univ. Paris*, vol. 8, pp. 229-231, 1959.

[49] R. Nelsen, *An introduction to copulas*. New York: Springer, 1999.

[50] E. Pradier, "Copula theory: an application to risk modeling," Grenoble, Technical report 2011.

[51] R. Idema, G. Papaefthymiou, D. Lahaye, C. Vuik, and L. Van der Sluis, "Towards faster solution of large power flow problems," *IEEE Transactions on Power Systems*, vol. 28, no. 4, pp. 3010-3017, 2013.

9 Appendix: The IEEE 118 Bus System

Most experiments in this report are performed on the IEEE 118 bus system, see Figure 115. The test system consists of 118 buses, 186 circuits and 54 generators. The data for the IEEE 118 bus system is listed in the following sections. The numbers are taken from the MATPOWER case file; irrelevant numbers to us are left out.

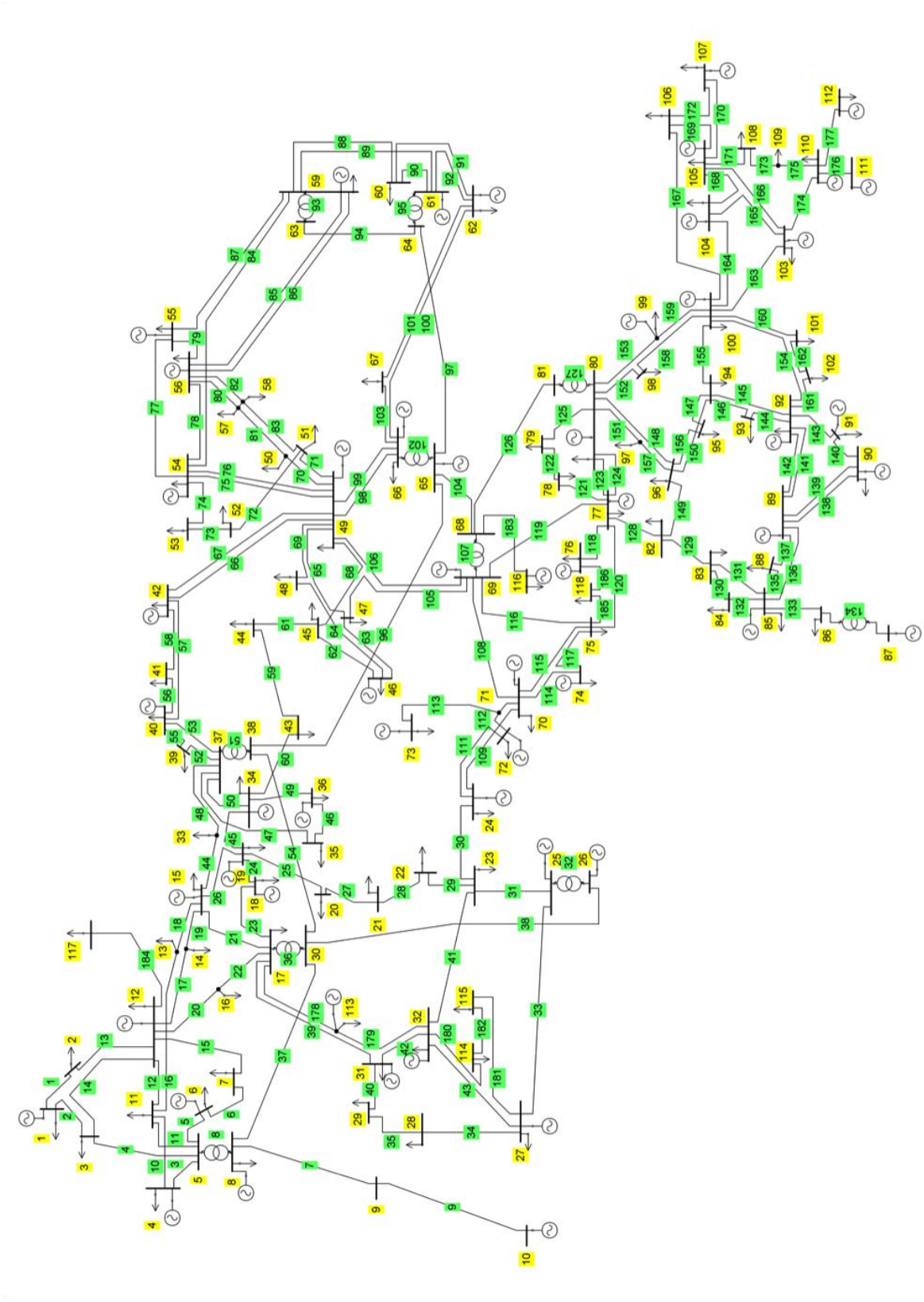

Figure 115: The IEEE 118 bus test system.

9.1.1 Bus data

bus	type	Pmu	Psigma	Qmu	Qsigma	corr(P,Q)	Bs	Vm	Va	baseKV	Vmax	Vmin
1	2	54.14	20.1769	8.66	10.4362	0.5663	0	0.955	10.67	138	1.05	0.94
2	1	21.23	7.6306	9.55	3.5067	-0.1014	0	0.971	11.22	138	1.06	0.95
3	1	41.40	17.2943	10.62	4.3443	-0.0928	0	0.968	11.56	138	1.06	0.95
4	2	31.85	17.1482	12.74	5.0621	0.7089	0	0.998	15.28	138	1.09	0.99
5	1	0.00	0	0	0	0.6535	-40	1.002	15.73	138	1.09	0.99
6	2	55.20	19.8511	23.35	8.1580	-0.1669	0	0.990	13.00	138	1.09	0.97
7	1	20.17	8.3330	2.12	0.7715	0.7443	0	0.989	12.56	138	1.09	0.97
8	2	0.00	10.1920	0	0	0.1251	0	1.015	20.77	345	1.09	0.98
9	1	0.00	0	0	0	0.6201	0	1.043	28.02	345	1.09	0.98
10	2	0.00	0	0	0	0.5357	0	1.050	35.61	345	1.09	0.98
11	1	74.31	28.0835	24.42	10.0801	0.7031	0	0.985	12.72	138	1.08	0.97
12	2	49.89	17.6623	10.62	3.8412	0.6635	0	0.990	12.20	138	1.09	0.98
13	1	36.09	12.4799	16.99	6.2962	0.1289	0	0.968	11.35	138	1.05	0.95
14	1	14.86	5.1064	1.06	0.3651	-0.6606	0	0.984	11.50	138	1.07	0.98
15	2	96.54	36.4855	31.85	12.1716	0.7502	0	0.970	11.23	138	1.05	0.98
16	1	26.54	9.6767	10.62	4.4060	0.0514	0	0.984	11.91	138	1.07	0.98
17	1	11.68	4.3716	3.18	1.2869	0.4692	0	0.995	13.74	138	1.09	0.98
18	2	63.69	26.0642	36.09	14.0795	0.0986	0	0.973	11.53	138	1.07	0.98
19	2	47.77	19.5492	26.54	9.2617	0.0517	0	0.963	11.05	138	1.06	0.98
20	1	19.11	7.1608	3.18	1.1341	0.7048	0	0.958	11.93	138	1.04	0.96
21	1	14.86	5.5362	8.49	3.5005	-0.0089	0	0.959	13.52	138	1.03	0.95
22	1	10.62	4.0705	5.31	1.9779	0.1109	0	0.970	16.08	138	1.04	0.97
23	1	7.43	2.9431	3.18	1.1561	0.782	0	1.000	21.00	138	1.09	0.98
24	2	0.00	5.0725	0	0	0.792	0	0.992	20.89	138	1.09	0.98
25	2	0.00	0	0	0	0.1134	0	1.050	27.93	138	1.09	0.98
26	2	0.00	0	0	0	0.6439	0	1.015	29.71	345	1.09	0.98
27	2	65.82	26.2331	13.8	5.1572	0.8506	0	0.968	15.35	138	1.09	0.96
28	1	18.05	6.1854	7.43	2.9604	0.6428	0	0.962	13.62	138	1.08	0.94
29	1	25.48	9.4702	4.25	1.4812	0.6073	0	0.963	12.63	138	1.08	0.93
30	1	0.00	0	0	0	0.6798	0	0.968	18.79	345	1.06	0.98
31	2	45.65	15.8845	28.66	11.7193	0.7565	0	0.967	12.75	138	1.09	0.94
32	2	62.63	21.9861	24.42	9.0077	0.0644	0	0.964	14.80	138	1.08	0.97
33	1	24.42	8.4217	9.55	3.3592	0.8071	0	0.972	10.63	138	1.04	0.96
34	2	62.63	23.9414	27.6	10.3481	0.7168	14	0.986	11.30	138	1.08	0.97
35	1	35.03	13.4889	9.55	3.6682	0.7708	0	0.981	10.87	138	1.08	0.96
36	2	32.91	12.5569	18.05	6.4789	0.6574	0	0.980	10.87	138	1.08	0.96
37	1	0.00	0	0	0	-0.0761	-25	0.992	11.77	138	1.09	0.98
38	1	0.00	0	0	0	0.5393	0	0.962	16.91	345	1.04	0.95
39	1	27.00	11.8853	11	4.3020	0.5761	0	0.970	8.41	138	1.09	0.93
40	2	20.00	27.2649	23	9.5970	0.693	0	0.970	7.35	138	1.09	0.93

Bus data (cont.)

bus	type	Pmu	Psigma	Qmu	Qsigma	corr(P,Q)	Bs	Vm	Va	baseKV	Vmax	Vmin
41	1	37.00	15.8214	10	4.0274	0.7888	0	0.967	6.92	138	1.09	0.93
42	2	37.00	35.4219	23	9.1770	0.5145	0	0.985	8.53	138	1.09	0.92
43	1	18.00	6.5864	7	2.5992	0.6562	0	0.978	11.28	138	1.06	0.96
44	1	16.00	6.6066	8	2.9678	0.5093	10	0.985	13.82	138	1.06	0.97
45	1	53.00	22.2932	22	8.7742	0.6326	10	0.987	15.67	138	1.06	0.98
46	2	28.00	10.5460	10	3.7211	0.6301	10	1.005	18.49	138	1.09	0.98
47	1	34.00	13.8599	0	0	0.7107	0	1.017	20.73	138	1.09	0.98
48	1	20.00	7.3395	11	4.7876	-0.0242	15	1.021	19.93	138	1.09	0.98
49	2	87.00	34.6078	30	12.1794	0.0259	0	1.025	20.94	138	1.09	0.98
50	1	17.00	7.4691	4	1.5957	-0.0005	0	1.001	18.90	138	1.09	0.99
51	1	17.00	6.6117	8	3.3927	0.7203	0	0.967	16.28	138	1.07	0.97
52	1	18.00	7.4414	5	2.1855	0.7282	0	0.957	15.32	138	1.06	0.97
53	1	23.00	9.5857	11	4.5279	0.1235	0	0.946	14.35	138	1.06	0.96
54	2	113.00	44.5616	32	12.0385	0.557	0	0.955	15.26	138	1.09	0.97
55	2	63.00	24.7312	22	8.6520	0.5744	0	0.952	14.97	138	1.09	0.97
56	2	84.00	34.4298	18	7.9072	0.6046	0	0.954	15.16	138	1.09	0.97
57	1	12.00	5.2065	3	1.2709	0.1071	0	0.971	16.36	138	1.08	0.98
58	1	12.00	4.8807	3	1.1070	0.5768	0	0.959	15.51	138	1.07	0.97
59	2	277.00	113.4571	113	44.3883	0.5389	0	0.985	19.37	138	1.09	0.98
60	1	78.00	28.5016	3	1.2658	0.5987	0	0.993	23.15	138	1.09	0.99
61	2	0	0	0	0	0.5853	0	0.995	24.04	138	1.09	0.99
62	2	77.00	30.9038	14	5.4937	0.5837	0	0.998	23.43	138	1.09	0.98
63	1	0	0	0	0	0.0869	0	0.969	22.75	345	1.06	0.96
64	1	0	0	0	0	0.6973	0	0.984	24.52	345	1.07	0.98
65	2	0	0	0	0	-0.6598	0	1.005	27.65	345	1.07	0.98
66	2	39.00	16.0660	18	6.6112	0.4922	0	1.050	27.48	138	1.09	0.98
67	1	28.00	10.4505	7	2.6101	0.4811	0	1.020	24.84	138	1.09	0.98
68	1	0	0	0	0	0.4061	0	1.003	27.55	345	1.08	0.98
69	3	0	0	0	0	0.5543	0	1.035	30.00	138	1.09	0.98
70	2	66.00	28.4205	20	7.8983	0.6732	0	0.984	22.58	138	1.06	0.98
71	1	0	0	0	0	-0.6221	0	0.987	22.15	138	1.06	0.99
72	2	0	4.7613	0	0	0.1801	0	0.980	20.98	138	1.09	0.99
73	2	0	2.6394	0	0	0.6269	0	0.991	21.94	138	1.06	0.99
74	2	68.00	27.0689	27	11.3764	0.6009	12	0.958	21.64	138	1.03	0.93
75	1	47.00	20.4314	11	4.0039	-0.0677	0	0.967	22.91	138	1.04	0.94
76	2	68.00	27.5830	36	14.6718	0.0753	0	0.943	21.77	138	1.02	0.93
77	2	61.00	26.2028	28	11.6308	0.707	0	1.006	26.72	138	1.08	0.98
78	1	71.00	29.8200	26	10.5065	0.6935	0	1.003	26.42	138	1.07	0.99
79	1	39.00	16.8618	32	13.9405	0.0878	20	1.009	26.72	138	1.07	0.99
80	2	130.00	56.4218	26	10.0377	0.1802	0	1.040	28.96	138	1.09	0.99

Bus data (cont.)

bus	type	Pmu	Psigma	Qmu	Qsigma	corr(P,Q)	Bs	Vm	Va	baseKV	Vmax	Vmin
81	1	0	0	0	0	0.6944	0	0.997	28.10	345	1.07	0.98
82	1	54.00	20.9909	27	10.4784	-0.7734	20	0.989	27.24	138	1.09	0.98
83	1	20.00	7.7836	10	3.7068	0.794	10	0.985	28.42	138	1.07	0.99
84	1	11.00	4.5089	7	2.6752	0.5824	0	0.980	30.95	138	1.03	0.96
85	2	24.00	10.5828	15	6.5882	0.8044	0	0.985	32.51	138	1.02	0.96
86	1	21.00	7.9644	10	3.7261	0.6255	0	0.987	31.14	138	0.96	0.93
87	2	0	0	0	0	0.5408	0	1.015	31.40	161	1.09	0.98
88	1	48.00	18.0462	10	4.2485	0.4253	0	0.987	35.64	138	1.06	0.98
89	2	0	0	0	0	0.6797	0	1.005	39.69	138	1.09	0.98
90	2	78.00	60.7616	42	15.8469	0.7963	0	0.985	33.29	138	1.09	0.98
91	2	0	4.3316	0	0	0.6359	0	0.980	33.31	138	1.09	0.98
92	2	65.00	27.4711	10	3.8634	0.1579	0	0.993	33.80	138	1.09	0.98
93	1	12.00	4.4247	7	2.8923	0.5519	0	0.987	30.79	138	1.08	0.98
94	1	30.00	11.2886	16	5.9923	-0.0803	0	0.991	28.64	138	1.07	0.98
95	1	42.00	15.3473	31	11.7803	0.1976	0	0.981	27.67	138	1.05	0.98
96	1	38.00	15.5788	15	6.3366	0.658	0	0.993	27.51	138	1.07	0.98
97	1	15.00	6.3891	9	3.6646	0.0885	0	1.011	27.88	138	1.08	0.98
98	1	34.00	12.4299	8	3.2707	-0.0324	0	1.024	27.40	138	1.08	0.98
99	2	0	17.3681	0	0	0.6127	0	1.010	27.04	138	1.09	0.98
100	2	37.00	15.4968	18	7.9298	0.6662	0	1.017	28.03	138	1.09	0.98
101	1	22.00	8.1089	15	5.5274	0.5216	0	0.993	29.61	138	1.08	0.98
102	1	5.00	1.8774	3	1.3238	0.157	0	0.991	32.30	138	1.09	0.98
103	2	23.00	9.1023	16	6.8813	0.1361	0	1.001	24.44	138	1.09	0.98
104	2	38.00	16.7590	25	9.4056	0.1454	0	0.971	21.69	138	1.08	0.99
105	2	31.00	12.7653	26	10.2932	0.6764	20	0.965	20.57	138	1.08	0.98
106	1	43.00	18.7248	16	6.7788	0.6838	0	0.962	20.32	138	1.07	0.96
107	2	28.00	18.7014	12	5.3098	0.5986	6	0.952	17.53	138	1.06	0.94
108	1	2.00	0.7852	1	0.3970	0.6082	0	0.967	19.38	138	1.08	0.98
109	1	8.00	3.5491	3	1.3021	0.7006	0	0.967	18.93	138	1.08	0.98
110	2	39.00	14.7566	30	12.1345	0.0138	6	0.973	18.09	138	1.09	0.97
111	2	0	0	0	0	0.5962	0	0.980	19.74	138	1.09	0.97
112	2	25.00	28.4185	13	5.0220	0.4522	0	0.975	14.99	138	1.09	0.97
113	2	0	2.6418	0	0	0.6465	0	0.993	13.74	138	1.09	0.98
114	1	8.49	3.2744	3.18	1.1215	0.7119	0	0.960	14.46	138	1.08	0.96
115	1	23.35	8.8275	7.43	2.6143	0.5187	0	0.960	14.46	138	1.08	0.96
116	2	0	77.9658	0	0	0.6417	0	1.005	27.12	138	1.09	0.98
117	1	21.23	8.8006	8.49	3.0676	0.6968	0	0.974	10.67	138	1.06	0.95
118	1	33.00	14.6173	15	5.6310	0.5396	0	0.949	21.92	138	1.03	0.93

9.1.2 Generator data

bus	Pg	Qmax	Qmin	Vg	mBase	Pmax	Pmin	c2	c1	c0	Pr(outage)
4	0	300	-300	0.998	100	30	5	0.069663	26.2438	31.67	0.0004
6	0	50	-13	0.990	100	30	5	0.069663	26.2438	31.67	0.0004
8	0	300	-300	1.015	100	30	5	0.069663	26.2438	31.67	0.0004
10	450	200	-147	1.050	100	300	150	0.010875	12.8875	6.78	0.0010
12	85	120	-35	0.990	100	300	100	0.010875	12.8875	6.78	0.0010
15	0	30	-10	0.970	100	30	10	0.069663	26.2438	31.67	0.0004
18	0	50	-16	0.973	100	100	25	0.012800	17.8200	10.15	0.0008
19	0	24	-8	0.962	100	30	5	0.069663	26.2438	31.67	0.0004
24	0	300	-300	0.992	100	30	5	0.069663	26.2438	31.67	0.0004
25	220	140	-47	1.050	100	300	100	0.010875	12.8875	6.78	0.0010
26	314	1000	-1000	1.015	100	350	100	0.003000	10.7600	32.96	0.0010
27	0	300	-300	0.968	100	30	8	0.069663	26.2438	31.67	0.0004
31	7	300	-300	0.967	100	30	8	0.069663	26.2438	31.67	0.0004
32	0	42	-14	0.963	100	100	25	0.012800	17.8200	10.15	0.0008
34	0	24	-8	0.984	100	30	8	0.069663	26.2438	31.67	0.0004
36	0	24	-8	0.980	100	100	25	0.012800	17.8200	10.15	0.0008
40	0	300	-300	0.970	100	30	8	0.069663	26.2438	31.67	0.0004
42	0	300	-300	0.985	100	30	8	0.069663	26.2438	31.67	0.0004
46	19	100	-100	1.005	100	100	25	0.012800	17.8200	10.15	0.0008
49	204	210	-85	1.025	100	250	50	0.002401	12.3299	28.00	0.0010
54	48	300	-300	0.955	100	250	50	0.002401	12.3299	28.00	0.0010
55	0	23	-8	0.952	100	100	25	0.012800	17.8200	10.15	0.0008
56	0	15	-8	0.954	100	100	25	0.012800	17.8200	10.15	0.0008
59	155	180	-60	0.985	100	200	50	0.004400	13.2900	39.00	0.0009
61	160	300	-100	0.995	100	200	50	0.004400	13.2900	39.00	0.0009
62	0	20	-20	0.998	100	100	25	0.012800	17.8200	10.15	0.0008
65	391	200	-67	1.005	100	420	100	0.010590	8.3391	64.16	n/a
66	392	200	-67	1.050	100	420	100	0.010590	8.3391	64.16	n/a
69	516.4	300	-300	1.035	100	300	80	0.010875	12.8875	6.78	0.0010
70	0	32	-10	0.984	100	80	30	0.045923	15.4708	74.33	0.0006
72	0	100	-100	0.980	100	30	10	0.069663	26.2438	31.67	0.0004
73	0	100	-100	0.991	100	30	5	0.069663	26.2438	31.67	0.0004
74	0	9	-6	0.958	100	20	5	0.028302	37.6968	17.95	0.0004
76	0	23	-8	0.943	100	100	25	0.012800	17.8200	10.15	0.0008
77	0	70	-20	1.006	100	100	25	0.012800	17.8200	10.15	0.0008
80	477	280	-165	1.040	100	300	150	0.010875	12.8875	6.78	0.0010
82	0	9900	-9900	0.989	100	100	25	0.012800	17.8200	10.15	0.0008
85	0	23	-8	0.985	100	30	10	0.069663	26.2438	31.67	0.0004
87	4	1000	-100	1.015	100	300	100	0.003000	10.7600	32.96	0.0010
89	607	300	-210	1.005	100	200	50	0.010875	12.8875	6.78	0.0009
90	0	300	-300	0.985	100	20	8	0.028302	37.6968	17.95	0.0004
91	0	100	-100	0.980	100	50	20	0.009774	22.9423	58.81	0.0005
92	0	9	-3	0.990	100	300	100	0.010875	12.8875	6.78	0.0010
99	0	100	-100	1.010	100	300	100	0.010875	12.8875	6.78	0.0010
100	252	155	-50	1.017	100	300	100	0.010875	12.8875	6.78	0.0010
103	40	40	-15	1.010	100	20	8	0.028302	37.6968	17.95	0.0004
104	0	23	-8	0.971	100	100	25	0.012800	17.8200	10.15	0.0008
105	0	23	-8	0.965	100	100	25	0.012800	17.8200	10.15	0.0008
107	0	200	-200	0.952	100	20	8	0.028302	37.6968	17.95	0.0004
110	0	23	-8	0.973	100	50	25	0.009774	22.9423	58.81	0.0005
111	36	1000	-100	0.980	100	100	25	0.012800	17.8200	10.15	0.0008
112	0	1000	-100	0.975	100	100	25	0.012800	17.8200	10.15	0.0008
113	0	200	-100	0.993	100	100	25	0.012800	17.8200	10.15	0.0008
116	0	1000	-1000	1.005	100	50	25	0.009774	22.9423	58.81	0.0005

9.1.3 Branch data

line	from	to	r	x	b	rating	ratio	Pr(outage)
1	1	2	0.03030	0.09990	0.02540	175	0	0.2347
2	1	3	0.01290	0.04240	0.01082	175	0	0.0987
3	4	5	0.00176	0.00798	0.00210	500	0	0.0173
4	3	5	0.02410	0.10800	0.02840	175	0	0.2539
5	5	6	0.01190	0.05400	0.01426	175	0	0.1261
6	6	7	0.00459	0.02080	0.00550	175	0	0.0476
7	8	9	0.00244	0.03050	1.16200	500	0	0.0705
8	8	5	0	0.02670	0	500	0.985	0.0615
9	9	10	0.00258	0.03220	1.23000	500	0	0.0745
10	4	11	0.02090	0.06880	0.01748	175	0	0.1611
11	5	11	0.02030	0.06820	0.01738	175	0	0.1597
12	11	12	0.00595	0.01960	0.00502	175	0	0.0447
13	2	12	0.01870	0.06160	0.01572	175	0	0.1441
14	3	12	0.04840	0.16000	0.04060	175	0	0.3769
15	7	12	0.00862	0.03400	0.00874	175	0	0.0788
16	11	13	0.02225	0.07310	0.01876	175	0	0.1713
17	12	14	0.02150	0.07070	0.01816	175	0	0.1656
18	13	15	0.07440	0.24440	0.06268	175	0	0.5765
19	14	15	0.05950	0.19500	0.05020	175	0	0.4597
20	12	16	0.02120	0.08340	0.02140	175	0	0.1957
21	15	17	0.01320	0.04370	0.04440	500	0	0.1018
22	16	17	0.04540	0.18010	0.04660	175	0	0.4244
23	17	18	0.01230	0.05050	0.01298	175	0	0.1178
24	18	19	0.01119	0.04930	0.01142	175	0	0.1150
25	19	20	0.02520	0.11700	0.02980	175	0	0.2752
26	15	19	0.01200	0.03940	0.01010	175	0	0.0916
27	20	21	0.01830	0.08490	0.02160	175	0	0.1992
28	21	22	0.02090	0.09700	0.02460	175	0	0.2278
29	22	23	0.03420	0.15900	0.04040	175	0	0.3745
30	23	24	0.01350	0.04920	0.04980	175	0	0.1148
31	23	25	0.01560	0.08000	0.08640	500	0	0.1876
32	26	25	0	0.03820	0	500	0.96	0.0887
33	25	27	0.03180	0.16300	0.17640	500	0	0.3840
34	27	28	0.01913	0.08550	0.02160	175	0	0.2006
35	28	29	0.02370	0.09430	0.02380	175	0	0.2215
36	30	17	0	0.03880	0	500	0.96	0.0902
37	8	30	0.00431	0.05040	0.51400	175	0	0.1176
38	26	30	0.00799	0.08600	0.90800	500	0	0.2018
39	17	31	0.04740	0.15630	0.03990	175	0	0.3681
40	29	31	0.01080	0.03310	0.00830	175	0	0.0767
41	23	32	0.03170	0.11530	0.11730	140	0	0.2711
42	31	32	0.02980	0.09850	0.02510	175	0	0.2314
43	27	32	0.02290	0.07550	0.01926	175	0	0.1770
44	15	33	0.03800	0.12440	0.03194	175	0	0.2927
45	19	34	0.07520	0.24700	0.06320	175	0	0.5827
46	35	36	0.00224	0.01020	0.00268	175	0	0.0225
47	35	37	0.01100	0.04970	0.01318	175	0	0.1159
48	33	37	0.04150	0.14200	0.03660	175	0	0.3343
49	34	36	0.00871	0.02680	0.00568	175	0	0.0618
50	34	37	0.00256	0.00940	0.00984	500	0	0.0206

Branch data (cont.)

line	from	to	r	x	b	rating	ratio	Pr(outage)
51	38	37	0	0.03750	0	500	0.935	0.0871
52	37	39	0.03210	0.10600	0.02700	175	0	0.2491
53	37	40	0.05930	0.16800	0.04200	175	0	0.3958
54	30	38	0.00464	0.05400	0.42200	175	0	0.1261
55	39	40	0.01840	0.06050	0.01552	175	0	0.1415
56	40	41	0.01450	0.04870	0.01222	175	0	0.1136
57	40	42	0.05550	0.18300	0.04660	175	0	0.4313
58	41	42	0.04100	0.13500	0.03440	175	0	0.3177
59	43	44	0.06080	0.24540	0.06068	175	0	0.5789
60	34	43	0.04130	0.16810	0.04226	175	0	0.3960
61	44	45	0.02240	0.09010	0.02240	175	0	0.2115
62	45	46	0.04000	0.13560	0.03320	175	0	0.3192
63	46	47	0.03800	0.12700	0.03160	175	0	0.2988
64	46	48	0.06010	0.18900	0.04720	175	0	0.4455
65	47	49	0.01910	0.06250	0.01604	175	0	0.1462
66	42	49	0.07150	0.32300	0.08600	175	0	0.7625
67	42	49	0.07150	0.32300	0.08600	175	0	0.7625
68	45	49	0.06840	0.18600	0.04440	175	0	0.4384
69	48	49	0.01790	0.05050	0.01258	175	0	0.1178
70	49	50	0.02670	0.07520	0.01874	175	0	0.1763
71	49	51	0.04860	0.13700	0.03420	175	0	0.3225
72	51	52	0.02030	0.05880	0.01396	175	0	0.1375
73	52	53	0.04050	0.16350	0.04058	175	0	0.3852
74	53	54	0.02630	0.12200	0.03100	175	0	0.2870
75	49	54	0.07300	0.28900	0.07380	175	0	0.6820
76	49	54	0.08690	0.29100	0.07300	175	0	0.6868
77	54	55	0.01690	0.07070	0.02020	175	0	0.1656
78	54	56	0.00275	0.00955	0.00732	175	0	0.0210
79	55	56	0.00488	0.01510	0.00374	175	0	0.0341
80	56	57	0.03430	0.09660	0.02420	175	0	0.2269
81	50	57	0.04740	0.13400	0.03320	175	0	0.3154
82	56	58	0.03430	0.09660	0.02420	175	0	0.2269
83	51	58	0.02550	0.07190	0.01788	175	0	0.1685
84	54	59	0.05030	0.22930	0.05980	175	0	0.5408
85	56	59	0.08250	0.25100	0.05690	175	0	0.5921
86	56	59	0.08030	0.23900	0.05360	175	0	0.5638
87	55	59	0.04739	0.21580	0.05646	175	0	0.5089
88	59	60	0.03170	0.14500	0.03760	175	0	0.3414
89	59	61	0.03280	0.15000	0.03880	175	0	0.3532
90	60	61	0.00264	0.01350	0.01456	500	0	0.0303
91	60	62	0.01230	0.05610	0.01468	175	0	0.1311
92	61	62	0.00824	0.03760	0.00980	175	0	0.0873
93	63	59	0	0.03860	0	500	0.96	0.0897
94	63	64	0.00172	0.02000	0.21600	500	0	0.0457
95	64	61	0	0.02680	0	500	0.985	0.0618
96	38	65	0.00901	0.09860	1.04600	500	0	0.2316
97	64	65	0.00269	0.03020	0.38000	500	0	0.0698
98	49	66	0.01800	0.09190	0.02480	500	0	0.2158
99	49	66	0.01800	0.09190	0.02480	500	0	0.2158
100	62	66	0.04820	0.21800	0.05780	175	0	0.5141

Branch data (cont.)

line	from	to	r	x	b	rating	ratio	Pr(outage)
101	62	67	0.02580	0.11700	0.03100	175	0	0.2752
102	65	66	0	0.03700	0	500	0.935	0.0859
103	66	67	0.02240	0.10150	0.02682	175	0	0.2385
104	65	68	0.00138	0.01600	0.63800	500	0	0.0362
105	47	69	0.08440	0.27780	0.07092	175	0	0.6555
106	49	69	0.09850	0.32400	0.08280	175	0	0.7648
107	68	69	0	0.03700	0	500	0.935	0.0859
108	69	70	0.03000	0.12700	0.12200	500	0	0.2988
109	24	70	0.00221	0.41150	0.10198	175	0	0.9718
110	70	71	0.00882	0.03550	0.00878	175	0	0.0824
111	24	72	0.04880	0.19600	0.04880	175	0	0.4620
112	71	72	0.04460	0.18000	0.04444	175	0	0.4242
113	71	73	0.00866	0.04540	0.01178	175	0	0.1058
114	70	74	0.04010	0.13230	0.03368	175	0	0.3113
115	70	75	0.04280	0.14100	0.03600	175	0	0.3319
116	69	75	0.04050	0.12200	0.12400	500	0	0.2870
117	74	75	0.01230	0.04060	0.01034	175	0	0.0944
118	76	77	0.04440	0.14800	0.03680	175	0	0.3485
119	69	77	0.03090	0.10100	0.10380	175	0	0.2373
120	75	77	0.06010	0.19990	0.04978	175	0	0.4713
121	77	78	0.00376	0.01240	0.01264	175	0	0.0277
122	78	79	0.00546	0.02440	0.00648	175	0	0.0561
123	77	80	0.01700	0.04850	0.04720	500	0	0.1131
124	77	80	0.02940	0.10500	0.02280	500	0	0.2468
125	79	80	0.01560	0.07040	0.01870	175	0	0.1649
126	68	81	0.00175	0.02020	0.80800	500	0	0.0462
127	81	80	0	0.03700	0	500	0.935	0.0859
128	77	82	0.02980	0.08530	0.08174	200	0	0.2002
129	82	83	0.01120	0.03665	0.03796	200	0	0.0851
130	83	84	0.06250	0.13200	0.02580	175	0	0.3106
131	83	85	0.04300	0.14800	0.03480	175	0	0.3485
132	84	85	0.03020	0.06410	0.01234	175	0	0.1500
133	85	86	0.03500	0.12300	0.02760	500	0	0.2893
134	86	87	0.02828	0.20740	0.04450	500	0	0.4890
135	85	88	0.02000	0.10200	0.02760	175	0	0.2397
136	85	89	0.02390	0.17300	0.04700	175	0	0.4076
137	88	89	0.01390	0.07120	0.01934	500	0	0.1668
138	89	90	0.05180	0.18800	0.05280	500	0	0.4431
139	89	90	0.02380	0.09970	0.10600	500	0	0.2342
140	90	91	0.02540	0.08360	0.02140	175	0	0.1961
141	89	92	0.00990	0.05050	0.05480	500	0	0.1178
142	89	92	0.03930	0.15810	0.04140	500	0	0.3724
143	91	92	0.03870	0.12720	0.03268	175	0	0.2993
144	92	93	0.02580	0.08480	0.02180	175	0	0.1990
145	92	94	0.04810	0.15800	0.04060	175	0	0.3721
146	93	94	0.02230	0.07320	0.01876	175	0	0.1715
147	94	95	0.01320	0.04340	0.01110	175	0	0.1010
148	80	96	0.03560	0.18200	0.04940	175	0	0.4289
149	82	96	0.01620	0.05300	0.05440	175	0	0.1238
150	94	96	0.02690	0.08690	0.02300	175	0	0.2039

Bus data (cont.)

line	from	to	r	x	b	rating	ratio	Pr(outage)
151	80	97	0.01830	0.09340	0.02540	175	0	0.2193
152	80	98	0.02380	0.10800	0.02860	175	0	0.2539
153	80	99	0.04540	0.20600	0.05460	200	0	0.4857
154	92	100	0.06480	0.29500	0.04720	175	0	0.6962
155	94	100	0.01780	0.05800	0.06040	175	0	0.1356
156	95	96	0.01710	0.05470	0.01474	175	0	0.1278
157	96	97	0.01730	0.08850	0.02400	175	0	0.2077
158	98	100	0.03970	0.17900	0.04760	175	0	0.4218
159	99	100	0.01800	0.08130	0.02160	175	0	0.1907
160	100	101	0.02770	0.12620	0.03280	175	0	0.2969
161	92	102	0.01230	0.05590	0.01464	175	0	0.1306
162	101	102	0.02460	0.11200	0.02940	175	0	0.2633
163	100	103	0.01600	0.05250	0.05360	500	0	0.1226
164	100	104	0.04510	0.20400	0.05410	175	0	0.4810
165	103	104	0.04660	0.15840	0.04070	175	0	0.3731
166	103	105	0.05350	0.16250	0.04080	175	0	0.3828
167	100	106	0.06050	0.22900	0.06200	175	0	0.5401
168	104	105	0.00994	0.03780	0.00986	175	0	0.0878
169	105	106	0.01400	0.05470	0.01434	175	0	0.1278
170	105	107	0.05300	0.18300	0.04720	175	0	0.4313
171	105	108	0.02610	0.07030	0.01844	175	0	0.1647
172	106	107	0.05300	0.18300	0.04720	175	0	0.4313
173	108	109	0.01050	0.02880	0.00760	175	0	0.0665
174	103	110	0.03906	0.18130	0.04610	175	0	0.4273
175	109	110	0.02780	0.07620	0.02020	175	0	0.1786
176	110	111	0.02200	0.07550	0.02000	175	0	0.1770
177	110	112	0.02470	0.06400	0.06200	175	0	0.1498
178	17	113	0.00913	0.03010	0.00768	175	0	0.0696
179	32	113	0.06150	0.20300	0.05180	500	0	0.4786
180	32	114	0.01350	0.06120	0.01628	175	0	0.1432
181	27	115	0.01640	0.07410	0.01972	175	0	0.1737
182	114	115	0.00230	0.01040	0.00276	175	0	0.0230
183	68	116	0.00034	0.00405	0.16400	500	0	0.0080
184	12	117	0.03290	0.14000	0.03580	175	0	0.3296
185	75	118	0.01450	0.04810	0.01198	175	0	0.1122
186	76	118	0.01640	0.05440	0.01356	175	0	0.1271